



# **BOTTOM UP NANOMACHINES (BUN)**

## **Final report**

**Covering period 1.1.2000-30.06.2003**

Report Version: **001**

Report Preparation Date: **23/01/01**

Classification: **Confidential**

Contract Start Date: **01/01/2000** Duration: **3 ½ Years**

Project Co-ordinator: **C. JOACHIM**

Partners: **TOULOUSE, KIEL, ORSAY, ZURICH, BASEL, AARHUS,  
CAMBRIDGE, LONDON**



**Project funded by the European Community under  
the “Information Society Technologies”  
Programme (1998-2002)**



## *Contents*

I) Introduction	5
II) Chemistry	
a) The lateral legs functional groups	7
b) Molecular wires with a small homo-lumo gap	10
c) Conformational switches: rotational Lander	11
d) Extended p systems in a molecule for future intramolecular circuits	13
e) Nano-communication groups	14
III) Molecular surface science in BUN	
a) Extracting and optimising a molecular conformation from an STM image	15
b) Lander molecule on a flat metallic surface	17
c) Lander molecule at a mono-atomic step edge	21
d) I-V STM spectroscopy on a Lander molecule	25
e) First images of organics molecules on the surface of a bulk insulator	26
f) Force spectroscopy on a leg of a molecule	30
g) Conclusion	32
IV) Transforming the surface for molecular electronics	
a) Fabrication of atomic holes and wires using single molecules	33
b) Transforming the surface before adsorbing the molecule	37
c) Combining SWCNT on an SiO <sub>2</sub> surface	41
V) Nano-communications	
a) Co-planar nano-junction fabrication by e-beam nanolithography down to 2 nm	43
b) I-V characteristics of SWCNT	51
c) Is an atomic scale technology possible?	54
d) Nanostencil: towards an atomic scale technology	58

VI) Hybrid molecular electronics	
a) Miniaturisation of the electronic circuit	62
b) Miniaturisation of the transistor in a hybrid circuit: the C60 transistor case	64
c) Limitations of the hybrid molecular electronic approach	73
VII) Mono-molecular electronics	
a) The tunnel transport regime	77
b) The intramolecular circuit laws and circuit simulator	83
c) The design and function of a full tight binding digital half adder	86
d) The design and function of a molecule-OR and a molecule-AND	90
e) Starting of the mono-molecular electronics experimental approach	92
f) Conclusion	96
VIII) Conclusion	97

## **I) Introduction**

The research summarized in this final report is the result of 3 ½ years of work of a consortium of 7 laboratories best in Chemistry, nanotechnologies, atomic and molecular manipulation, UHV-STM, UHV-AFM, surface science and computer circuit architecture.

The objective of BUN was to establish new sciences and technologies at the nanoscale for the fabrication of a calculator with a minimum number of molecule and ideally with only one, integrating all the function inside this single molecule. This new field can be considered as a part of a more general field of fundamental technology: the design, assembly and communication of a mono-molecular machine made of a single and always the same molecule supported by a surface. Those nano-machines belong to the “nano” world which will encompass in the future: computer (calculators and memory), mechanical machine (motor, carriers...), transducers (sensors, amperemeters ...) and communication devices. The BUN project was only dedicated to the nano-calculator machines. But the sciences and fundamental technologies developed under the BUN direction will also contribute to the development of other types of nano-machines.

There are a few possible choices for the architecture of a calculator: Hybrid, semi-classical mono-molecular, quantum mono-molecular and quantum computer like architectures.

The simple Hybrid architecture consider that a properly designed molecule, interacting with 3 metallic electrodes will play the role of a transistor. In this case, the full circuit is made of an underneath metallic net constituting the electronic circuit and the molecular transistors are positioned on dedicated places pre-fabricated on the metallic net. This is the Hybrid approach of molecular electronics. In principle, it can be practiced with small molecules like C60. But the experimental realisation are using macromolecules like carbon nanotubes. It is important here to insist on the fact that it is not the molecule alone which creates the transistor functionality (if any). It is the molecule + its 3 electrodes.

The semi-classical mono-molecular is base on the integration of the full electronic circuit of the calculator inside (on) the same molecule. This suppresses the metallic underneath net. Ideally, only the nano-communication circuit outside the single molecule is metallic. Basically, the designer will be able here to preserve the spatial representation of the calculator electronic functions. But due to the fact that the information inside the molecule is quantum in nature, new intramolecular circuit laws taking into account the quantum origin of the true bond electron transfer process have been established as described in section V.

The quantum mono-molecular approach is more advances. It was introduced by BUN in answer to the fundamental problem that a complex circuit in a semi-classical mono-molecular approach is unrealistic. This is due to the fact that the tunnelling current intensity true an intramolecular circuit decay exponentially when the spatial extension of the circuit is increased. One solution is to recognize the powerness of the intramolecular behaviour inside a single molecule without any reference to electronic circuit concept. There is no special rules in the design of the calculator. But simple quantum rules. This approach is now developed in the CHIC project.

Finally, the quantum computer approach is based on the subdivision of the molecule is qbits. This approach permits to apply the quantum algorithm developed in the context of quantum

computer. This usually requires molecules with relatively isolated groups. This is not an approach explored in BUN even if the previous quantum mono-molecular approach is positioned between the semi-classical mono-molecular approach and this quantum computer approach.

Any choice of architecture relying on the use of molecules requires the transition from nanotechnology to atomic scale technology. This was not so clear at the beginning of BUN. But after a year of BUN work, the atomic technology becomes the next frontier of technology to be reach. The BUN consortium was first in pushing hard in this direction and to establish the roots of this fundamental technology. As presented in section IV, this requires to master the surface preparation at a truly atomic scale in an ultra-clean environment. This also require to master atomic and molecular positioning with a precision better than 0.1 nm.

Another side of this new atomic scale technology is the design and synthesis of molecules not only with an electronic function useful in the assembling of a calculator. The chemical structure of the molecule must be adapted to others constraints like solubility, protection of the electronic functional group when adsorbed on a surface and proper end group to ensure a good electronic interaction between the molecular electronic molecules and the nano-communication circuit. Section II is dedicated to the BUN progresses in organic chemistry towards this goal.

Of course, BUN had beneficiated form mature sciences like organics chemistry, surface science and electron transfer theory through a molecule. Furthermore, BUN had made a large use of the just mature near field microscopy technique especially UHV-STM and LT-UHV-STM. BUN has introduced specific computation techniques like conformation refinement and intramolecular circuit rules theory. BUN also pushed strongly for the complete development of the nanostencil technique and for the improvement of the non-contact UHV-AFM microscopy.

The present document is not organised following the work-package definition of BUN. It was re-organised in an order which may be more suitable for example in teaching the foundation of molecular electronic technology at a truly atomic scale at a post-doc level. All the sections are supposed to defined a specific subject of research which may develop independently. If the chemistry section II is pivotal for molecular electronics, section III and IV about surface science at the atomic scale with large molecules are new and result from the work done by the BUN partners. What is totally new is the division practiced between section V on nano-communications, VI on hybrid molecular electronics and VII on mono-molecular electronics. It is the real contribution of the BUN work to have identified, created and culture those field as independent entities. We expect that this final report will please the readers as all the BUN partners have be very pleased to work together during those years.

C. Joachim  
BUN co-ordinator  
August 2003



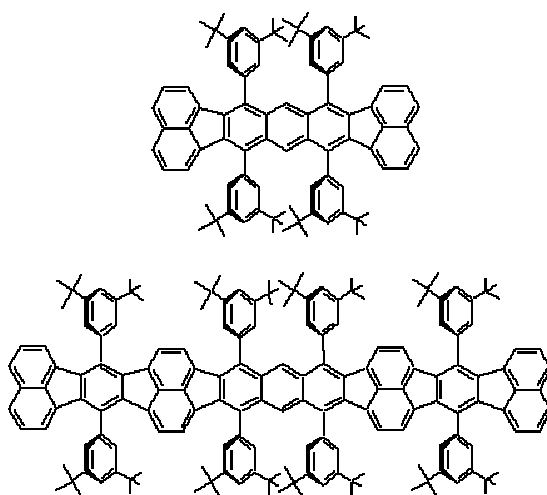
## II) Chemistry

Chemistry was central in BUN. Chemistry provides new molecules for experiments which can not be found in the catalogue and require a specific design. Aside the molecule internal electronic functions which depend on this dedicated design to obtained for example a long molecular wire, an intramolecular switch or in the near future an intramolecular circuit, the molecule must be equipped with a few other functional groups for :

- (1) maintaining the intrinsic electronic function away from the underneath supporting surface
- (2) helping the molecules to be soluble during their synthesis away from the surface
- (3) clipping the molecule at a given position and conformation on the surface
- (4) maintaining the nano-communication group of the molecule in good electronic interaction with the interconnection nano-electrodes

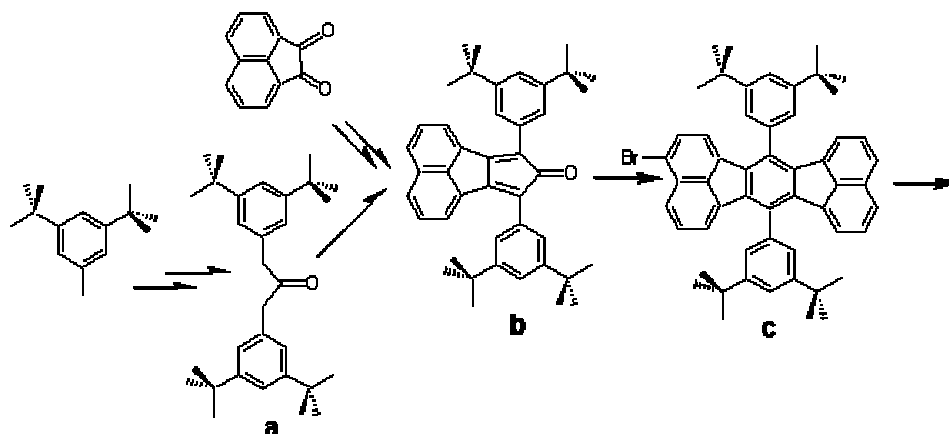
In some cases, part of those functionalities are shared between the surface and the molecule. For example, anchoring groups are pre-deposited on the surface before the sublimation of the functional molecules. In some other cases, even the intramolecular electronic function results from an interaction between the molecule and the surface. This is the case of some conformational switches studied in BUN where the double well energy potential of the system is created by both the surface and the molecule.

In BUN, our starting and model molecule have been the single Lander molecule shown below which is constituted of a conjugated central plateau and 4 lateral legs to fulfil (1). The initial concept was that the end naphthalene groups can be put in interaction with an atomic ordered electrode to control the electronic contact between the molecule and the nano-electrode at the atomic scale. The double Lander molecules with 8 legs shown also below is an extension of the concept toward very long molecular wires (the length of the central board is approaching 5 nm).



### IIa) The lateral legs functional groups

To keep the central molecular wire board away from the surface, the first lateral group used in BUN were 3,5-di(*tert*Butyl)phenyl spacers. The multi-step synthesis of these legs also preparing for the central molecular wire board as presented below:



The 3,5-ditertButyltoluene is first brominated and this derivative is then used in a carbonylative coupling reaction to get the symmetric ketone **a**. Double Knoevenagel on the brominated acenaphthenequinone yields the activated diene **b** which is transformed in **c** by Diels-Alder with acenaphthylene. **c** is then lithiated to give access to its boronic acid derivative. Suzuki couplings with, for instance, dibromonaphthalene or dibromoperylene using Buchwald's catalysts yield the precursors **1** and **2**.

In the case of the single and the double Lander, UHV-STM images were used to observe the actual conformation of those molecules equipped with the legs on a metal surface (see section III). The STM-ESQC calculation technique (see section III) was used as a conformation refinement tool to extract the molecular conformation. Contrary to what was expected, the central board is only 0.36 nm away from the surface and not 0.68 nm. Those important distortions of the overall geometries of polyaromatic molecules on metallic surfaces as shown in Fig.1 led us to investigate new types of spacers designed for a better control of the molecular wire-surface distances and of the interconnection geometry.

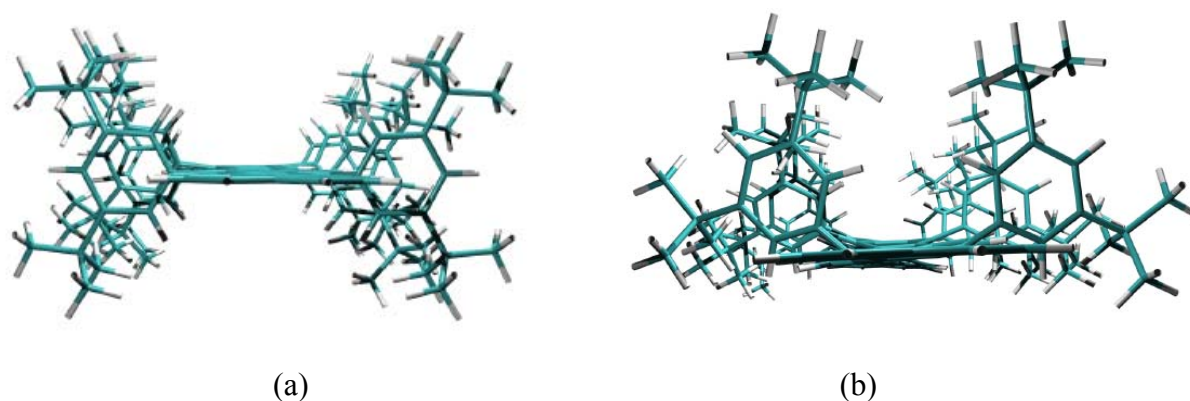
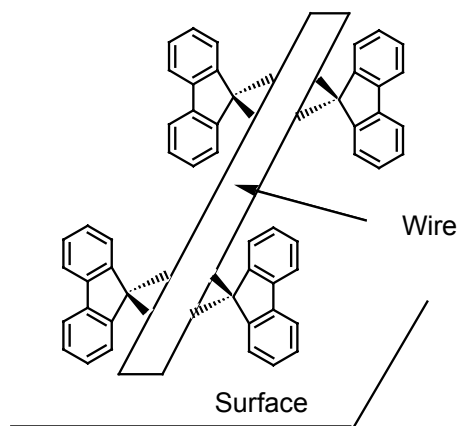


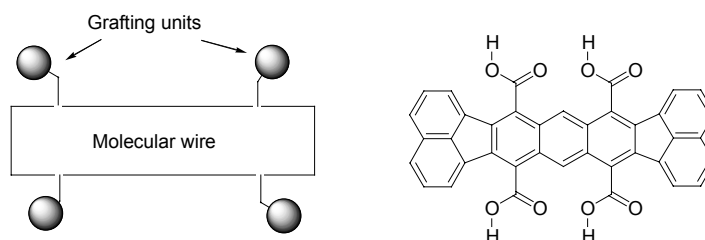
**Figure 1:** View of a double Lander along the wire main axis. (a) the optimised calculated conformation of a free single Lander molecule in vacuum. (b) the refined conformation of the same molecule when adsorbed on a Cu(100) surface obtained from the experimental STM scans.

For example, STM studies by the Kiel group have (*vide supra*) shown that the spiro-bifluorene core is the most rigid group known so far toward surface-induced distortions. Therefore, the Toulouse group has started to investigate the synthesis of new types of Lander bearing similar fluorene-based spacers.

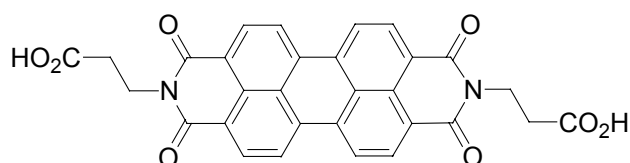


With this architecture, the molecule will be very rigid, without possible rotation along a single C-C axis. The wire-surface distance will be similar in vacuum and on a surface. This will simplify the design of new devices. It requires an exploration of new synthetic routes since the chemistry of this type of compound is essentially unknown.

For insulating surfaces investigated by AFM significantly different molecular legs are needed. Whereas STM experiments on metallic surfaces require molecules equipped with molecular spacers in order to decouple the molecular wire from the surface, one of the main problems in AFM experiments on single molecules is the large mobility of these molecules on the surface. One possible solution to this difficulty is to attach grafting units on each side of the studied molecular device. Consequently, the Toulouse group has prepared a molecular board bearing four carboxylic groups as shown on the scheme below:

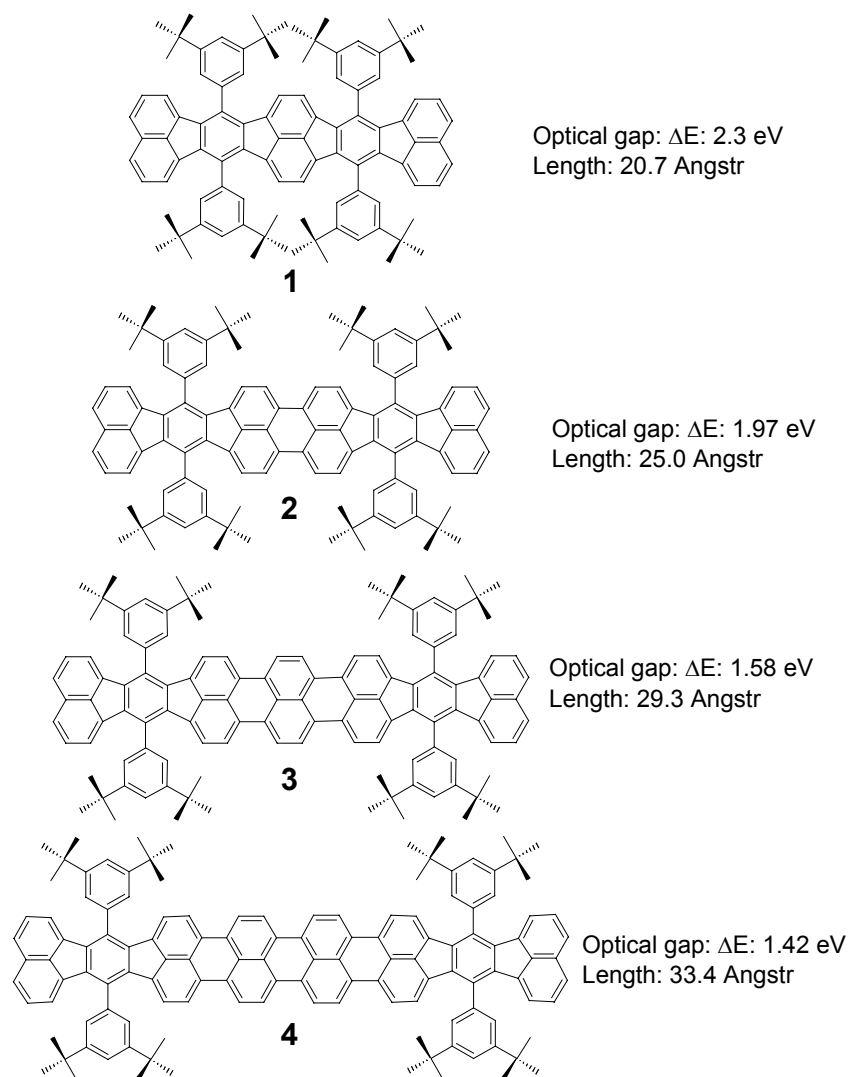


This compound was studied by the Basel group using NC-AFM on alumina. Preliminary AFM studies showed that, in this molecule, the anchoring groups were too close from the main board, which prevents efficient bonding to the oxide surfaces. Therefore, the preparation of molecules bearing short alkane chains ended with a carboxylic group has been carried out. An example of such compound is the substituted perylene-3,4,9,10-tetracarboxdiimide shown below. This molecule is currently studied in the Basel group.



## IIb) Molecular wires with a low homo-lumo gap

The tunnel current intensity through a molecular wire is decaying exponentially with the length of the wire (see section VII for more detail). One parameter controlling the decay factor is the homo-lumo gap of the wire. Therefore, For further studies of the long-distance electron transport process through a single molecular wire, it has been found necessary to prepare long small-gap landers. We have therefore synthesised a series of oligorylenes bearing four 3,5-di(*tert*Butyl)phenyl spacers such as shown on the figure below with a overall length ranging from 20.7 Å to 33.4 Å:



The HOMO-LUMO gap of these new Landers decreases rapidly with the overall length as shown in Fig. 2 by comparison with the previous family of Landers which were integrated on an anthracene core. According to the theory of tunnel transport (section VII), those Landers must present a much higher conductance than our past ones. This opens the synthesis of much longer Lander than before, Lander which may support measurable tunnel current intensity over distances up to 6 or 7 nm.

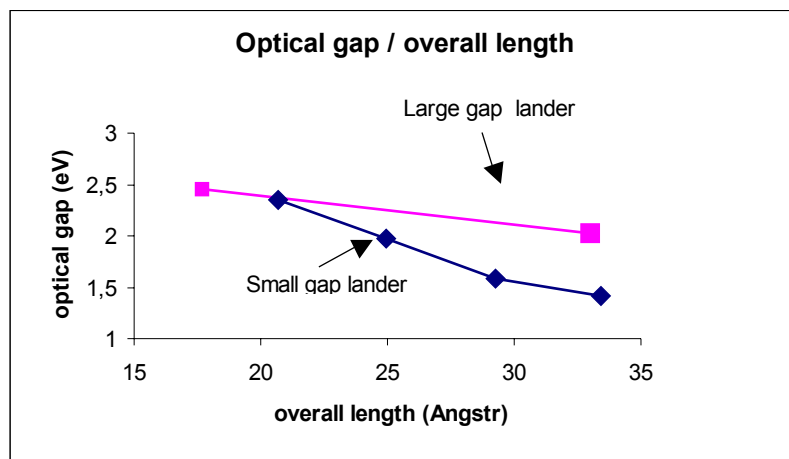
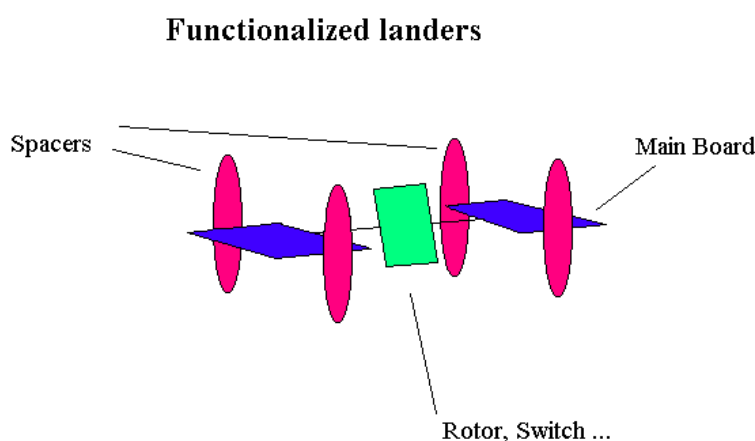


**Figure 2 :** Experimental variation of the Lander optical gap as a function of the overall length of its molecular wire board. Pink is for the old Lander series and blue is for the gap of the new Lander series.

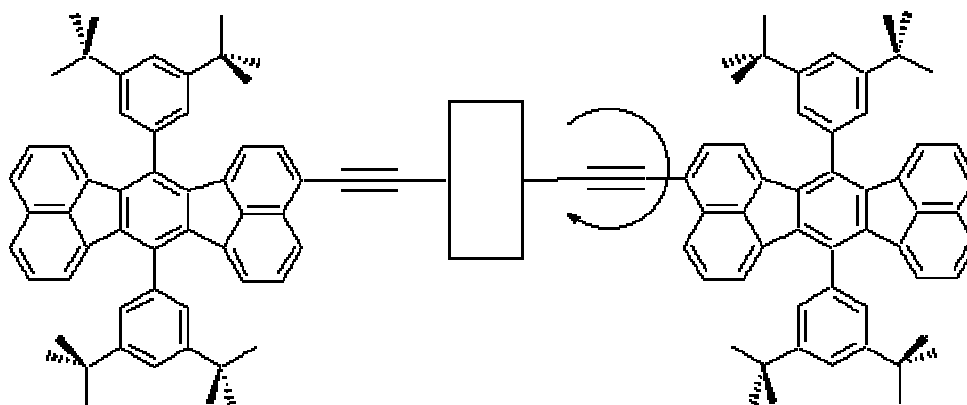
These molecules have required an important effort to improve the multiple steps syntheses in order to provide significant amounts (30 to 200 mgs) of pure products for various UHV-STM studies. For instance, Lander **2**, previously obtained only at low yields (<10 %) by metal catalyzed homo-coupling of the bromo-derivative (R= Br) and cyclodehydrogenation, can now be accessed in good yields (60 %) by direct oxidative coupling of the reduced analogue (R=H) in one step.

### IIc) Conformational switches: rotational Lander

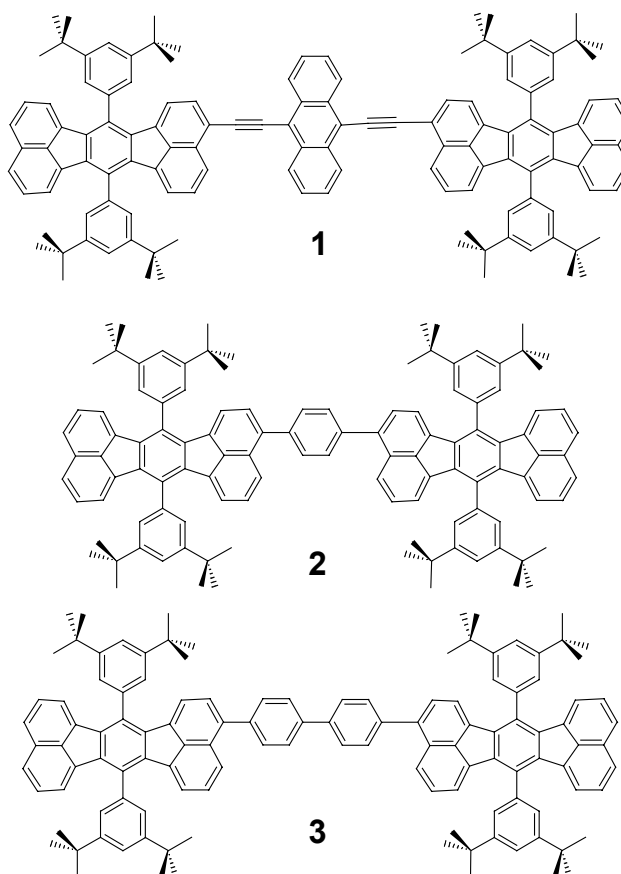
The BUN interest in investigating intramolecular movements induced by through bond inelastic electron tunnelling has led to the design of functionalised Landers bearing a central mobile part as shown on the scheme below:



The synthesised molecules comprise as usual the four 3,5-di(tertButyl)phenyl groups to support the molecule on the surface and a central rotor (an anthracene unit) hold by two ethyne groups:



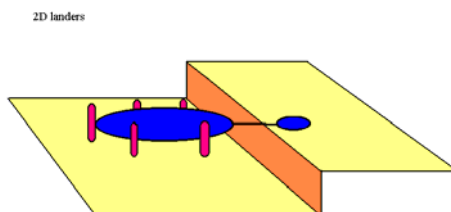
The first molecule **1** below was too fragile for deposition on bare copper surfaces despite the bulky spacers. They are fragile probably because of the presence of the alkyne functions and of the anthracene groups. It was then decided to prepare more robust rotating Landers comprising a phenyl and a biphenyl as a rotor (respectively rotating Lander **2** and **3**):



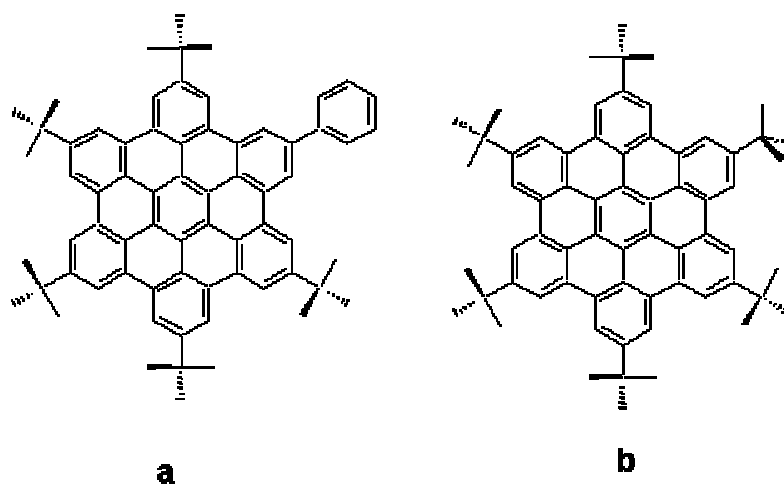
The first UHV-STM images of these special Lander are given in section VII. Further developments of this study will lead the choice of other central rotating units bearing for example bulky groups, donor-acceptor functions, switching groups...

## II d) Extended $\pi$ system in a molecule for future intramolecular circuits

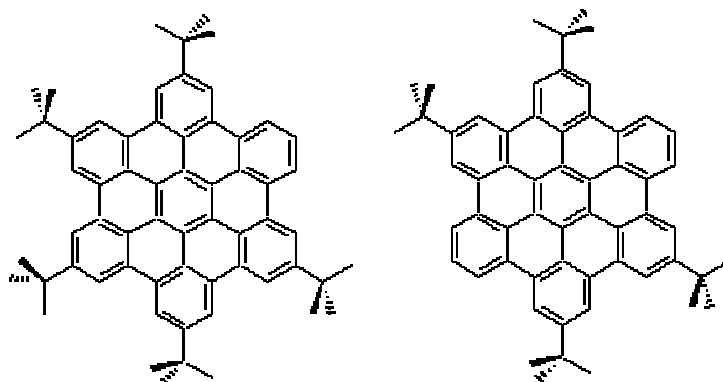
The original goal was to extend the  $\pi$  system of the Lander molecule laterally in preparation of the design of intramolecular circuit integrated inside a single molecular Lander. Therefore, the molecules must comprise a large polyaromatic plateau and a connector as shown below:



In Bun, we have prepared molecule **a** comprising a hexabenzocoronene core held up by five *tert*-Butyl groups and linked to a phenyl connector and molecule **b** as a reference compound:



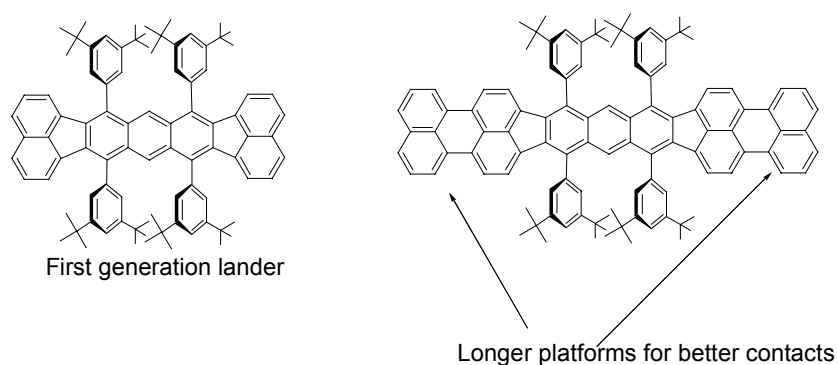
Since preliminary UHV-STM studies have shown surprising differences between the images of **a** and **b**, we have undertaken the syntheses of other similar molecules with the same hexabenzocoronene plateau and different repartitions of the legs such as:



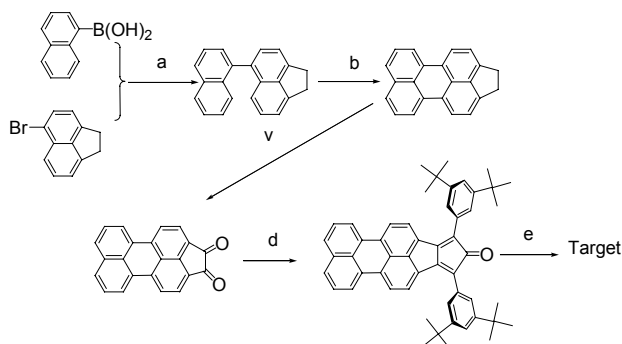
## IIe) nano-communication groups

The molecule of the Lander series, integrating a molecular wire, a rotor or even an extended  $\pi$  system are all terminated by 1 or 2 chemical groups whose task will be to interact electronically with metallic nano-electrodes in a well ordered atomic configuration. These groups are called nano-communication groups because they are in charge of transforming the electron delivered by the tunnel junction in transferable electrons adapted to the molecular orbital organisation and symmetry of the Lander. The contact conductance (see section VII) is a way to measure the efficiency of those terminal groups.

Theoretical calculations in BUN have shown that a higher contact conductance between the metallic electrode and the molecular wire is achieved by adsorption of larger connecting polyaromatic ends. According to these results and because of the success in measuring the contact bump of a single Lander (see section V), the synthesis of a molecular wire, with the same main board core and spacers as in the "single lander" but with two extended platforms, has been undertaken.



The preparation proceeds according to the scheme below. However, the lack of solubility of the target long lander and its precursors hindered the last step of the synthesis (e) when carried out in conditions similar to that used for several other landers, *ie* in situ room temperature oxidation of diaminodihydrobenzobistriazole. Work in progress on this last step involves the use of recently described 1,4-Bis(phenyliodonio)benzene-2,5-dicarboxylate as a benzadiyne precursor by pyrolysis at high temperature in polar solvents, conditions which should improve the solubility of reactants and intermediates.



Synthetic steps: a) Suzuki coupling b) cyclodehydrogenation by alkali reduction, then air oxidation c) oxidation d) double Knoevenagel e) reaction with benzadiyne.

### III) Molecular surface science in BUN

The goal here was to master the adsorption site and conformation of the well equipped molecule synthesized in section II together with a full development of the tools requires for imaging and performing spectroscopy at the atomic scale. At a single molecule basis, the microscopy used to determine the molecule adsorption geometry and conformation were the UHV-STM at room temperature, the variable temperature one down to 80 K and the low temperature one down to 10 K. In BUN, we also start to explore “imaging on insulator surfaces” using UHV-AFM. The reason is that technology will demand circuitry at the atomic scale fabricated on the surface of an insulator combining molecular devices and atomic scale interconnects. Extraction and understanding of the conformation of a given molecule were obtained by an intensive use of STM-ESQC calculation technique. We do not develop a specific sublimation technique yet for the Lander molecule series. But the double Lander was the largest possible molecule to be able to be simply deposited. We have clearly demonstrated in BUN that new deposition technique in the UHV must be developed for molecular electronics at the atomic scale.

#### IIIa) Extracting and optimising a molecular conformation from an STM image

To interpret the UHV-STM images and extract the conformation of a given molecule from its given STM image, we have developed our STM image calculation technique. Its kernel is based on the EHMO-ESQC technique using a scattering approach and quantum chemistry routine to compute the molecular orbitals and the corresponding energy levels. The computation time had been reduced to a week (in average for a single lander image in a constant current mode) instead of a few months by the use of a large IBM 22 processor SP 375 MHz machine dedicated only to image calculations. This machine was donated by IBM to the Toulouse group.

We have explored how a calculated image i.e. an x, y, z file can converge toward the experimental x, y, z STM image file. This is unique since usually the comparison is only in the x, y plane. This requires the optimisation of the atomic and orbital composition of the tip apex and of the conformation of the molecule. If using a few experimental scans over a step edge, one can easily built an effective tip apex for a given set of images, we do not yet have an automatic way for the conformation of the molecule to be optimised toward the experimental image using standard image processing distance criterion. As presented in Fig.3, this is still practised by hand, the know-how of the quantum chemist being still faster (a month or two) than many month of automatic conformation exploration.

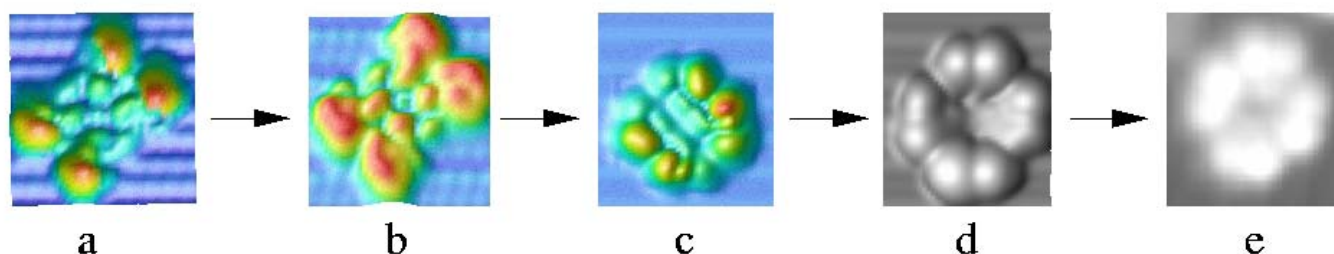


**Figure 3:** an example of successive conformation optimisation performed on a TerButyl Phenyl Porphyrin toward the corresponding experimental UHV-STM image (e). (a) 60°, (b) 45°, (c) 30° and the final optimisation (d) 10° for the legs angle on a Cu(111) surface.

The table given Fig.4 presents a few example of the image interpretation provided to the experimentalist by BUN. One important fact obtained from these calculation is that the leg conformation of the Lander molecule is not as frozen as we assumed at the time of its design. The conjugated board of the molecule appears to be lower on the surface that estimated with a pronounced deformation of the legs.

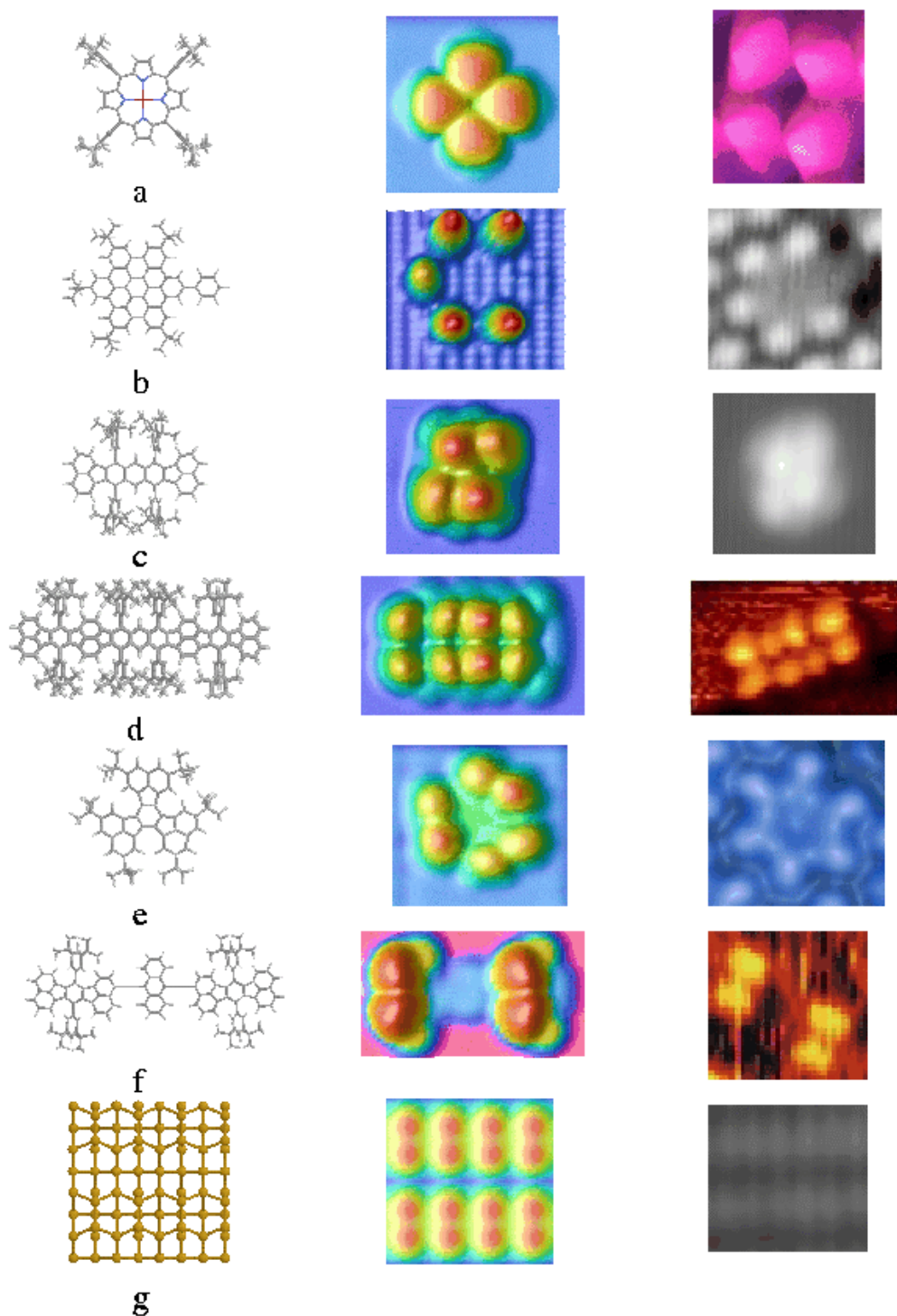
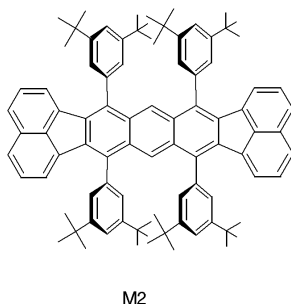


**Figure 4:** a table of the STM images calculated in BUN: (a) Porphyrin, (b) intramolecular corral (c) single lander, (d) double lander, (e) propeller (f) rotating lander (g) Si(100) 2x1 H.

### IIIb) Lander molecule on a flat metallic surface

The first molecule studied in BUN was the single Lander molecule whose chemical structure is recalled below. It was imaged on a lot of surfaces like Cu(100), Cu(110), Cu(111), Ag(111), Cu<sub>3</sub>Au(100), Cu(110)O and its adsorption geometry extracted in all those cases. The experimental images were obtained by 5 different groups in BUN.



As presented in Fig. 5a, well prepared surfaces with atomic steps decorated by the molecules can be routinely achieved. By varying the coverage, the molecules tend to grow short lines along specific crystallographic directions (Fig. 5b). This feature was very pronounced on Ag(111), probably due to the low diffusion barrier on that surface compared to Cu(001). This tendency to self-assemble very long (up to 150 nm were observed) molecular lines was exploited on the Cu(110) surface (see section IV). By comparison with low-energy electron diffraction (LEED) images the orientation of the sample in the STM images was determined. Near monolayer coverage, the molecules form extended domains on Cu(001) that are directed along the  $\langle 120 \rangle$  directions (Fig.2c). Already at very low coverage the molecules start to align along these directions, indicating a specific molecule-surface interaction which is responsible for the growth direction.

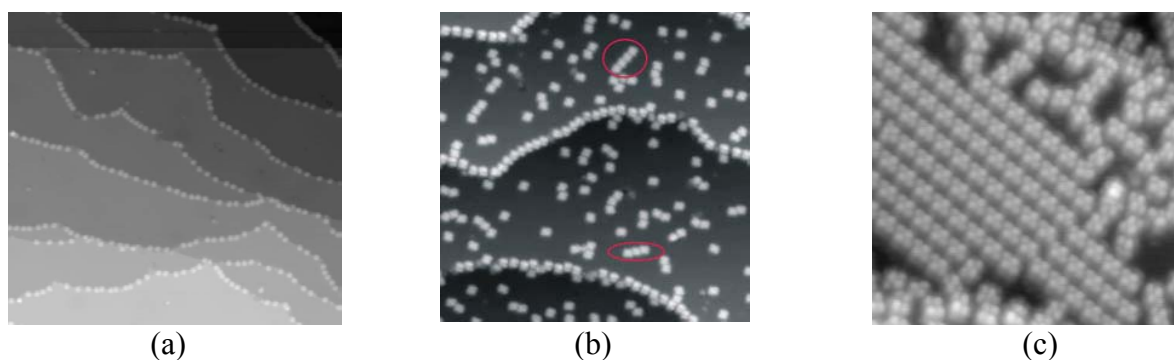


**Figure 5:** Low temperature UHV-STM images of the Lander molecules adsorbed on Cu(001) and Ag(111). (a) 130 nm STM image of landers adsorbed at Cu(001) steps, (b) Intermediate coverage also on Cu(001) (the red marks indicate early stages of domain growth.) and (c) near monolayer coverage forms extended domains along specific crystallographic directions (here:  $[120]$ ) on Cu(001).

Since the legs have many rotational degrees of freedom, it is a pre-requisite for molecular leg optimisation to image the different conformations that the Lander adopts on the substrate. The Lander conformation was extensively studied on flat terraces of Cu(100). Three molecular conformations were identified: two of which are presented in Fig.6a along with the schematic drawings in Fig.6b sketching the main differences between these conformations: A) The DTP-legs on both sides of the central wire rotate in the same direction. We call this conformation

the parallel-legs conformation. It leads to an overall square shape of the molecule in STM images. B) The DTP-legs on both sides rotate in different directions, therefore we name it the crossed-legs conformation. It leads to rhombic shaped molecules when imaged by STM. The third conformation is a mirror symmetric to the latter. The ratio of 1:50 between parallel-legs and crossed-legs molecules on the images indicates that the latter conformation is more stable, in agreement with molecular mechanics calculations which predict a 87 meV energy difference in favour of the crossed-legs conformation. Since in the gas phase the DTP-legs are perpendicular to the central molecular wire, but clearly not for adsorbed molecules, this underlines the existence of a molecule-substrate interaction, which forces the DTP-legs to change their orientation. To gain more insight, we have compared these Lander conformations with calculated ESQC images. The comparison clearly underlines the existence of a van der Waals attraction of the polyaromatic wire towards the surface that induces a substantial lowering of the wire from 0.7 nm to 0.37 nm above the surface and constrains at the same time the DTP-legs to be twisted.

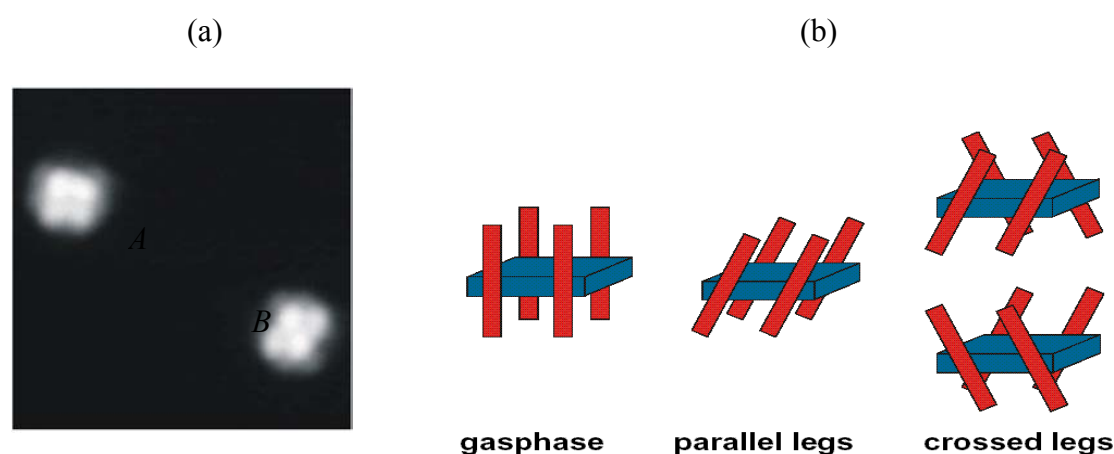


**Figure 6:** (a) The Landers on Cu(100) in two different conformations (image is  $14 \times 14 \text{ nm}^2$ ): (A) parallel-legs and (B) crossed-legs. (b) Sketch of the different conformations on a flat terrace of Cu(100). The wire is represented by a board flanked by four legs.

In the Aarhus group, the same Lander molecules were also deposited by Organic Molecular Beam Deposition on a Cu(110) surface, previously cleaned by standard sputter / anneal cycles. In Fig. 7a, a low temperature (LT,  $T = 100 \text{ K}$ ), high resolution STM image of a single Lander molecule deposited on the Cu(110) surface is presented, with its corresponding height profile (Fig. 7b) across the molecule. The STM images a single molecule as four lobes arranged in either a parallelogram-like or rectangular geometry like on the Cu(100) surface as discussed above for the Cu(100) surface..

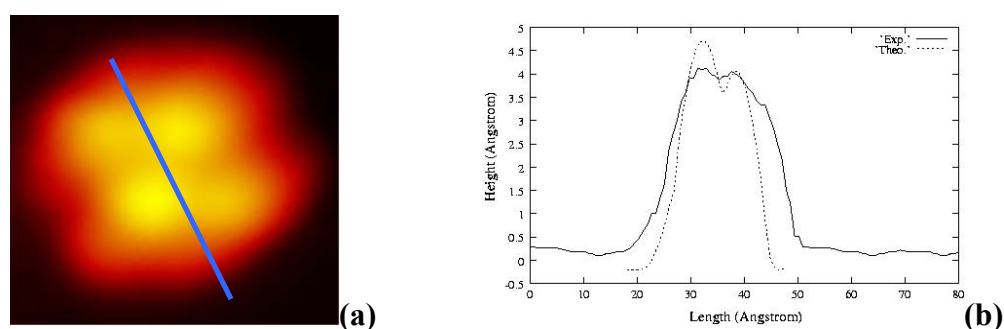


**Figure 7:** (a) High resolution STM image of a single Lander molecule in parallelogram-like conformation on Cu(110) at LT (100 K). Image dimensions are  $5 \times 5 \text{ nm}^2$ ; (b) line scan on the image reported in (a) and taken across the lobes, and corresponding calculated height profile.

A long Lander (LL) version of the single Lander where the polyaromatic board extends up to 2.5 nm (see Fig. 8) was also studied. The aim here was to check if an increased length of the wire favours a conformation where there is an electronic coupling to the step edge of the metallic substrate. The study of the conformations adopted by these new Landers on various metallic substrates was performed in the Toulouse home-made UHV-STM apparatus at room temperature.

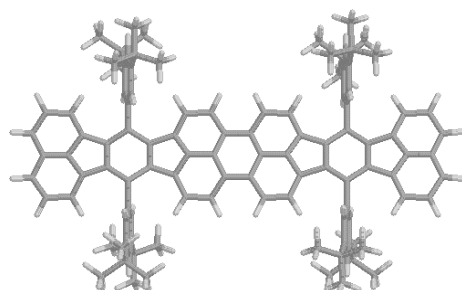


**Figure 8:** A top view model of the L-Lander molecule

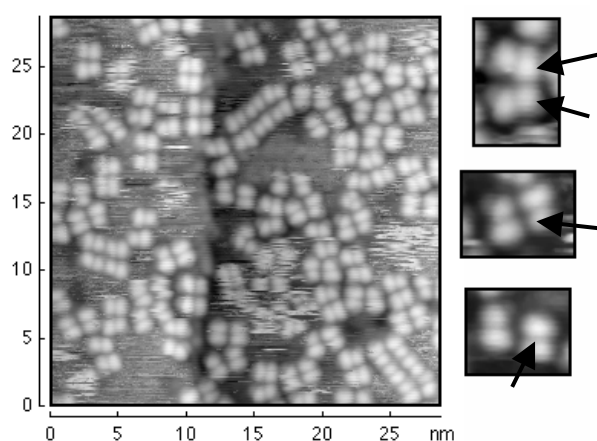


**Figure 9:** STM constant-current image ( $I_t = 10$  pA,  $V_{\text{bias}} = 2.5$  V) of LL adsorbed on Cu(100). The arrows of the zoomed molecules point to shoulders as discussed in the text.

The LL was designed in such a way that the distance  $L = 1.22$  nm between the front and the back legs is much larger than the  $L = 0.7$  nm of the simple Lander resulting in a very small steric crowding of the spacers. As presented in Fig. 9, an adsorbed LL appears in the STM experimental images as 4 elongated lobes in a nearly rectangular configuration with again no intramolecular contrast associated with the central board. As for many molecules of the Lander series, only the legs are imaged.

Some lobes are accompanied with a shoulder (indicated by arrows in Fig.9). This is an indication that the corresponding legs are sufficiently rotated relative to the designed perpendicular conformation, for their lower part to be imaged. The histogram of the distances between the legs in the lateral ( $l$ ) and longitudinal ( $L$ ) directions shows a much higher dispersion in the longitudinal direction ( $L = 1.48 \pm 0.17$  nm) than in the lateral direction ( $l = 0.74 \pm 0.07$  nm).

To further identify the detailed conformations adopted by a L-Lander on a Cu(100) surface, we have first calculated, using the ESQC technique, the constant current STM image of the L-Lander in the conformation Fig. 8 of the free molecule, under the assumption of complete

rigidity, i.e. without authorizing any mechanical relaxation. The experimental rectangular four lobes shape is easily recovered by calculation (Fig. 10a) but not with the good  $l$  value (Fig. 10d).

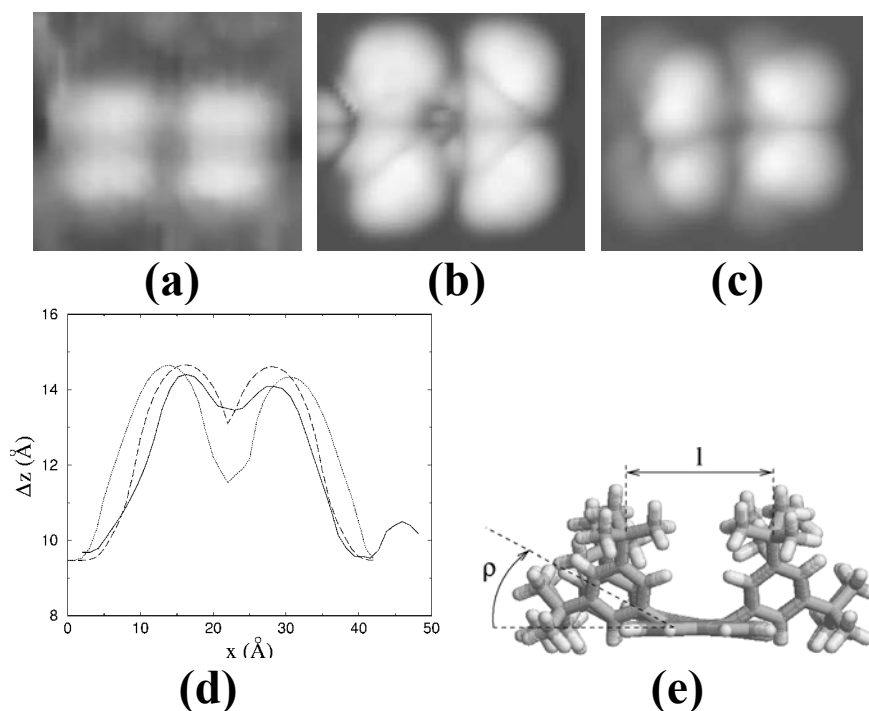
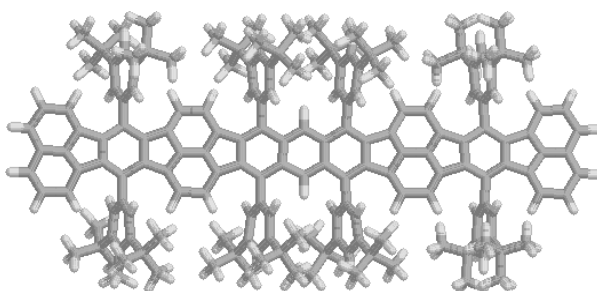


**Figure 10:** a) Experimental image b) and c) calculated image for the rigid (b) and relaxed (c) adsorbed molecule. d) Comparison of experimental and calculated profiles. e) structure of the adsorbed molecule.

After many ESQC-calculated conformation images, we concluded that it is not possible to reproduce by calculation the experimental image while keeping the assumption of rigidity of the  $\sigma$  bond attaching each leg to the board, whatever the angles of the legs were. The image Fig. 10c was calculated using a fully relaxed molecule. It is in good agreement with the experimental result, as attested by the comparison of the profiles of Fig. 10d. The legs are strongly distorted leading to a much shorter distance between the central board and the substrate than the one given by the naïve picture of a rigid aromatic board connected to the leg by rigid bonds.

The same experimental study was carried out in Toulouse on the longer member of the series: the double Lander molecule. The chemical structure of the Double Lander is recalled below:



The problem of the sublimation of such large molecule on Cu(100) was solved using a flash sublimation technique. Molecules diffuse at room temperature at the step edges where they can be UHV-STM imaged (Fig. 11). This is the largest well identified molecule ever image with an STM in UHV.

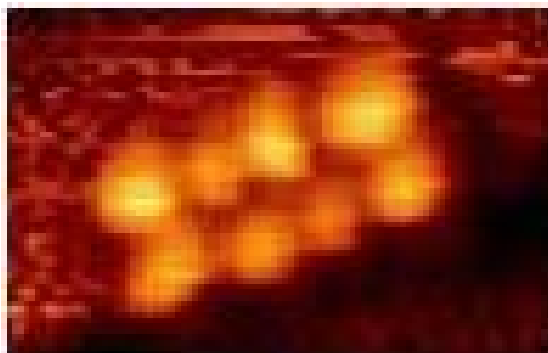


**Figure 11:** UHV-STM images of a double lander molecule with 8 legs on a Cu(100) surface ( $I = 1$  nA,  $V = 2$  V). (STM image size 1.5 nm x 2.0 nm)

### IIIc) Lander molecules at mono-atomic step edges.

After understanding the conformation of the Lander molecule family on a flat metallic terrace, it was necessary to understand the conformation of those Lander at step edge. The goal here was to follow up on the Toulouse-IBM initial 1999 experiment showing that the board of a simple Lander can be put in electronic contact with a double atomic step on Cu(100). The atomic step is used in place of the end of a nano-electrode whose facets are well defined for the electronic contact to be unambiguously defined. Going further than a first experimental demonstration of a concept is always very tedious compared to the original excitement. This tedious work was practiced carefully in BUN, learning step by step how a Lander molecule is able to adsorb at a mono atomic step on different metal surface. After a lot of experiments, the solution was to work on the Cu(111) surface. This is explained in section V. We described here all the other tentatives which were as important as the final conclusive experiment in the BUN knowledge on how a single molecular wire can be properly contacted at the atomic scale and with a picometer precision to a nanoscopic electrode.

For ideal electronic coupling, the four DTP-legs should adsorb on the lower terrace of the step with the polyaromatic wire perpendicular to it. At single steps of Cu(100) ( $\sim 0.18$  nm) we find a completely different adsorption geometry. From the comparison of the calculated STM images via the ESQC technique with the experimental data of the Lander adsorbed on step edges, we conclude that the molecule adsorbs with the wire parallel to the step, preventing a good electronic coupling. Two legs remain on the upper terrace and the two other legs adsorb on the lower terrace (see for example Fig.12b).

Only 2 conformations are present (parallel and crossed) in agreement with the molecular mechanics calculations, which places other adsorption geometries at higher energies. In view of these results it is clear that the molecular wire of the Lander cannot be contacted electronically when adsorbed at a single step edge of Cu(100) as the 0.37 nm distance from the wire to the surface is still too large for a good overlap between the electronic wave functions of the wire and the metal.

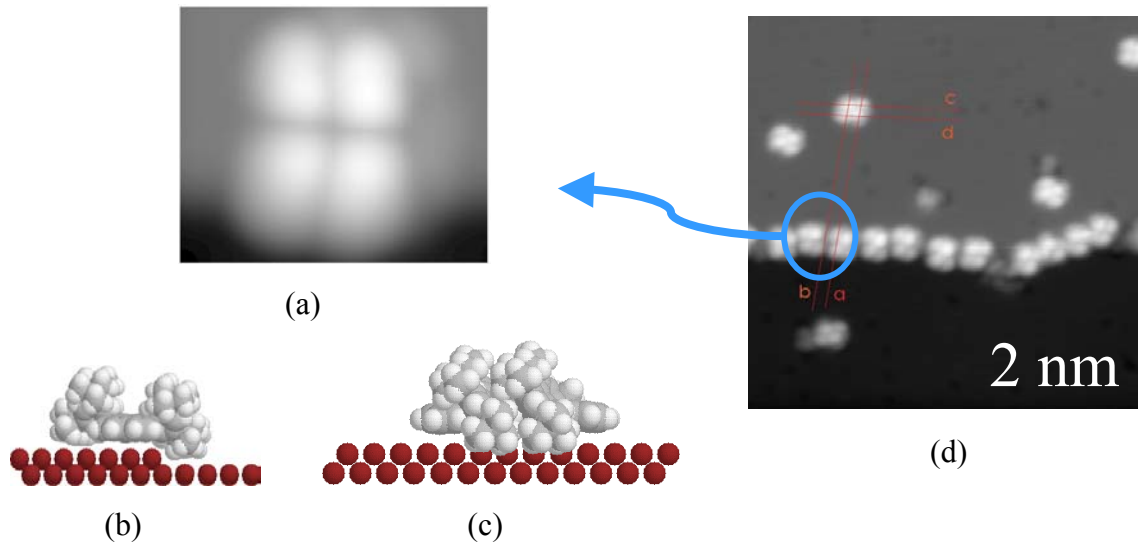


**Figure 12:** conformation extraction and experimental image of simple Lander molecule natively adsorbed at a mono-atomic step edge on Cu(100). (a) calculated image of one single Lander, (b) side view of the extracted conformation, (c) front view of the same conformation and (d) experimental image of 11 single Lander molecules adsorbed at the step edge. The image was taken at 10 K to avoid a molecule diffusion process.

Notice that in the early work on Landers adsorbed on Cu(100) it was asserted that electronic coupling is achieved on double steps of this substrate. Since the double atomic step of Cu(100) ( $\sim 0.36$  nm) ideally matches the height of the molecular wire on a flat terrace of Cu(100) (0.37 nm), one may conclude that this geometrical feature is an essential property for a good overlapping of the electronic wave functions of the wire and of the metallic step edge. However, the low density of double steps on the Cu(100) substrate has limited further observations of such a coupling. Hence, experimental evidence is too scarce at present to allow definitive conclusions.

As an attempt to overcome this problem, the alloy substrate  $\text{Cu}_3\text{Au}(100)$  was used. This alloy has an ordered structure made up of an alternating stacking of Cu planes and of CuAu planes with a lattice parameter of  $3.75 \text{ \AA}$  (Fig. 13 a). After an adequate preparation, the  $\text{Cu}_3\text{Au}(100)$  surface yields single steps of  $\sim 0.19$  nm (separation between the Cu plane and the CuAu plane) and double steps of  $\sim 0.37$  nm (CuAu plane to CuAu plane).

The double step of  $\sim 0.37$  nm matches perfectly the wire height on Cu(100) and should favour the electronic coupling of the Lander to the double step edge. After sublimation of the molecules and adsorption of submonolayer coverage, we routinely acquired high-resolution STM images of the Landers on  $\text{Cu}_3\text{Au}(100)$ . Fig. 13b summarizes our observations. The adsorption geometry of the Lander on steps of both heights closely resembles the one on single steps of Cu(100): two DTP-legs are on the top terrace and two on the bottom terrace for both single and double steps of  $\text{Cu}_3\text{Au}(100)$ . This resemblance, further underlined by the striking similarity between their cross-section profiles, points to a molecular wire parallel to the step and hence to an absence of a good electronic coupling. The easier diffusion of the Lander we observe on  $\text{Cu}_3\text{Au}(100)$  terraces does suggest a weaker interaction compared to Cu(100).

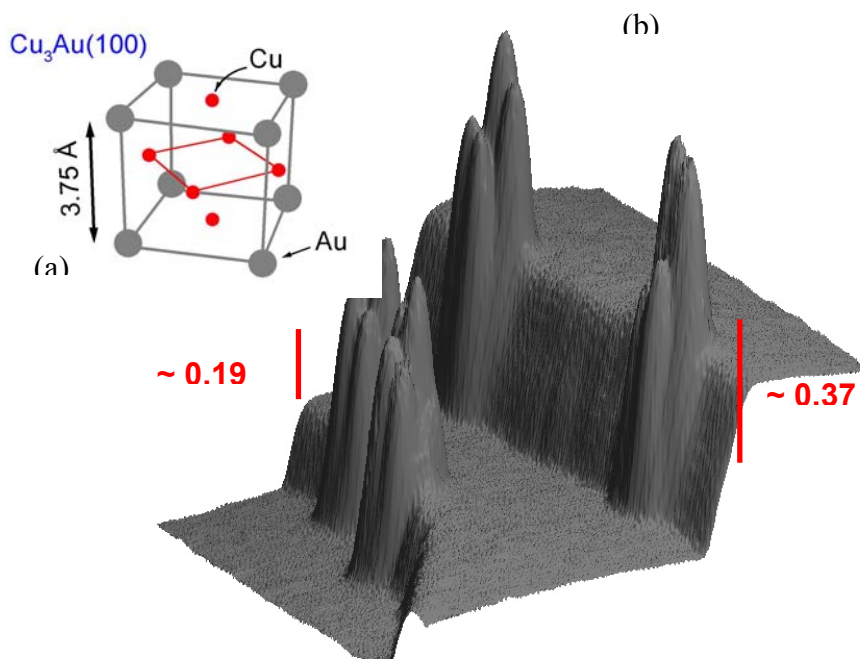


**Figure 13:** (a) the Cu<sub>3</sub>Au(100) ordered structure. (b) a pseudo 3-dimensional image of 4 Landers molecules, 2 on single mono-atomic step and 2 on a double atomic step on the Cu<sub>3</sub>Au(100) surface.

We have also tried to contact a double Lander molecule at a step edge using a specific fabricated stepped surface by evaporating more Co metal on a Cu metal surface. Inspired by the work of de la Figuera *et al.* on the cobalt deposition onto the Cu(111) surface, a simple method was elaborated to fabricate double atomic steps in a controlled way. In fact, during its initial growth at RT on Cu(111), cobalt creates triangular islands which are strictly bilayer. Since cobalt is pseudo-morphically arranged conserving the lattice parameters of the Cu crystal, the perimeter of every Co island offers a step with the required height. Therefore, after cleaning the Cu(111) surface, small amounts of Co were evaporated onto the surface to adapt it to the DL deposition. DL-molecules adsorbed on the Co/Cu(111) surface are displayed in Fig.14. Recognizable through their eight lobes, the DL-molecules may be found both on top of the Co islands and at the double steps.

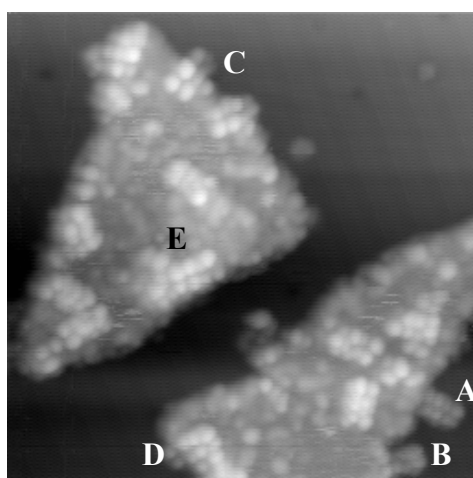


**Figure 14:** UHV-STM constant-current image ( $I_t = 30$  pA,  $V_{\text{bias}} = -2.9$  V,  $36$  nm  $\times$   $36$  nm) of DL adsorbed on Co/Cu(111).

When adsorbed at the double steps, isolated DL-molecules show a multiplicity of configurations as indicated in Fig. 14. They may lay both parallel and perpendicular to the step edge. If parallel, they are found both at the upper and at the lower side of the step. If perpendicular, they are found in five configurations which are practically equal probable in the error range: With all eight legs at the lower side (A), with six legs on the lower terrace (down) and two on the upper one (up) (B), with four down and four up (C), with two legs down and six up (D) and with all eight legs up (E). All these configurations are very stable at room temperature.

As for the simple Lander and the LL, we have extracted the geometrical conformation of a DL adsorbed on the flat terraces of Cu(100) by comparing experimental and calculated STM images. Indeed, the spacers tilt in the two planes perpendicular and parallel to the sigma bond while the central board remaining flat and parallel to the terrace. In Fig.15, the experimental profile (solid line) along the maxima of the lobes in the longitudinal direction is plotted for the case of a molecule with two spacers on the Co island and six on the Cu terrace. To obtain a good agreement with the calculated profile (crosses), not only the spacers but also the central board were allowed to relax. Therefore, the polyaromatic wire undergoes a deformation to adapt itself to the step edge.

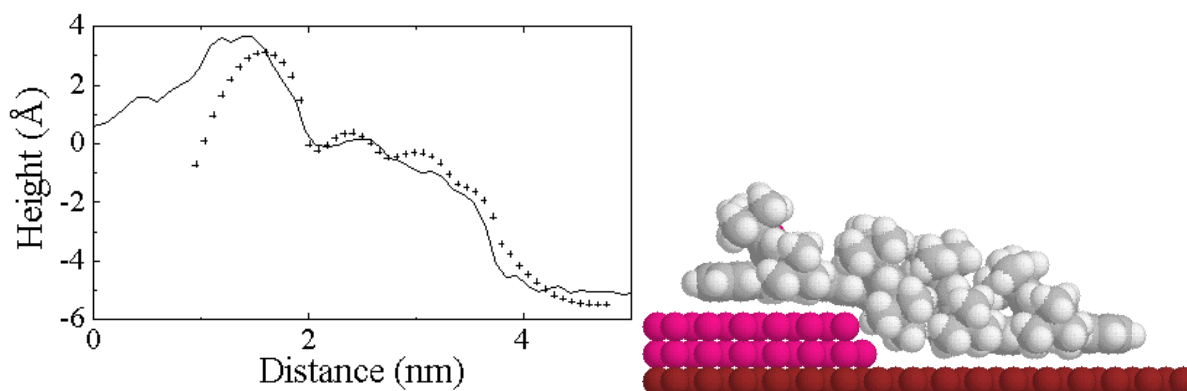


**Figure 15:** On the left experimental (solid) and calculated (crosses) profiles. On the right structure of the adsorbed molecule.

Calculations show that the driving energy for the distortion of the legs and of the wire is provided by the electronic interaction between the central conjugated board and the substrate. The energy associated with the deformation obtained by comparing the energy of the free molecule with the energy of the deformed molecule rigidly removed from the surface, is much lower than the van der Waals energy : the legs are too soft to keep the board away from the surface. But this Co/Cu(111) step strategy was again not the good one.

As described in section V, the success of the connection of a Lander relies on a very fine tuning of the height of the molecular board of the Lander as compared to the step apparent electronic height. What is important is not the van der Walls height but the apparent height created by the surface states. It took 2 years of work to the BUN consortium to determine that on Cu(100), the surface state at the mono-atomic step are too low and that the double atomic step is too high. This double mono-atomic step leads to a deformation of the molecule along the step facet which may be taken as a contact as experienced for the first time in 1999 in the original experiment. The surface state on a Cu(111) mono-atomic step provides just the good apparent height as demonstrated in section V. This search for a precise matching

between the molecule and the step height with a precision better than 0.05 nm is very important for the future of molecular electronic in demand of an ultra-precise and clean interconnection technology (see section V).

### IIIId) I-V STM spectroscopy on a Lander leg

A very important surface tool with STM is special resolved spectroscopy. Current-voltage I-V curves are recorded at different points on a molecule to determine the more electronically transparent region of a molecule. This helps in understanding STM images. This is also a formidable tool when a molecular Lander is connected at one end to a step edge and the tip apex of the STM positioned as a second ultra clean electrode at the other end of the molecular wire. In BUN we have pushed the technique in the prevision of the success on the interconnection experiment. This was performed on the  $\text{Cu}_3\text{Au}(100)$  surface by the Kiel group. The  $\text{Cu}_3\text{Au}(100)$  substrate is ideal for scanning tunnelling spectroscopy on the Landers

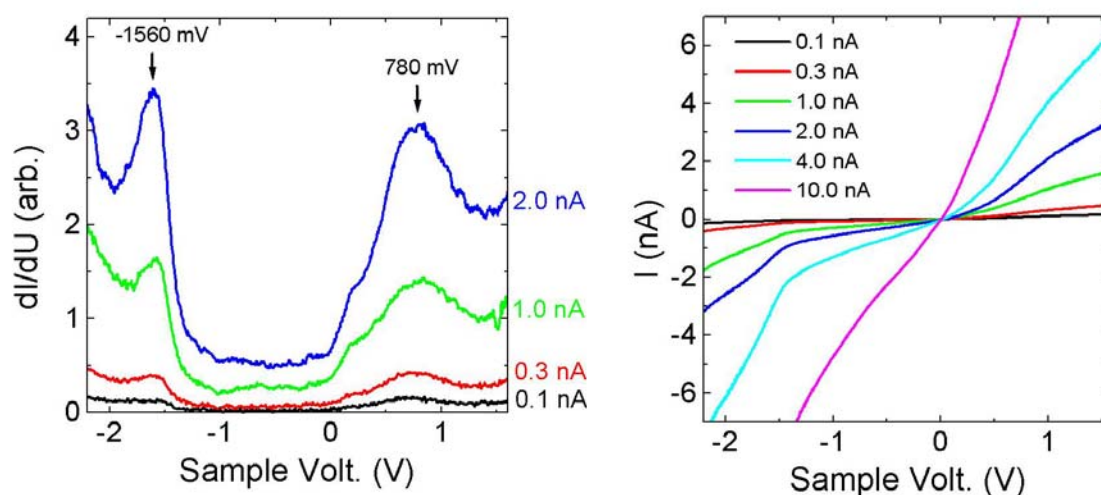


**Figure 16:** (a) The tunneling spectra (differential conductance,  $dI/dU$ ) and (b) the current versus voltage curves for increasing currents acquired at the center of a single Lander adsorbed on a double step of  $\text{Cu}_3\text{Au}(100)$ . The sample voltage was set to 1 V before cutting the feedback loop.

adsorbed on single and double steps. The tunnelling spectra acquired on a bare terrace of  $\text{Cu}_3\text{Au}(100)$  provided a solid reference to check the status of the STM tip, allowing to perform reliable spectroscopy and to discard tip artefacts affecting the Landers spectra. As shown in Fig.16, all the spectra exhibit a gaped region, estimated at  $\sim 2.3$  eV.

No difference was evidenced in the spectra of Landers adsorbed on single and double steps, consistent with the STM image analysis mentioned above. Turning to the value of the gap, we found it to be considerably lower than the  $\sim 2.9$  eV gap we observed in the spectra taken on Landers on single steps of  $\text{Ag}(111)$  (step height  $\sim 24$  nm). The variation in the gap underlines an influence of the Landers interaction with the substrate and, given the lower value in  $\text{Cu}_3\text{Au}(100)$ , the Lander-substrate interaction is weaker on this substrate compared to  $\text{Ag}(111)$ . The gap in  $\text{Cu}_3\text{Au}(100)$  is actually extremely close to the optical gap of the Lander in the gas phase (2.4-2.5 eV), suggesting a nearly zero molecular orbital mixing between the board part of the Lander and the substrate. This viewpoint may be consistent with the absence

of an electronic coupling of the Lander with the double step edges of  $\text{Cu}_3\text{Au}(100)$ , since if the Lander is less deformed by the substrate it must yield a wire height closer to the gas phase height of  $\sim 0.7$  nm and may therefore not be suited to electronically couple to  $\text{Cu}_3\text{Au}(100)$  double steps of  $\sim 0.37$  nm. No significant change was evidenced in the spectra for set point currents ranging from 0.1 nA to 10 nA. Note that by doing so, we decreased considerably the STM tip-Lander distance and hence the Lander's spectroscopic features on the  $\text{Cu}_3\text{Au}(100)$  substrate are robust to a possible deformation of the molecule.

Finally, we performed spatially resolved spectroscopy over various Landers. In Fig.17 we present the typical spectra recorded over five different parts of a Lander on a single step of  $\text{Cu}_3\text{Au}(100)$ : the center of the Lander and the four DTP-legs which appear as four bright lobes in the STM images. The spectra show little spatial dependency over the Lander. Since the 2.3 eV gap is inconsistent with the high-energy gap expected for DTP-legs, all the spectra are dominated by the molecular wire wavefunction. This means that there is a substantial leaking of the wires wavefunction over the four DTP-legs. However, when comparing spatially resolved spectra of various Landers we note that there is a random variation in the height of the left peak flanking the gap, suggesting a dependence of this peak's intensity on the Lander orientation with respect to the atomic step.

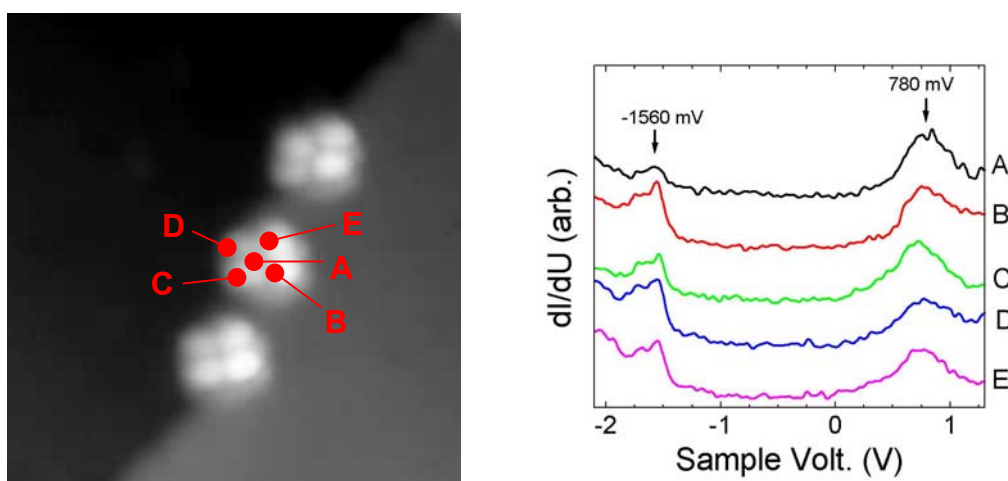


**Figure 17:** Spatially resolved spectroscopy of a Lander on a single step of  $\text{Cu}_3\text{Au}(100)$  (image is  $12 \times 12 \text{ nm}^2$ ). The spectra shown are shifted for clarity and were acquired at 0.1 nA with a sample voltage set to 1 V before cutting the feedback loop.

### IIIe) First images of organic Molecules on the surface of a bulk insulator

All the experiments presented up to now in BUN have been performed with single molecules adsorbed on a metal surface. Clearly, the next step toward the creation of a new technology for molecular electronics is to generalise this know-how to insulating surfaces. The main reason is that the fabrication of the metallic circuit for nano-interconnects requires an insulating support. This support must be atomically clean. The adsorption of molecular devices and in a near future mono-molecular machines, requires an imaging ability at the atomic scale that is equivalent to what is currently achieved on metallic surfaces. For this purpose, we have pushed in BUN the development of non-contact UHV AFM microscopy. This was assured by the Basel group in parallel with the Toulouse group.

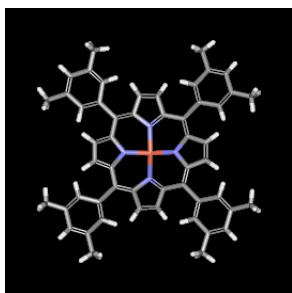


**Figure 18a :** Cu-tetra (3,5 di-t-butylphenyl) porphyrin (Cu-TBPP). The porphyrin board holds a Cu atom (red) surrounded by four N atoms (blue). Four di-t-butylphenyl surrounds the board.

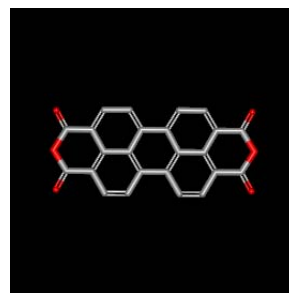


**Figure 18b:** 3,4,9,10-perylenetetracarboxylic-dianhydride (PTCDA) molecule. The molecule essentially consists of a  $\pi$  conjugated system holding three O atoms at both extremities (red).

The Basel group has studied two kinds of organic molecules, namely a Cu-tetra (3,5 di-*t*-butylphenyl) porphyrin (Cu-TBPP) and a 3,4,9,10-perylenetetracarboxylic-dianhydride (PTCDA) molecule (Fig. 18a and b, respectively), on insulating surfaces by means of UHV NC-AFM. The chosen insulating surfaces are KBr(001), thin films of NaCl grown on Cu(100) and Al<sub>2</sub>O<sub>3</sub>(0001). The experiments are carried out at room temperature with an home built combined STM-AFM operating in non-contact (NC-AFM mode) in a UHV chamber whose base pressure is less than 10<sup>-10</sup> mbar.

The porphyrins molecules were evaporated with the same parameters than on normal sublimation on Cu(100) except that the KBr was kept at room temperature during the procedure. The images obtained are shown in Figs.19.

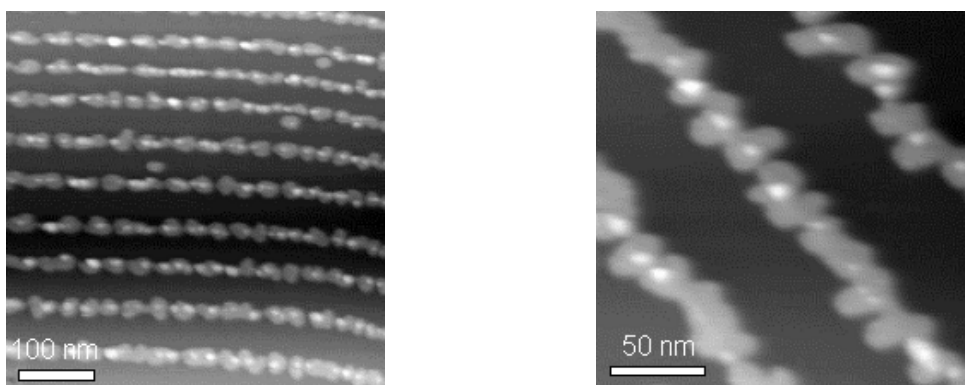
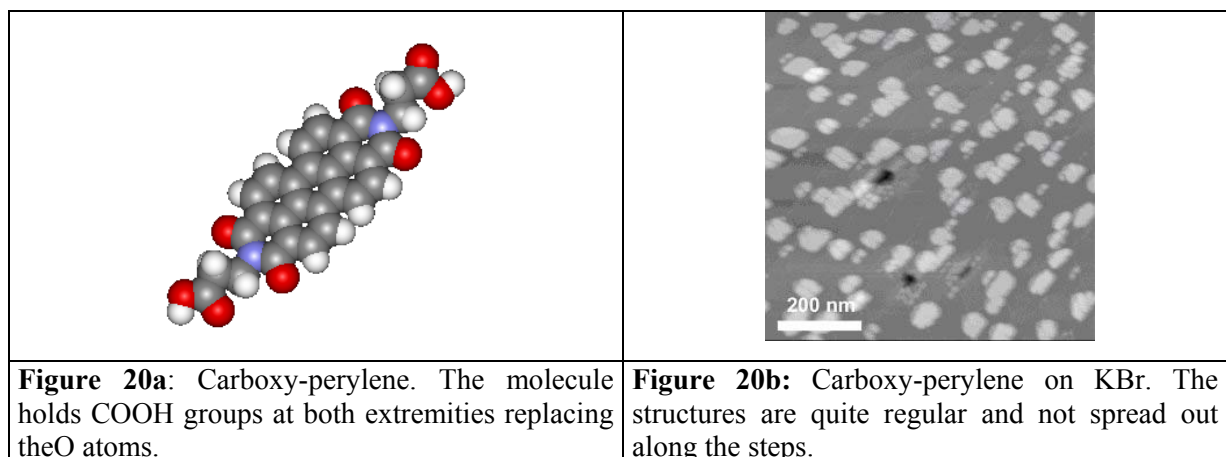


**Figure 19:** The first NC-AFM image of the Cu-TBPP molecule on the KBr surface at 2 different scales.

The molecules aggregate along the steps of the KBr and the molecular islands start to grow. At large scale (Fig.19a), this creates quite well-defined molecular lines along the mono-atomic step edges. At smaller scale (Fig.19b) the islands don't seem to be so ordered and it was impossible to resolve single molecules one at a time. The height of these islands is about 1 nm which corresponds to a single monolayer.

The Basel group had also imaged conjugated molecules equipped with carboxylic groups specially prepared by the Toulouse group. Preliminary results have been achieved with a perylene-based molecule holding carboxylic groups at both extremities replacing the O atoms (Fig.20a). The molecules were evaporated on KBr at room temperature. The substrate had

initially been heated at 380°C during half an hour to create the regular monatomic steps. The structures observed are arranged along the steps but each of them stays isolated (Fig. 20b). They do not coalesce in contrary to the Cu-TBPP on KBr. The so called “molecular lines” are not created. Here, the clusters have rather regular shapes and are quite high, typically 9 nm. The molecules favour the 3D growth instead of keeping on diffusing on the surface. Further experiments are required, but the couple carboxy-perylen/KBr sounds promising.



Aside from the alkali halides crystal like NaCl or KBr, adsorption of molecules on an oxide surface was studied as well. The oxygen atoms might indeed make it more reactive to the molecules. The  $\text{Al}_2\text{O}_3$  surface is often modelled as an ideal hexagonal unit cell whose parameters are  $a=4.758 \text{ \AA}$  (plane  $0001$ ) and  $c=12.992 \text{ \AA}$  (plane  $01\bar{1}0$ ).

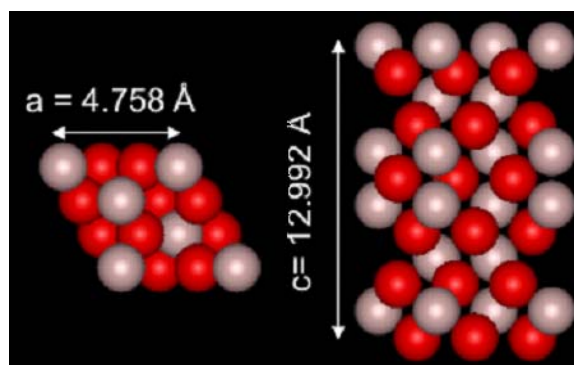


**Figure 21:** Idealized hexagonal unit cell of  $\text{Al}_2\text{O}_3$

In the  $(01\bar{1}0)$  plane, the unit cell consists of 6 bilayers of Al and O atoms. This layered structure leads to sub-unit cell step height (Fig. 21). The sample is heated in air at 1400°C during 36 hours and then placed in the UHV chamber. Further thermal cycles ( $\sim 1200^\circ\text{C}$ ) are then performed, each of them being 20 minutes long. The sample is clean and some steps are observable.

The apparent step height measured on this surface is smaller than the  $c$  parameter of the unit cell, typically 0.75nm, e.g. here  $c/2$ . Then, if the top most step consists of an Al enriched layer (top most layer in Fig. 21), then the bottom one also. However, our preparation protocol leads to quite rough terraces (Fig. 22), making unachievable high resolution. Further investigations regarding the optimisation of the preparation recipe are clearly needed here.

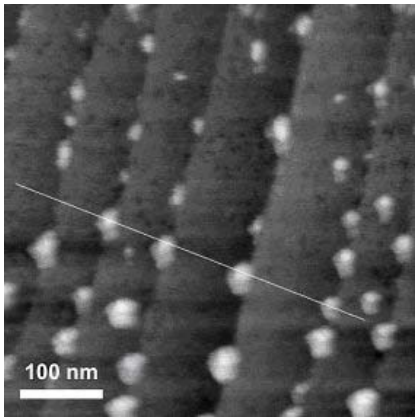


**Figure 22a:** Cu-TBPP on  $\text{Al}_2\text{O}_3$ . The molecules decorate the steps and form clusters almost similar to those observed on KBr

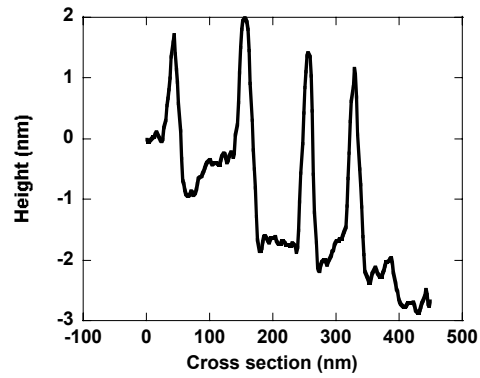


**Figure 22b:** Related cross section. The clusters' height is typically larger than 1 nm, which means that they consist of multiplayer, like on KBr.

The Cu-TBPP molecules were evaporated about half a monolayer on  $\text{Al}_2\text{O}_3$  at room temperature. Fig.22 displays the results observed. It turns out that the molecules decorate the steps and form clusters similarly to what had been observed on KBr. The clusters height is always larger than the apparent height of a single molecule implying that they again probably consist of multilayers of molecules.

Another striking evidence of the large diffusion occurring on the surface was obtained. Fig. 23a depicts an image acquired on a spot scanned from top to bottom. Some molecules clusters lying along the  $\text{Al}_2\text{O}_3$  steps are clearly visible. But while scanning the same spot from bottom to top (Fig. 23b), almost all the clusters have been removed, except two (white arrows).

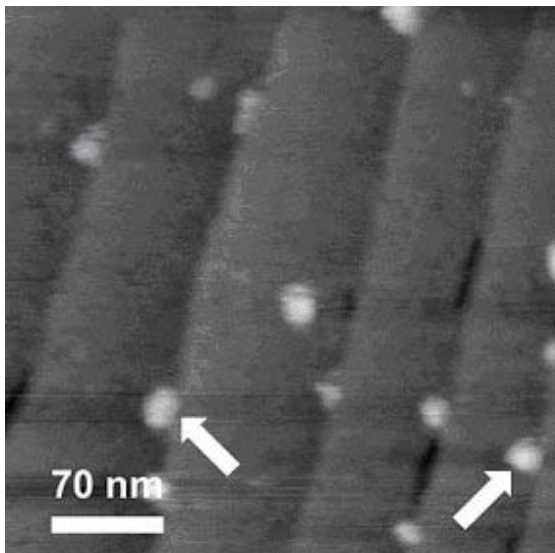


**Figure 23a :** The frame is acquired from top to bottom. Some clusters are visible.

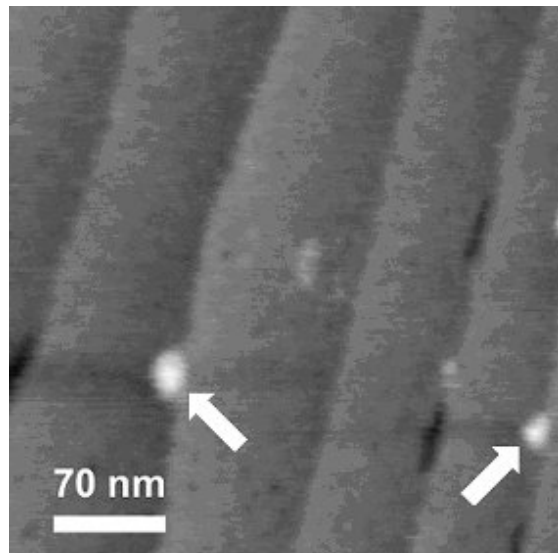


**Figure 23b:** While scanning the same frame from bottom to top, almost all the clusters have been removed.

The tip wipes the molecules around, but the “wiping” process is enhanced by the low interaction of the molecules with the surface. This had confirmed the importance of equipping the BUN molecules with lateral groups adapted for the surface used to support a given experiment at the atomic scale.

### III f) Force spectroscopy on the leg of a molecule

Like the I-V STM spectroscopy performed on a single molecule to understand transport mechanism through and along a single molecule, BUN had developed a force spectroscopy technique to be able to measure for example the switching energy of a single molecule molecular switch. For example, to measure the energy required to change the conformation of a part of a single molecule, the Basel group uses its new UHV non contact AFM (NC-AFM) with a metallic tip apex to have access at the same time to the energy required to change the conformation of the molecule and to the tunnelling current intensity through this molecule.

The aim of a NC-AFM is to give access to the frequency shift (hereafter noted  $\Delta f$ ) with respect to the free frequency of the oscillating tip as a function of the distance when the tip approaches the surface and therefore the molecule. These “ $\Delta f$  versus distance” curves are performed at a given (X,Y) location and provide the interaction force of the object located here.

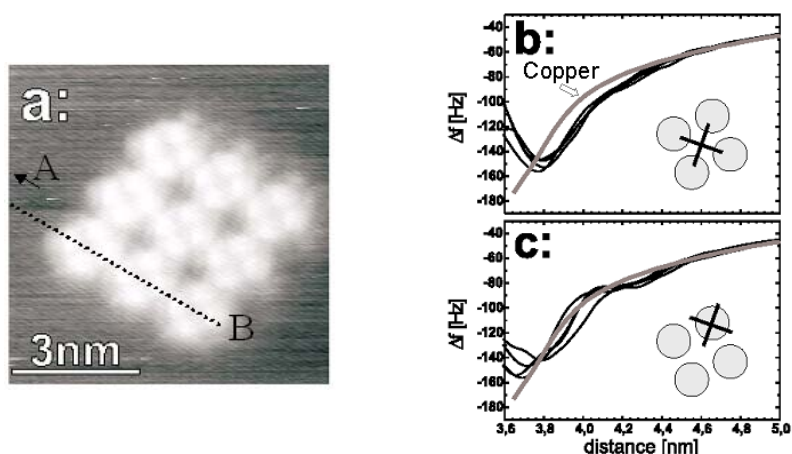


**Figure 24 :** (a) AFM image of an array of terbutylphenylporphyrins. The  $\Delta f$  versus distance curves are performed along the (AB) axis. (b) and (c)  $\Delta f$  versus distance curves obtained along the (AB) axis.

Let us consider the molecule island shown in Fig.24a. Along the (AB) axis, 20 curves were recorded. Three main features are observed in Fig. 24b and c. The first one corresponds unambiguously to the copper substrate (the grey curves in Fig. 24b and 24c). The others on Fig. 24b are the contribution of the porphyrin’s core. The last one on Fig. 24c exhibits a different shape and is the contribution of one porphyrin’s TBP leg substituent.

A further detailed analysis was performed by subtracting the contribution of the copper which acts here as a “long-range background”. The “short-range” contribution to  $\Delta f$ , hereafter noted  $\Delta f_{\text{chem}}$ , whose origin is due to forces taking place in the close vicinity of the molecule, typically a few angstroms, is shown in Fig.25.

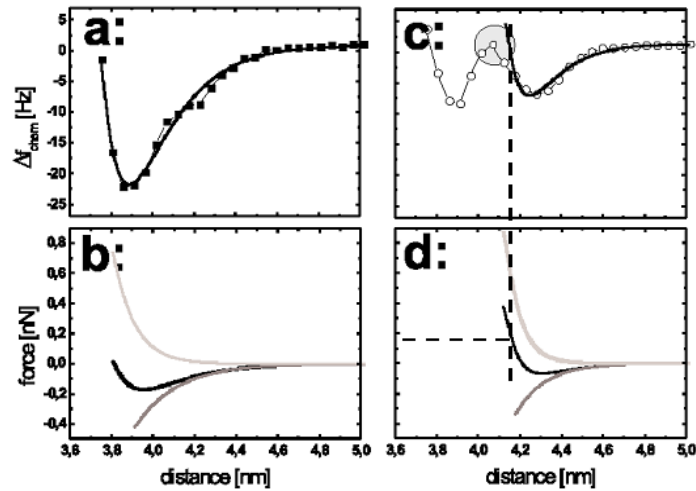


**Figure 25** : Short range contribution to the  $\Delta f$  measured on the core (a) or on the leg (c) of the molecule and the associated force variation (b and c, respectively).

Fig.25a is the  $\Delta f_{\text{chem}}$  deduced from Fig.24b and corresponds to the short-range contribution of the porphyrin's core. Its variation is unambiguously distinguishable from the one shown in Fig.25c that corresponds to the short-range contribution above the leg. The Figs.25b and d are the force spectra deduced from a model-dependent approach on the porphyrin's core and leg, respectively. Assuming that the short-range forces can be derived from a Morse potential, the  $\Delta f_{\text{chem}}$  has a simple expression involving the potential depth,  $U_0$  and the decay length  $\lambda$  of the interaction. Then these two parameters can be fitted from the  $\Delta f_{\text{chem}}$  (black continuous line in Figs.25a and c) measurements and the force spectrum deduced. One find  $U_0 = 0.07$  aJ and  $\lambda = 0.2$  nm for the porphyrin's core and  $U_0 = 0.02$  aJ and  $\lambda = 0.14$  nm for the porphyrin's leg.

On the curve Fig.25c, the second minimum observed indicates that the tip investigates a second attractive and repulsive interaction on the leg. As a consequence of the rotation of the leg around its  $\sigma$  bond, the force spectrum changes. The distance of 4 Å between the two minima is in good agreement with the height of the leg over the porphyrin ring. The force at which the leg is assumed to bend down is of about 0.1 nN which is good agreement with the previous value (Fig. 26).

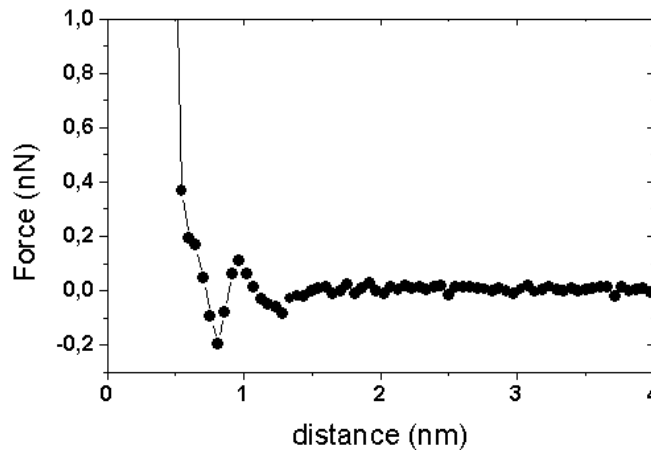


**Figure 26** : Force spectrum deduced from  $\Delta f_{\text{chem}}$  measure of fig.13c from the Giessibl's approach.

The corresponding molecular mechanics calculation was performed by the Toulouse group. One can get the force acting between the tip and the porphyrin's leg depending on the tip apex to surface distance (Fig.27). Here the copper contribution was not subtracted, but one can see in the inset that similar variations of the force are obtained so that the assumption of the bending of the leg is reasonable.

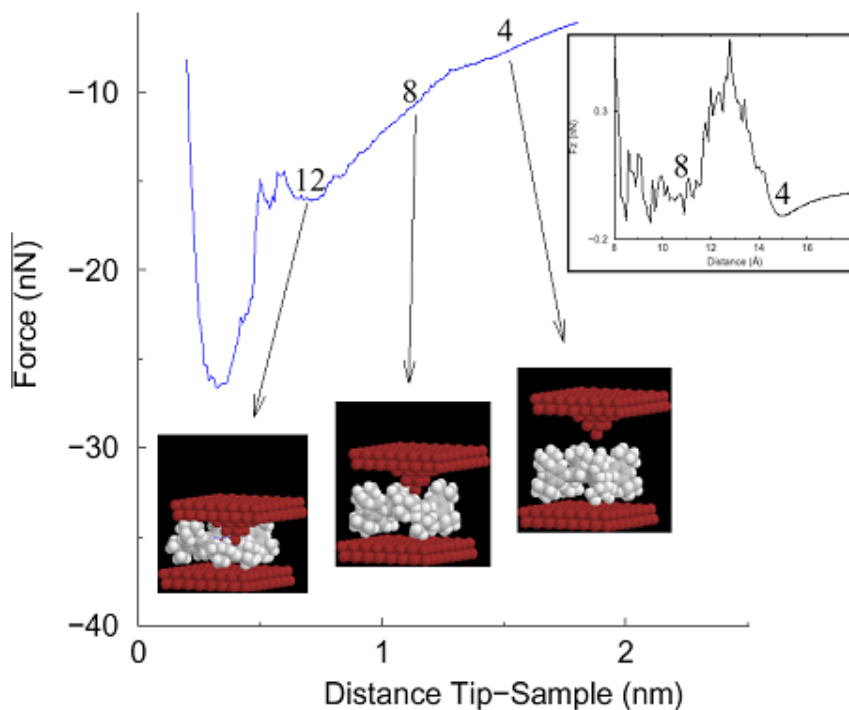


**Figure 27** : Molecular mechanics calculations of the force acting between the tip and the porphyrin's leg.

From those 2 force curves, one can deduce that the energy to switch a single leg from a perpendicular to a parallel conformation relative to the surface is 18 kcal/mol. This is comparable to the 20 kcal/mol measured in solution using NMR techniques on the same family of molecules. With such a conformation change, the tunnelling current intensity will change by more than one order of magnitude for a tip apex positioned on the switched leg at the same distance in both the on and the off states.

### IIIg) Conclusion

We had shown here how the BUN consortium had developed a definite set of instruments devoted to imaging and spectroscopy at the atomic scale. The transition from a metal to an insulator surface occurs during the BUN project as an effort to prepare the future of an atomic scale technology. In instrumentation, there is still more to gain on the capability of UHV-STM and UHV-AFM. This is for example the case of STM imaging on an insulator surface which develops during the BUN project as described in the next section.

## IV) Transforming the surface for molecular electronics

In BUN, a surface prepared and imaged at the atomic scale is the support of our experiments with single molecules. It is also a support for the future technology of interconnecting a single molecule to nanoscale metallic wire with a picometer precision. Therefore, BUN was very attentive in taking benefit of atomic scale transformation of a surface which can help in imaging the molecule, in ordering them spontaneously or preparing an interconnection to an atomic wire. It turns out that the molecules themselves are very good in handling surface atoms. The design of dedicated molecule for this task is very promising and very closed to the emerging field of mechanical molecular machine. In complement, BUN kept a more traditional chemical physics approach by improving the adsorption of macromolecular single walled carbon nanotubes on a well prepared and chemically modified SiO<sub>2</sub> surface where nano-electrodes have been nano-lithographed.

### IVa) Fabrication of atomic holes and atomic wires using single molecules.

All the atomic scale surface processes induced by single molecules are more easily observed at low temperature. For BUN, the Aarhus group had built a fast-scanning variable-temperature, liquid He-cooled scanning tunnelling microscope (STM) capable of operating at sample temperatures from 25 K up to 400 K in ultrahigh vacuum (UHV). The first prototype molecule was the hexa-*tert*-butyl decacyclene (HtBDC, C<sub>60</sub>H<sub>66</sub>), see Fig.28. This molecule possesses the basic chemical groups required for future molecular electronic: a conducting backbone (aromatic  $\pi$  system) and spacer lateral groups (*t*-butyl groups) separating the conducting parts of the molecule from the substrate.

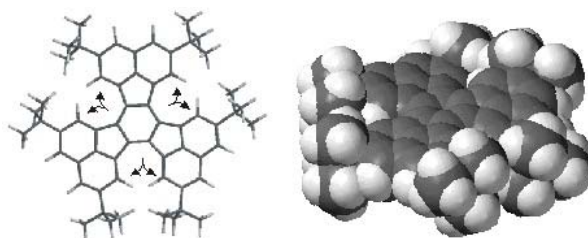


**Figure 28:** models of the HtBDC showing the propeller-shaped conformation of the molecule. HtBDC consists of an aromatic ring system (decacyclene) built from a centred benzene ring interconnected by three five-member rings to three naphthalene subunits (each with two butyl groups attached to it).

The deposition of HtBDC onto the Cu(110) surface was done by organic molecular beam deposition (OMBD) out of a heated glass crucible. When a sample is kept at room temperature during deposition, the STM images reveal double rows of HtBDC molecules aligned along the equivalent  $[1\bar{1}2]$  and  $[1\bar{1}2]$  directions (see Fig. 29a). Each molecule is imaged as six lobes, corresponding to tunnelling through the six spacer legs. STM movies at room temperature demonstrate that the double rows are immobile but fluctuate in size, growing or shrinking at the ends. Utilising the variable-temperature ability of the Aarhus STM, it was confirmed that molecules are fast-diffusing in between the double rows when the sample is cooled down after the deposition of HtBDC at room temperature. At 25 K the double rows are fixed in size and single molecules are randomly immobilised in between them. This is illustrated in Fig.29b.

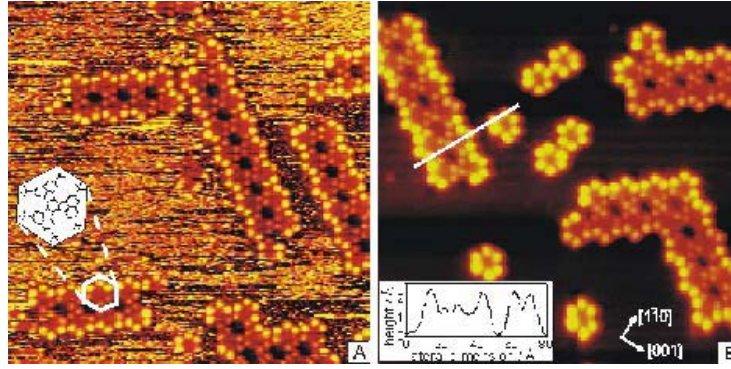


**Figure 29:** Constant current STM images of HtBDC on Cu(110) at low coverage. (a) At room temperature ( $V=1051$  mV,  $I=0.43$  nA,  $200 \times 200 \text{ \AA}^2$ ). The orientation of the six lobes in the imaged molecules is illustrated in the inserted model. (b) At  $T= 26$  K ( $V=1250$  mV,  $I=0.42$  nA,  $200 \times 200 \text{ \AA}^2$ ). The insert shows the height plot along the white line in  $\text{\AA}$  units, the arrows indicate the crystal directions.

Compared to single molecules, which are imaged as six lobes that lie parallel to the surface, the molecules located in the double rows seem to be tilted inwards, the three outer lobes being brighter as compared to the three inner ones. By manipulation of the double rows with the STM tip at low temperatures in the scanning mode at tunnelling resistances as low as  $1 \text{ M}\Omega$  (imaging usually above  $1 \text{ G}\Omega$ ), the molecules were pushed away. Most surprisingly, a HtBDC-induced restructuring of the underlying Cu(110) surface was revealed, referred to as a hole reconstruction. We find that about 14 Cu atoms are expelled from the surface in two adjacent  $[1\bar{1}0]$  rows, forming a trench-like base for anchoring of the molecules. Images of the row structure before and after the manipulation are shown in Figs.30a and b, and a model is sketched in Fig.30c. By simple effective medium theory calculations, we can demonstrate that the increase in adsorption energy of the molecules due to the holes is at least  $0.45 \text{ eV}$ , which is responsible for anchoring the molecules to the surface at RT.

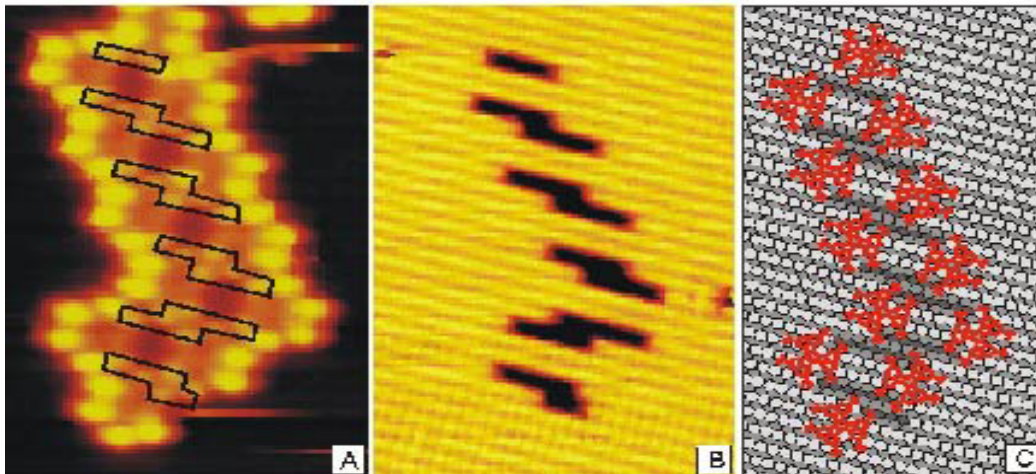


**Figure 30:** Constant current images ( $105 \times 69 \text{ \AA}^2$ ) at  $41 \text{ K}$ . (a) HtBDC double row structure ( $V=1070$  mV,  $I=0.45$  nA). The trenches in the underlying surface are sketched. (b) The trenches in the surface layers are disclosed after manipulating the molecules aside ( $V=7$  mV,  $I=1.82$  nA). (c) Ball model of the double row structure - the substrate atoms are shaded darker the deeper the layers lie, whereas the molecules are shown in red.

This was the first proof for BUN that simple molecules can reconstruct a metal surface. The most interesting outcomes of this observation is that the legs of the molecules are in a depression and the board central part seems to stabilise a double atomic row (Fig. 30). This pushed the Arrhus group to experiment with the simple Lander molecule on the same surface. Upon sub-monolayer deposition of the simple Lander at RT on Cu(110), it was found that the molecules diffuse readily across the surface and anchor preferentially to the *upper* edges of a mono-atomic step, as shown in Fig. 31a. To investigate in detail the anchoring of the molecules on the surface, STM manipulation experiments were also performed at LT (in the range 100 – 200 K) on isolated molecules (previously deposited at RT) adsorbed on step edges. The manipulation was obtained by reducing the resistance in the STM tunneling junction by about 3 orders of magnitude, from 1 G $\Omega$  to a few M $\Omega$ . This corresponds to a tip – surface approach of up to about 0.3 nm.

The manipulation reveals an underlying restructuring of the mono-atomic Cu steps induced by the docked molecules. When removing the molecules from the step edge, a “tooth-like” metal nanostructure appears at the site where the molecule was attached. A manipulation sequence is shown in Fig. 31a and b in which a molecule is removed from the step edge [(a)], and where the molecule was previously attached the step now appears to be locally restructured [(b)]. Fig. 31c shows a zoom in on the structure, with atomic resolution. We can rule out that the tooth-like structure may be artificially induced (in the sense of being pulled out) by the STM tip, since no such structures are formed when we use the same manipulation procedure at a step region where no molecules were present initially.

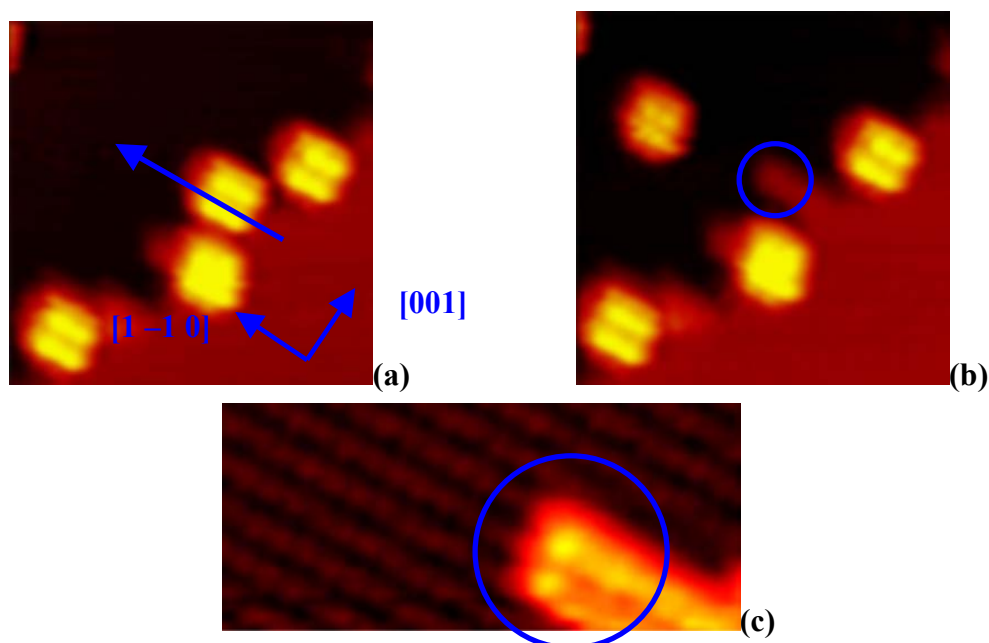


**Figure 31:** Manipulation sequence (a) – (b) of the Lander molecules from a step edge on Cu(110). The arrow shows which molecule is being pushed aside; the circle marks the tooth – like structure that is visible on the step where the molecule was attached. Image dimensions are 13 x 13 nm<sup>2</sup>. (c) Zoom – in STM image showing the characteristic two row width of the tooth – like structure (right corner) after removal of a single Lander molecule from the step edge. The Cu rows are also visible. The arrows show the directions on the surface.

A statistical analysis of the tooth like nanostructure’s width and length (performed on about 100 structures) yields  $0.75 \pm 0.05$  nm and  $1.85 \pm 0.35$  nm, respectively. This corresponds to a width of two atomic Cu rows aligned along the close packed direction [1 –1 0], and a length

of 7 Cu atoms along the  $[1 -1 0]$  direction. For comparison the Lander is expected to be only 1.37 nm long. Notably, the measured width corresponds approximately to the distance between opposite legs within a Lander.

The conformation extraction of the Lander molecule on the 2 copper atomic rows was performed by the Toulouse group. A scan by scan images comparison between the experimental and the calculated image leads to a best fit between the 2 images ( $\Delta z$  by  $\Delta z$  scans) corresponding to the Lander molecule with its molecular wire board parallel to the copper atomic wire (see Fig. 32). The Lander is more stable close to the step edge where the copper atomic row is attached than at the end of wire. The reason is that the 2 rear legs are attracted towards the step edge. Calculations show that the conformation found with the Lander board parallel to the copper rows on the tooth is more stable by 19 kcal/mol as opposed to a perpendicular conformation. The comparison of the calculated scans across the Lander on a flat terrace and on the tooth and with experimental results shows that with 2 copper atomic rows underneath it, the molecule restores a more vertical conformation of the legs compared to its conformation on the flat terrace. The leg-board sigma bond almost restores its planarity relative to the board, due to the steric interaction between the bottom of the legs and the two copper atomic rows.

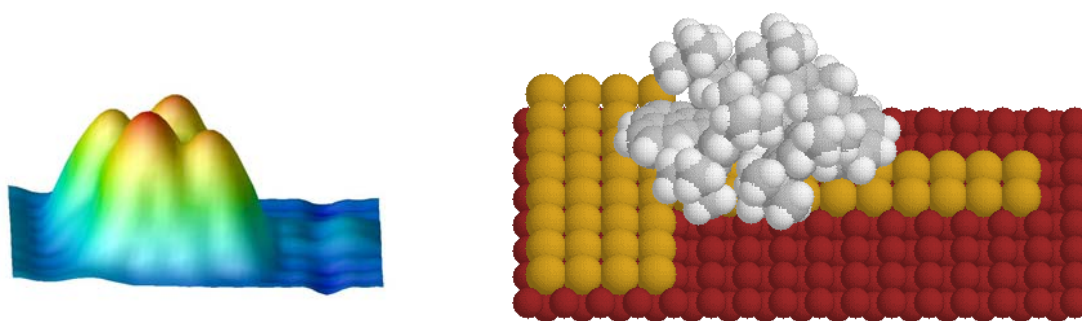


**Figure 32:** Calculated STM images and the corresponding molecular model of the Lander molecule on the copper atomic line observed in Aarhus

In view of the conformation of the Lander on the tooth compared to that on a flat terrace, the overall process can be qualitatively described as follows. At RT the molecules land on the surface and migrate towards the steps. At 300 K steps on Cu surfaces appear frizzy in STM images because the motion of kinks along the steps is so rapid that the mean residence time for a step is shorter than the time needed to scan across the corresponding distance. The molecule encourages the fluctuating step adatoms to arrange themselves in the tooth – like structures we reported, and at the same time, or subsequently, the molecule locally anchors to the structure. More specifically, the Lander’s conducting board is high enough and the distance between 2 opposite legs is large enough for 2 atomic rows to be accommodated between the legs under the board. This forms a perfect mold for the double row to be stabilized at LT and often even extend further than the length of the molecule. The observed process occurs only when the mobility of the adatoms at the step edge is high enough. a Cu surface kept at LT (about 150 K), when repeating the same manipulation experiments, no restructuring of the Cu step edges is found. In this case, the molecules simply attach to a step edge, on the upper terrace. This was verified by checking the apparent height of the molecules with respect to the lower and upper terraces ( $0.45 \pm 0.02$  nm with respect to the

upper terrace). Therefore we conclude that the process of step restructuring is thermally activated.

These nanostructures self-fabricated by the molecule are very well atomically ordered and clean. We have exploited them in BUN to electronically contact the simple Lander molecule to the end of an atomic wire (see section V). New molecules will have to be designed to self-fabricated longer metallic wires and to generalize the process for insulating surface with some metal on it.

#### IVb) Transforming the surface before adsorbing the molecule

Another way explored by BUN for preparing the interconnection of a molecule is to modify the atomic structure of the surface before adsorbing the molecules. It has been claimed often that self-assembly processes could play an important role to address the problem of the wiring between the different molecular components in an electronic nanoscale circuit. However, molecules that present clearly defined geometric assemblies usually contain chemical functional groups (like electron or proton donors or acceptors, etc...) that could change the electronic properties of the molecule. Thus, it is desirable to find a method to assemble the different molecules taking advantage of the interaction with the substrate rather than the interaction between the molecules, i.e., find a method to nano-template the substrate so that the molecules adsorb only at predefined places on the surface. One experiment performed by the Aarhus group was to show that the single Lander molecules can self-align on a specifically patterned surface. After a few tries, the best was to pre-pattern a Cu(110) surface. It is well known that upon O<sub>2</sub> chemisorption, the Cu(110) surface undergoes a partial reconstruction, being divided into bare Cu areas and 2x1 reconstructed Cu – O areas, as shown in Fig. 33a.

The single Lander molecules (Fig.1, section II) were deposited on such pre-patterned surfaces. They adsorb preferentially on the bare Cu areas. By varying the O<sub>2</sub> dose, the width of the bare Cu areas are tuned with respect to the Cu – O areas, thereby selectively changing the dimensions of the Lander's adsorption domains. In particular, as shown in Fig. 33b, when the bare Cu area's width corresponds to the dimensions of the molecule, the Lander forms long rows of molecular wires.

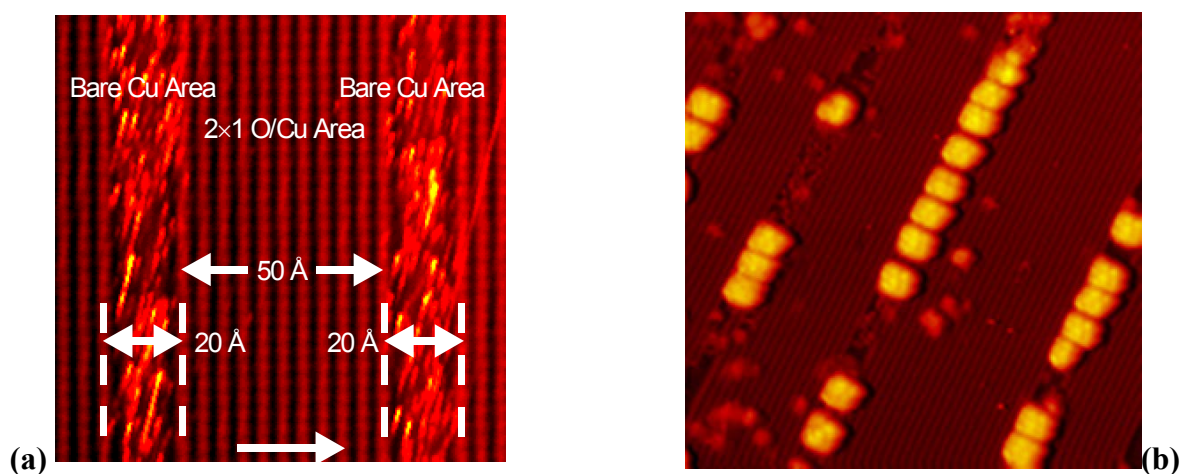


**Figure 33:** (a) Cu(110) surface after exposure to approximately 1 L of oxygen. The 2 x 1 reconstructed areas are visible at the upper left and lower right sides of the image, while the bare Cu area is located in the middle. (b) Formation of long molecular wires. The Lander molecule is deposited on the Cu(110) surface after exposure to oxygen. The O<sub>2</sub> dosing is fine tuned for the width of the bare Cu to correspond to the dimensions of the molecule.

After this initial try as presented in Fig. 33, the pattern method have been further improved up to the point to reach a very high degree of order on the nano-templated surface as presented in Fig. 34. This kind of improvement is a demonstration that we have ensure in BUN the transition between an observed phenomenon and the first step in developing a technology for the atomic scale.

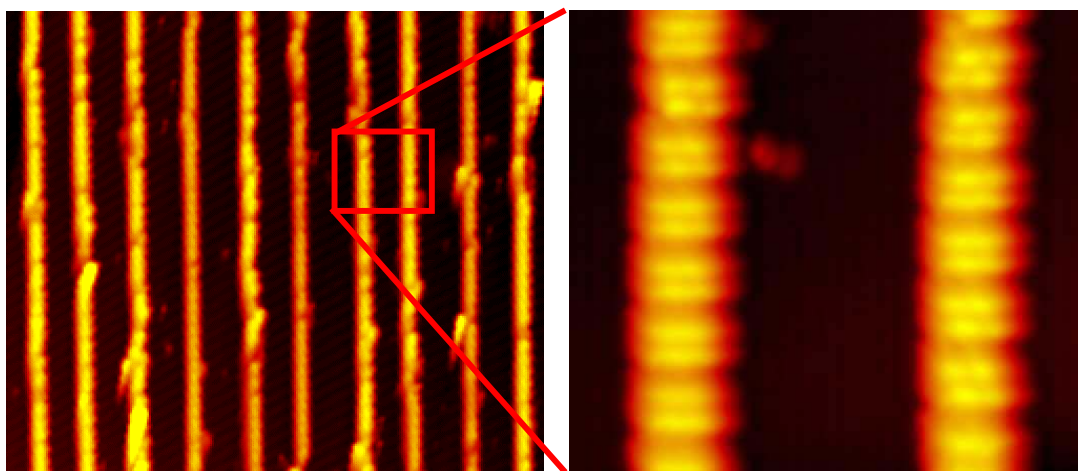


**Figure 34:** The deposition of the Lander molecules on top of the nanotemplated surface leads to a selective adsorption on the bare Cu stripes. The molecular rows show a high degree of order both along the lines (see inset) and perpendicular to them.

One other surface transformation studied in BUN was the deposition of a few layer of insulator on a metal surface. This presents the advantage to built a large gap material on the surface of a metal for separating the molecule from the metal surface without using legs. At the same time, if the number of layer is small enough, STM images can still be obtained at a lower current. Therefore, the STM resolution is kept and single molecule manipulation becomes possible with a much better resolution than with the non contact UHV-AFM described in section III.

In BUN, the Kiel group was in charge to explore this field starting with the adsorption of simple Lander molecules on thin insulating films of NaCl grown on Cu(001). NaCl is one of the few candidates for thin insulating films useful for the assembly of future experimental molecular devices. Fig. 35a shows a NaCl island on Cu(001). NaCl grows with fcc(100) termination on Cu(001) at a sub-monolayer coverage and covers substrate steps in a carpet like fashion. The nominal step height is 0.36 nm for the first NaCl-Cu step, and 0.11 nm for the second NaCl layer. The STM image of such a structure was calculated by the Toulouse group to identified the chlorine atoms as the imaged protuberance. After adsorption of Lander molecules, an atomic square lattice of approx. 0.4 nm and anomalous corrugation of 0.18 nm (Fig. 35b) was repeatedly observed at 1 V sample bias and 20 pA tunnel current, indicating the trapping of a molecule under the tip, acting as an amplifier of the atomic corrugation.

Fig. 35 c,d show the situation after room-temperature adsorption of Lander molecules onto this surface. The molecules do not stick on NaCl layers and diffusion is too fast at RT. The NaCl islands remain free of molecules. However, images of anomalous corrugation as shown in Fig. 35b indicate that there may be molecules on the NaCl islands.

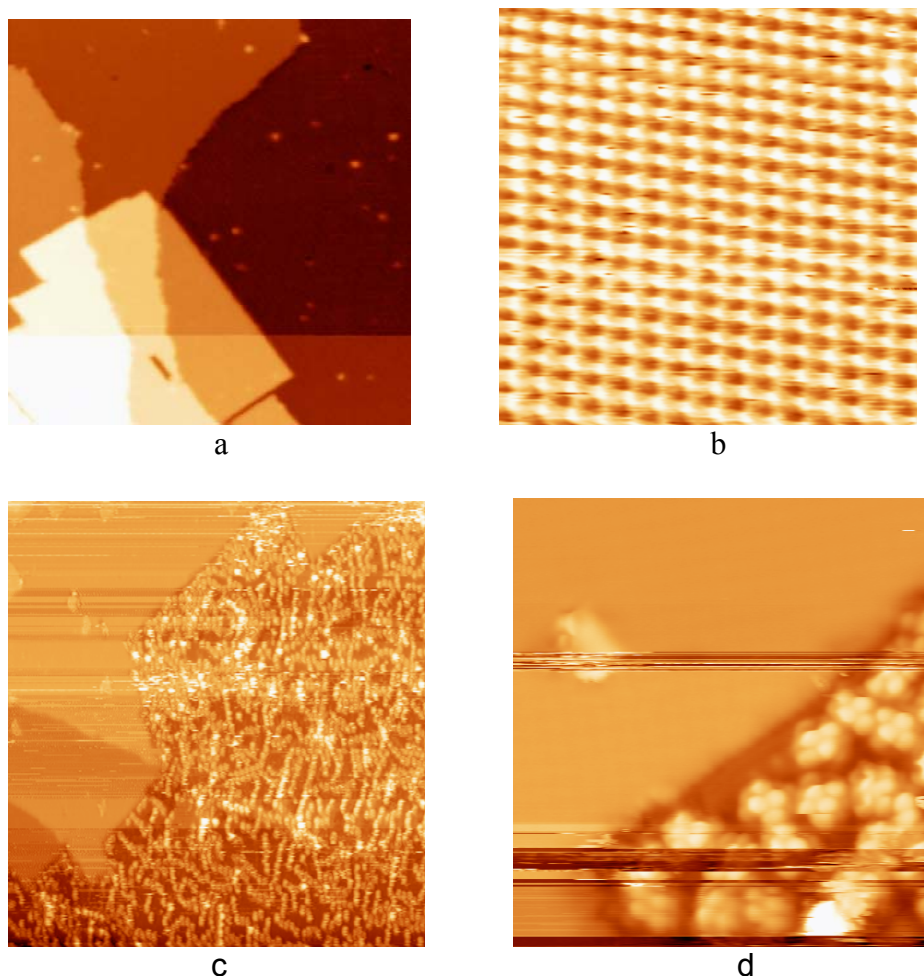


**Figure 35:** (a) NaCl island on Cu(001), image size 86 nm. Defects are due to residual impurities in the NaCl powder (early stage of cleaning). (b) Atomic resolution on a NaCl island due to molecular amplification (see text), image size 5.7 nm. (c),(d) Surface after adsorption of lander molecules, image sizes 129 nm and 14 nm, respectively. NaCl islands apparently remain free of molecules.

Since tip-molecule interactions is greatly reduced at low tunnel currents (hence large tip-sample separation), the electronics and wiring of the STM were modified as to minimize our detectable tunnel current. We are now able of tunneling at currents as low as 500 fA, whereas before it was limited to approximately 10 pA. Despite this effort, we could not acquire stable images of Lander molecules adsorbed on NaCl.

We note that imaging so far was done at approximately 60K. At lower temperature it may be possible to stabilize single molecules on NaCl. Such experiments with a low Lander coverage and manipulation of single molecules onto NaCl islands are currently in progress. However, in view of the rapid diffusion and/or low sticking probability of Lander molecules, the NaCl surface does not seem to be a suitable substrate for molecular assembly. This problem was already faced by BUN on bulk insulators as described in section III. This open the design of

grafting groups very well adapted to an insulating surface as the Lander legs were adapted to a metal surface.

In another approach to fix a single molecule to the surface, the BUN groups have also explored the well known slow but efficient STM tip atomic manipulation mode to create mold of the size of the molecule to be stabilized it on a semiconductor surface. In BUN, the Orsay group have pioneered a new molding method where the patterns are tailored to the form of the molecules by creating molecular molds. This enables the active site geometry to be controlled so that the molecules adsorb not only at a selected place but moreover, in the desired position giving the potential to select molecules according to their physical size or chemical properties.

Fabricating these molecular molds requires atomic-scale precision. The hydrogenated Si(100)-2x1:H is an ideal surface on which to create these molds. The reconstructed surface composed of rows of silicon dimers is rendered unreactive to molecular species by passivating with hydrogen. By applying a voltage pulse to the surface for a short duration (typically 1-10 ms at + 4 V and 10 nA), with the tip positioned over a selected Si-H bond, it is easy to create an isolated silicon

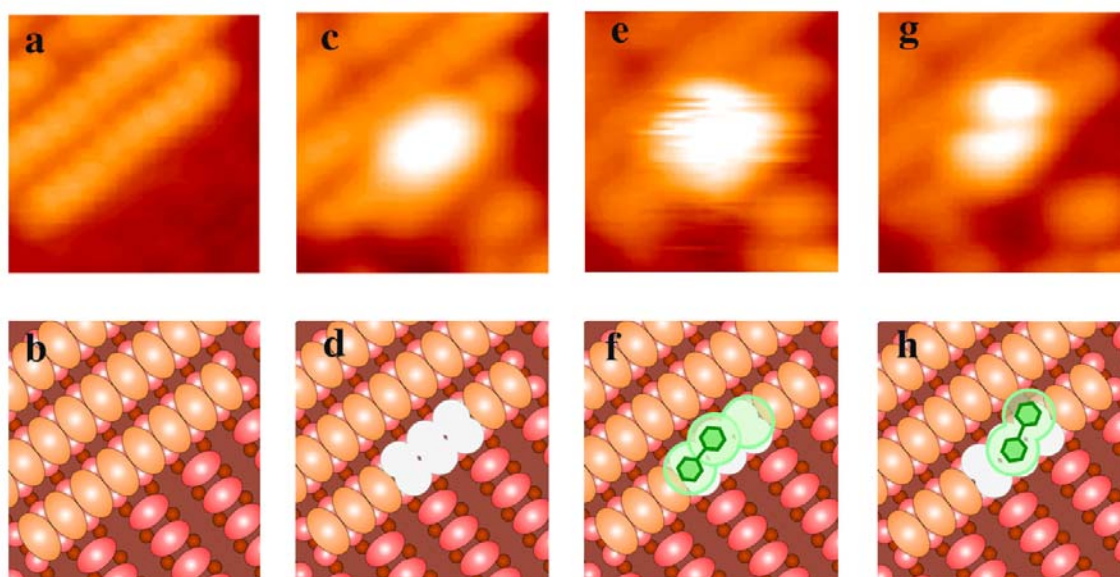


**Figure 36:** Adsorption of a biphenyl molecule in an artificially created individual molecular mold on the hydrogenated Si(100) surface.

An STM image of the hydrogenated silicon surface can be seen in Fig. 36a ( 5 nm x 5 nm,  $V_S = -1.5V$ ,  $I = 0.5nA$ ). Once the surface has been imaged, the hydrogen atoms are removed using feedback control lithography. The result of removing hydrogen atoms can be seen in figure 36c. Here, silicon dangling bonds are visible, appearing brighter than the surrounding terrace. 6 hydrogen atoms have been removed creating a molecular mold of 3 clean neighboring dimers. The fabricated mold is then exposed to a small dose of biphenyl molecules. This was done by retracting the STM tip by about 2 microns and then filling the chamber with  $2 \times 10^{-10}$  torr of biphenyl for 500 seconds (0.1 Langmuir). The tip was then returned to the surface and the same area imaged. The result can be seen in Fig. 36e. It is clear that the visual aspect of the group of dangling bonds have changed markedly from that shown in Fig. 36c. Molecular adsorption has evidently taken place on the silicon dangling bonds. After exposure to the biphenyl, the site appears striped indicating that the adsorbed species is

moving (Fig. 36e and 36f). This looks like the bistable chemisorbed biphenyl sites observed with the same molecule on the clean surface. In Fig. 36g, the same area was imaged some 70 minutes later. This image confirms that a single molecule has adsorbed in the molecular mold. This molecular adsorption site looks just like the fixed site we had previously observed (Fig. 36g and 36h). We only found molecules adsorbed in the mold, not attached to the edges of the molds. The important point is that the adsorption is determined by the final configuration which is in turn determined by the form of the mold. So the method should be very efficient for depositing molecules into fabricated molds. Furthermore, it is still possible, after locating the molecule in the mold in a well determined orientation to pattern, afterwards, atomic lines of Si dangling bond using the same hydrogen desorption method (see section V).

#### IVc) Combing SWCNT on an SiO<sub>2</sub> surface.

Up to now, we have described the preparation technique explored in BUN for a precise location of the molecule, opening the path for an atomic scale technology. In BUN, we have also explored a simple chemical physics way which does not require the UHV environment to deposit macromolecules at a predetermined position on an insulating surface. The method is based on molecular combing i.e. on the capillary force exerted by a receding liquid front on an object adsorbed on the surface. As a first prototype of molecular wire to be planar connected between nano-electrodes, we have chosen in Toulouse the SWCNT macromolecule. But the technique can be further developed for polymer and with a good control of the cleanliness of the combing to long oligomers too. The fabrication of the required nano-electrodes is described in section V.

A systematic study of the combing process showed that the balance between the tube-surface interaction force and the capillary force can be favourable and leads to a good alignment of the tubes in the direction of motion of the liquid (Fig. 37 a-b). The originality of this method is that it requires a weak adsorption (by hydrophobic interaction) of the tube on the electrodes so that it can be manipulated by the capillary force. Other methods based on strong interactions to force the tube to adhere to the electrodes were not successful in particular for transistor-like structures because, in this case, the tubes connect the gate electrodes as well as the source and drain electrodes. Molecular combing provides a great control of the orientation of the tubes which is primordial to avoid contact with the gate electrode (Fig 37c).

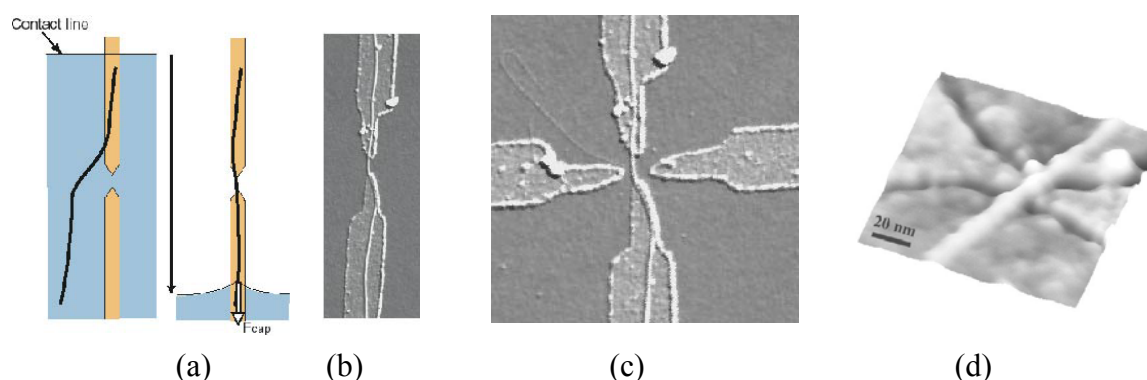


**Figure 37 :** (a) In a first step the tube adsorbs weakly on the electrodes previously chemically modified. (b) The liquid front aligns the tube parallel to the electrodes. (c) AFM image of a nanotube transistor :only the source and drain electrodes are connected. (d) AFM image of a single-wall nanotube on a 20 nm nanojunction.

The technique gives yields of about 45 % of two-electrode as well as four-electrode devices connected by nanotubes. This good result shows that, even in a geometry much more demanding than the parallel electrodes used usually in this kind of experiments, molecular combing provides a parallel deposition process. We were able to realise devices much smaller than the ones realised before (fig 37d).

But this first molecular combing method can not be applied directly to very small interconnection circuit as the OR like circuit presented below (Fig. 38). It requires the deposition of two CNT on a very small area and therefore a larger CNT density on the electrodes than achieved by the previous method. Increasing the adsorption time in the solution was not efficient enough. The Toulouse group therefore changed the surface treatment of the electrodes in order to give a strong adsorption to the nanotubes. Of course, the efficiency of the alignment of the nanotubes by the liquid front will decreased in this case. The electrodes surface were modified using aminothiophenol self-assembled monolayer. The amino group gives a strong interaction with the CNT while the conjugated part of the molecule insures a good electrical contact between the tube and the electrodes.

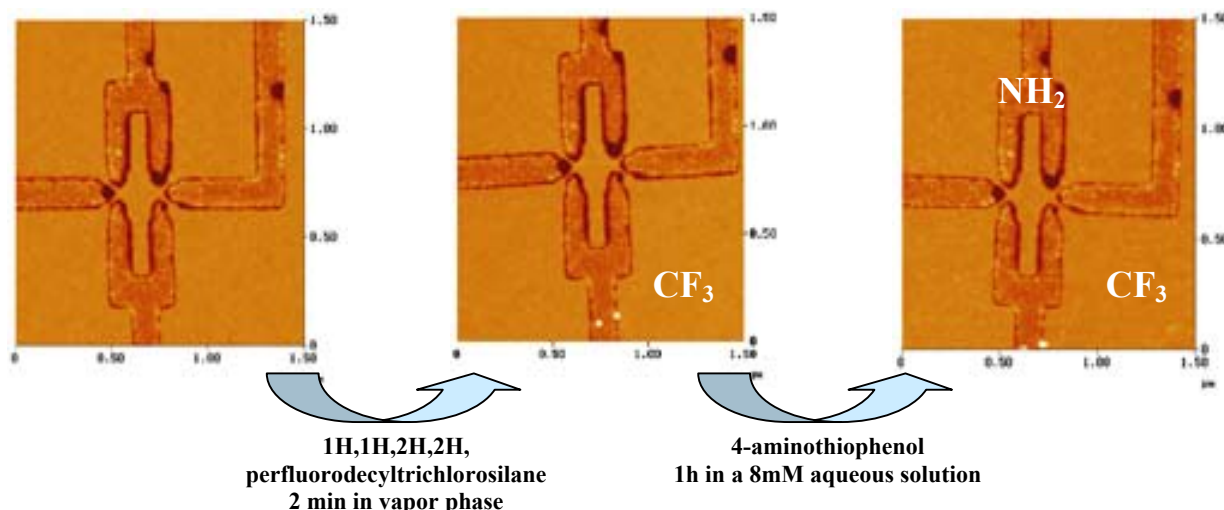


**Figure 38:** AFM images of the same OR like circuit before, and after the two steps of surface treatment.

Before doing this surface modification, it was necessary to protect the silica surface : this was done using 1H,1H,2H,2H, perfluorodecyl trichlorosilane which also gives an hydrophobic surface needed for good combing method. Both reactions were optimised to obtain very clean surface without any aggregate. The experimental procedure is shown on Fig. 38.

This new combing method was applied to deposit nanotubes on modified electrodes where the surface in regard is smaller than in fig. 38. Examples of results are shown on Fig. 39. Transistors with NT well positioned in the junction are obtained with a yield of 36 %. An interesting point is that on 94 % of the junctions one NT is positioned exactly on the source-drain electrode. This nearly perfect positioning results from the combination of preferential adsorption and molecular combing which work together. The alignment is also probably favoured by the strong wettability contrast between hydrophobic fluorinated silica and hydrophilic aminothiophenol modified electrodes. It may deform the triple line leading to a capillary force which pulls the NT on the electrodes (Fig. 40).

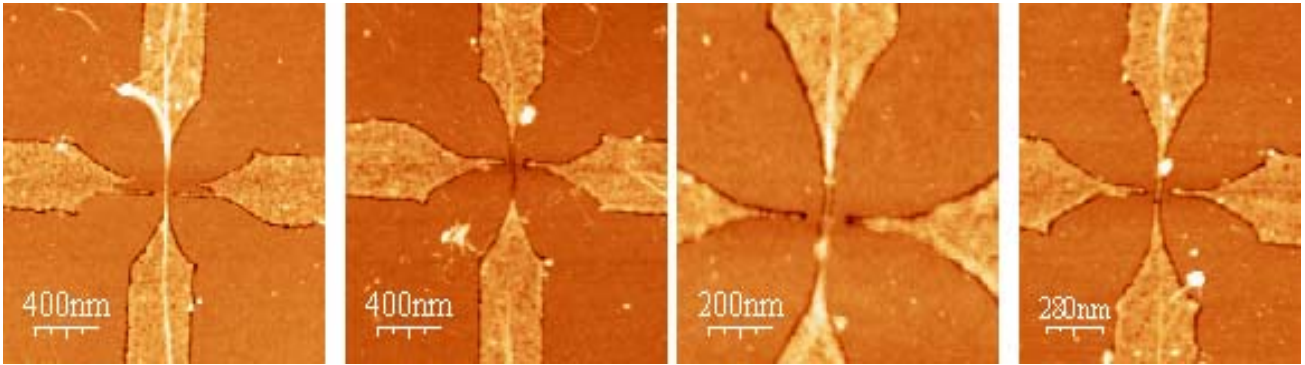


**Figure 39 :** AFM images of four transistors with NT deposited on gaps of about 10 nm.

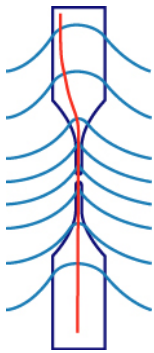


**Figure 40:** Schematic representation of a triple line moving on a circuit with hydrophilic (electrodes) – hydrophobic (silica) patterned surface. The combing force, which is perpendicular to the triple line, aligns the NT perfectly on the electrodes.

The new conditions used in the combing method allow fabricating NT transistors with lateral dimensions in the 10nm range with a reasonable yield. This is a significant decrease in the dimensions of the NT devices.

## V) Nano-communications

Nano-communication means the exchange of information with a single molecule. This requires the preparation of electrons (or photons) in a quantum or semi-classical states to carry this information (input, output, orders) from and to the molecule. A tunnel junction is doing this task spontaneously, transforming Bloch wave electronics states of the mesoscopic pads in single wave packets to be transfer through the molecular device. In BUN, we master the fabrication of tunnel junctions in a planar technology down to gaps of about 2 nm. At the same time, we explored a new atomic technology where the interconnections between a molecule and its pads are mastered at the atomic scale in an ultra-clean environment.

### Va) Co-planar nanojunctions fabricated by e - beam nano-lithography

Two terminal nanojunctions were fabricated by the Cambridge group with the prospect to interconnect first a SWCNT. At the beginning of BUN, the process used in Cambridge was the one established in the mid 90's by the Toulouse group. The gap between the junctions was quite reproducible for gap distances above 20 nm. For gaps below 20 nm, the reproducibility was not good. Gaps as small as 7 nm could be produced (Fig. 41). But the relation  $\lambda_a = f(\lambda_p)$  between the experimental gap size  $\lambda_a$  as a function of the programmed gap  $\lambda_p$  was not very good as shown in Fig. 42.

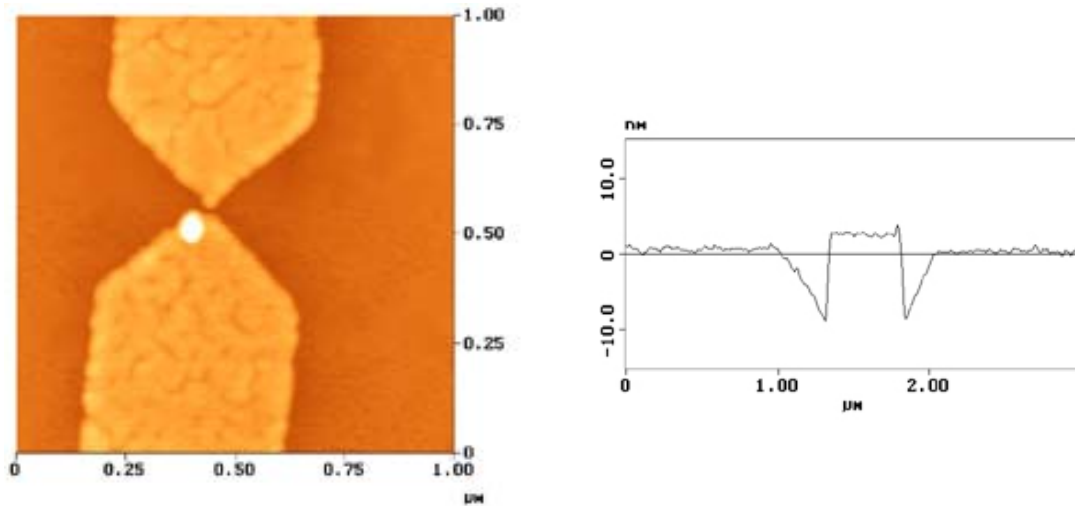


**Figure 41:** AFM image and scan (for planarity test) of a 7 nm co-planar nanojunction.

To fabricate better co-planar nano-junctions and to reach a better  $f(\lambda_p)$  curves, the process was modified according to standard e-beam technology. The embedded in  $\text{SiO}_2$ , thermally oxidized Si wafer ( $\text{SiO}_2$  thickness = 97 nm) was sawed into square pieces of dimensions 5 x 5 mm. They were ultrasonically cleaned in acetone and then in iso-propanol. De-ionized water was used to rinse these wafers. Then, they were plasma-cleaned for 5 minutes and subjected to HMDS treatment for 20 minutes. A double layer positive PMMA was spin-coated on the cut wafers. They were baked at  $180^\circ\text{C}$  for 2 hours. The coated wafers were exposed in a JEOL 4000EX nano-writer operating at 100 kV. After electron beam exposure, the development was carried out in a 1:2.5 mixture of MIBK and IPA for 30 seconds. To produce the co-planar junctions, thermally oxidized wafer needs to be etched before gold deposition. The wafer was dipped in a diluted buffered oxide etch for 3.5 minutes to achieve an approximately 10 nm deep trench. After cleaning in de-ionized water, the wafer was transferred inside a metal evaporator where 3 nm of chromium was deposited before depositing 7 nm of Pd-Au on top of it to achieve the co-planarity.

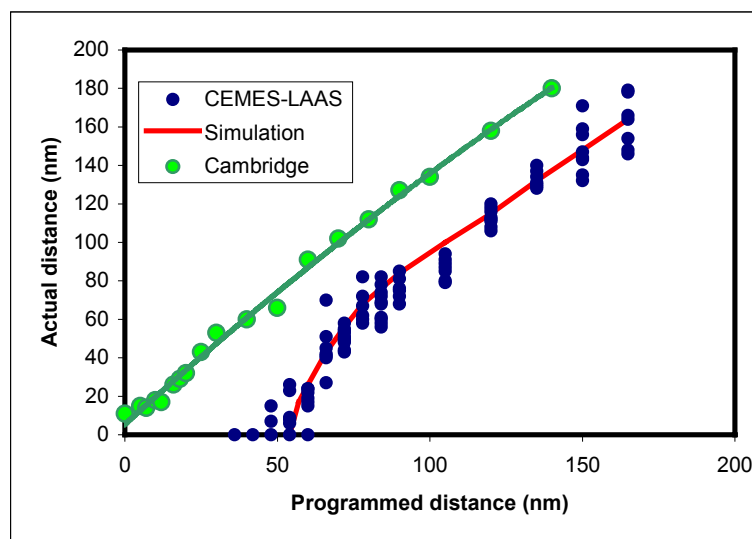


**Figure 42:** Variation (in green) of the measured distance versus the programmed distance of the gap between the two electrodes for the new nanojunctions fabricated in Cambridge. For comparison (in blue), the old result of the process in Toulouse.

The quality of co-planar nano-junctions was studied using AFM by the Toulouse group. It was found that the gap in a given junction was now reproducible for gap distances above 20 nm. For gaps below 20 nm, the reproducibility was not exceptionally high. But Fig. 42 shows that the  $\lambda_a = f(\lambda_p)$  curve improved a lot, offering a reliable process for nano-junctions down to 20 nm. At smaller gap distances, the error margin is quite high due to experimental as well as statistical reasons. Nevertheless, gaps as small as 7 nm were produced too.

To break this 20 nm wall with a good yield of nanojunction fabrication down to 5 nm, the Cambridge group had completely changed the exposure strategy. A 150 nm thick uniform film of 950k poly(methylmethacrylate), PMMA [MicroChem Corp., Nano™], resist was first spun on thermally oxidised and hexamethyldisilazane (HMDS) treated SiO<sub>2</sub> (97 nm)/Si wafers. They were baked at 180°C for two hours. A modified JEOL 4000EX nanowriter operating at 100 kV was used to expose a pattern consisting of 12×12 array of narrow gap electrodes, each column (twelve in a column) containing a different inter-electrode distance. The beam current of the nanowriter was set at 1 pA and the resist was exposed at an electron dose of 1.06 mC cm<sup>-2</sup>. This is a much larger dose than in the previous processes. The exposed samples were developed in a 7:3 isopropanol (IPA) and water solution with ultrasonic agitation (Total output power = 100 W) for 10 seconds. To produce co-planar narrow gap electrodes, thermally oxidised wafers were dipped in a 4% solution of 7:1 buffered oxide etch maintained at 20°C to achieve an approximately 10 nm deep trench. After cleaning in de-ionised water, the wafer was transferred inside a metal evaporator maintained at a vacuum of 10<sup>-8</sup> mbar where 3 nm of Cr was deposited followed by 7 nm of Pd-Au on top to achieve the co-planarity.

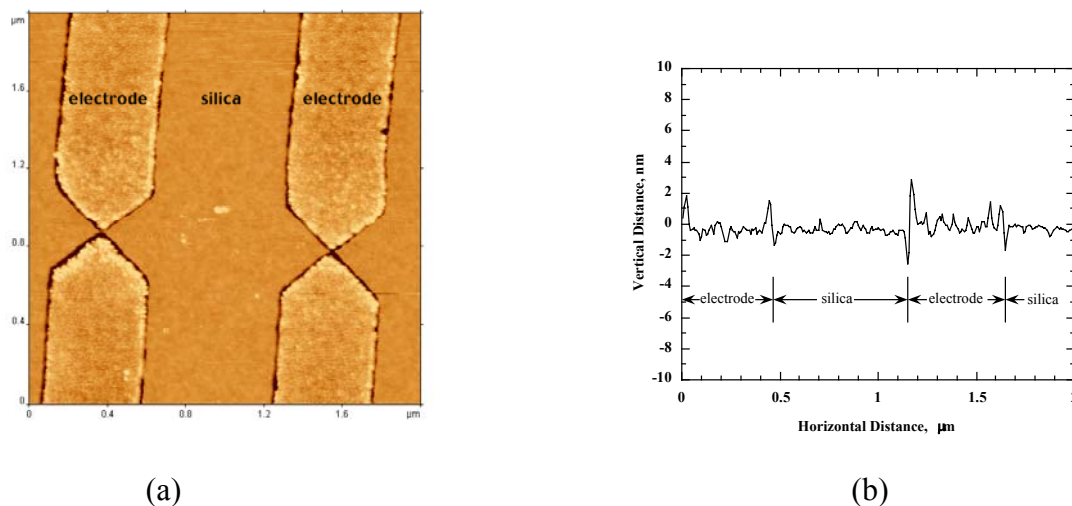


**Figure 43:** (a) An AFM image of co-planar electrodes with narrow gaps and (b) the line plot showing co-planarity of the electrodes with silica surface.

The lift-off took place in acetone. The wafer was abundantly washed in acetone, then in IPA and finally in de-ionised water. It was cleaned in an argon-oxygen plasma before imaging in an AFM equipped with a carbon nanotube tip so as to study the effect of small inter-electrode spacings down to 2 nm. Fig. 43a and b show an AFM image of co-planar electrodes and a measure of the co-planarity, respectively. The difference in height between electrode and SiO<sub>2</sub> surface as shown in Fig. 43b is better than 1 nm.

Fig. 44a shows the range of the measured inter-electrode gaps obtained for a particular value of designed inter-electrode gap. The data used in this plot includes local constrictions and sites with larger separations that were rarely observed, and were most likely due to lift-off effects. The data, however, does not include the gaps where there was an uncertainty in the measurement of their distances. This is especially true when the distance between the electrodes is  $< 2$  nm.

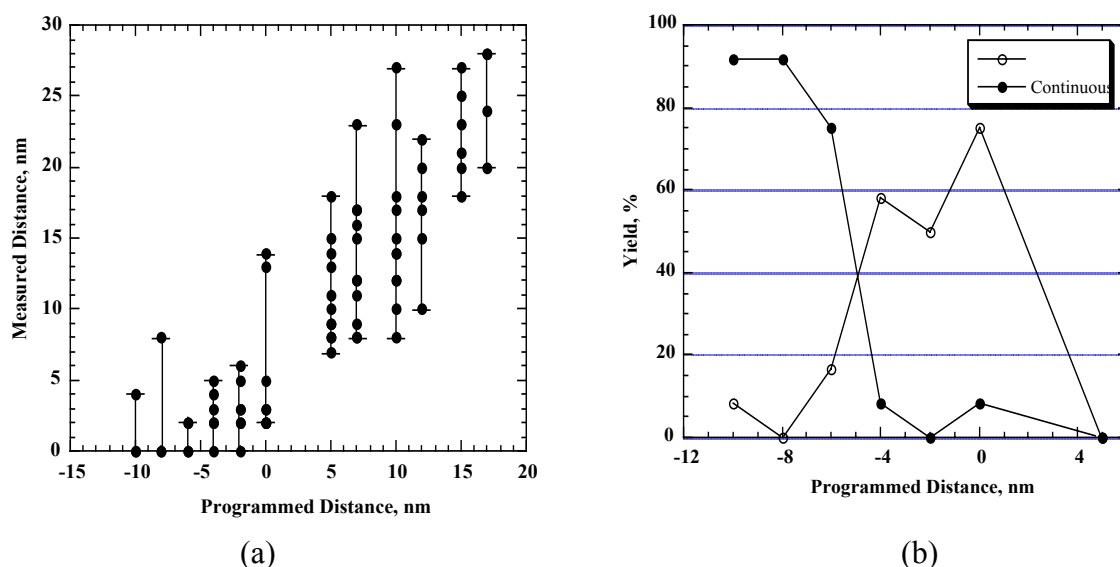


**Figure 44:** (a) Range of measured inter-electrode gaps obtained for a particular value of programmed inter-electrode distance. (b) The yield of gaps  $\leq 5$  nm and continuous junctions at various programmed distances.

The data in Fig. 44a were very useful in determining the range of inter-electrode gaps that can possibly be obtained for a given value of a programmed distance. The smallest measured gap obtained was  $\sim 2$  nm. For a programmed inter-electrode gap, the percentage yields of gaps are shown in Fig. 44b. It can be seen from Fig. 44b that the yield of  $\leq 5$  nm gaps jumps to a maximum value of about 75% at a programmed value of 0 nm. At negative programmed values the yield decreases slowly and below  $-4$  nm the yield drops significantly due to the joining of electrodes..

Previous attempts to fabricate nano-gaps of  $\sim 4$  nm gave a yield  $< 10\%$ . Our technique, on the other hand, gave a yield of about 75% for gaps  $\leq 5$  nm at a designed gap of 0 nm and furthermore is able to reproducibly fabricate  $\sim 2$  nm gaps – the size of a single molecule. The leakage resistance of our co-planar gaps was found to be of the order of  $10^{12} \Omega$ . This suggests that they have very good insulating properties and can be used for molecular electronics. Fig. 45 shows images of electrode structures with various gap distances achieved. With this work, BUN still hold the world record in the fabrication of the smallest gap in co-planar nano-junctions.

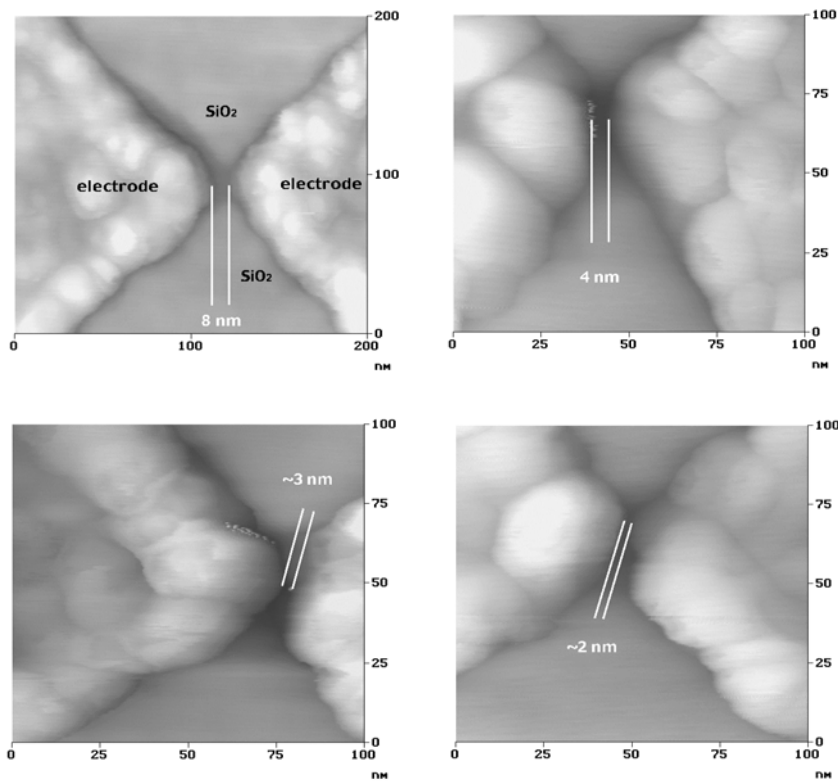


**Figure 45:** AFM images of the narrow gap electrodes show the distances (a) 8 nm, (b) 4 nm, (c) ~3 nm and (d) ~2 nm.

The next challenge in e-beam fabrication took over by BUN was the problem of multi-electrodes access to a junction in the prospect to master not only a single molecular device but a full molecular circuit interconnected by electrodes. There are many interpretations of what a molecular circuit may be in the future. The first case is that molecular devices are well separated by long mesoscopic and later nanoscopic metallic wire. This was easily fabricated by the Cambridge group using the BUN standard e-beam process as shown in fig. 46.

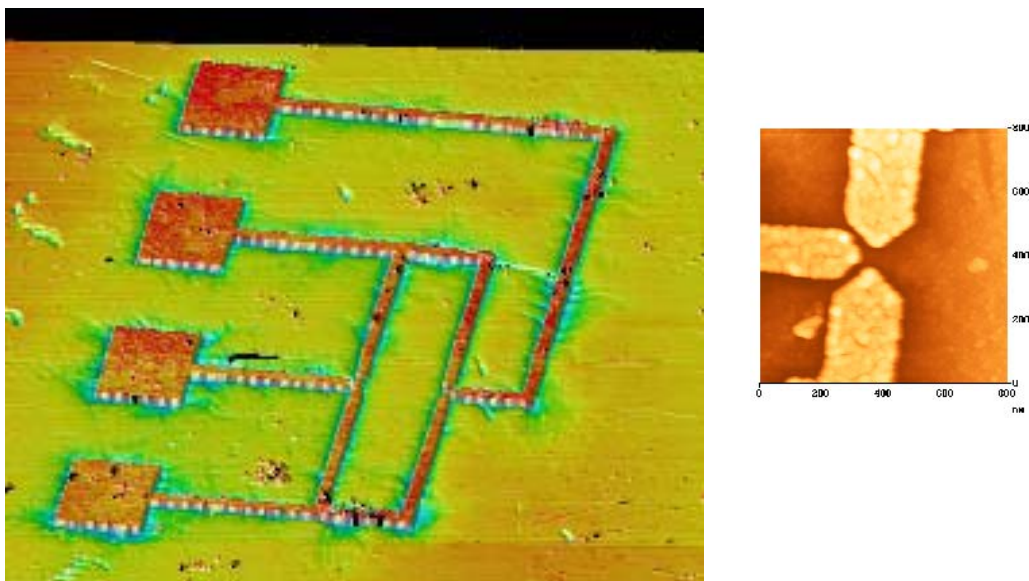


**Figure 46:** AFM image of the full OR microcircuit with a zoom in one of the 3-terminal nanojunctions. The contacting pads are 3  $\mu\text{m}$  x 3  $\mu\text{m}$  and the full AFM image is 23  $\mu\text{m}$  x 23  $\mu\text{m}$ .

This OR gate was designed for nanotube transistors taking into account the specific metallic cantilever interconnection strategy now in use in Toulouse. This requires the fabrication of micro-circuit with very small  $3\ \mu\text{m} \times 3\ \mu\text{m}$  interconnecting pads. The process is identical than for the nano-junction. Two 3-terminal nano-junctions are required to make an OR gate. The AFM image of the circuit is presented in Fig. 46 together with an image of one of the 3-terminal nano-junction. The size of the OR circuit is still very large compared to the dimension of a SWCNT.

The next step was to reduce the size of the full micro-circuit while keeping the design of the interconnecting pads at  $3\ \mu\text{m}$ . Compared to the Fig. 46 result where the wafer surface occupied by an OR gate is  $36\ \mu\text{m}^2$ , the new OR gate wafer surface is now  $0.25\ \mu\text{m}^2$  (Fig. 47). This was possible after a very large improvement of the process which requires a lot of runs. The demonstration of such integration with the development of specific combing process of molecule for this size of gate opens the way to fabricate more complicated hybrid molecular electronic circuits (see section IV).

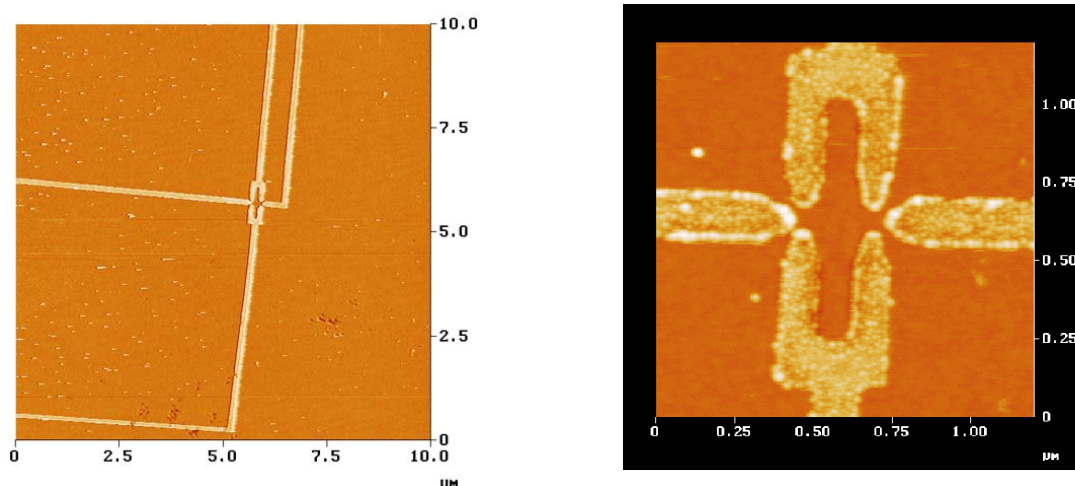


**Figure 47:** A bird's eye view of one OR gate imaged in tapping mode AFM and of central part of the OR gate with 2 nano-junctions in.

The last step in the miniaturisation of such a circuit is to integrate all the circuit inside the same molecule and to fabricate just a nano-junction with a multiple N-electrode access. The e-beam exposure strategy was to fabricate the mesoscopic portion of each electrode by a multi-exposure and to stop this exposure a distance  $L$  away from the centre of the N-electrode nanojunction. Then, each metallic nanowire is only exposed once. Of course,  $L$  is depending of  $N$  to avoid the backscattered electron effect and a too strong overlap of the resist exposure between 2 consecutive nanowires on the junction.

The Toulouse and the Cambridge group had already shown that  $N = 4$  can be reached with an inter-electrode distance around  $10\ \text{nm}$  as presented in Fig. 48. If a single OR molecule is interconnected to these 4 nano-electrodes, the full size of the OR gate will be around  $0.0001\ \mu\text{m}^2$ . Compared with the initial  $36\ \mu\text{m}^2$  of BUN shown in Fig.46, this is a huge miniaturisation factor which is possible to increase again if one is able to used the atomic wires fabricated by the molecules as presented in section IV. But this represents a new technology jump whose exploration starts in BUN as presented below with the nanostencil technique.

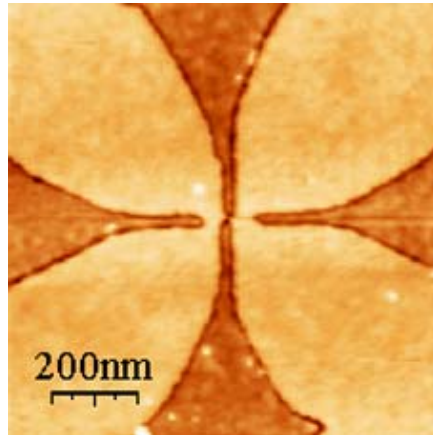


**Figure 46:** AFM image of a  $N = 4$  nano-junction with 20 nm-wide electrodes and a gap of the order of 10 nm in the centre of the junction.

For the surface profile, the previous co-planar buried electrodes design was kept here because of the AFM characterization step which is facilitated using metallic nano-electrodes being at the same height than the wafer surface. We have also kept our interconnection technology consisting of metallic micro-cantilevers. At the end of each metallic nanowire of the  $N$ -electrodes nano-junction, a metallic pad  $3\mu\text{m} \times 3\mu\text{m}$  in size is fabricated during the same process (Fig. 49).

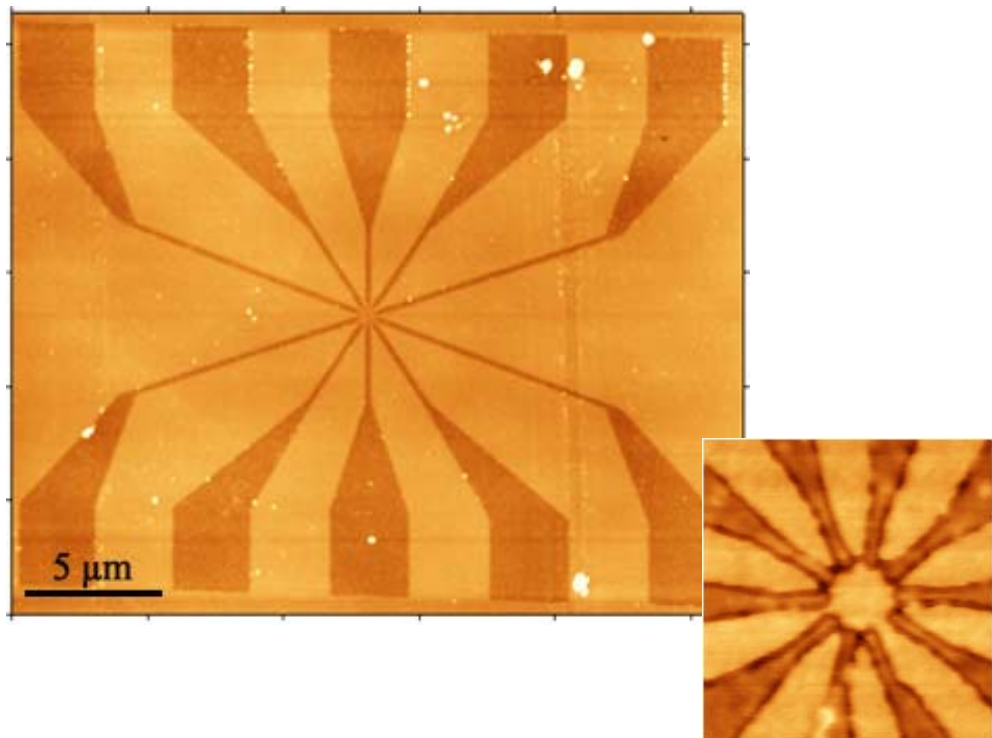


**Figure 49:** an AFM image of an e-beam fabricated  $N = 10$  electrode junction with single electrode width down to 20 nm in average. The overall diameter of the junction is 90 nm. The drawing of the micro-circuit is composed of  $N$  electrodes terminated each, on one side, by a nanowire and, on the other side, by a  $3\mu\text{m} \times 3\mu\text{m}$  pad. The top AFM image is presenting the interconnection pads at the micron scale.

To reach a larger N value as presented in Fig. 50, the STEM at 200kV (PHILIPS CM20 FEG) column in LAAS-Toulouse was used for the e-beam exposure. In the process, we have completely modified the electron dose, current intensity and resist thickness. In previous works, the proximity effects were under control to get 4 nm nanojunction for  $N = 2$  using a 20 KeV e-beam source. As shown above by the Cambridge group, the proximity effects can also be exaggerated using a very thick 150 nm resist under a 100 KeV e-beam source. In our new process, we use the new strategy to suppress proximity effect to be as closed as possible to the geometric law:  $N = \pi D / (d + \delta)$  with D the nominal diameter of the junction, d the distance between 2 nanowires and  $\delta$  the width of a nanowire.

The first step of the process developed in Toulouse is a thermal oxidation at 1100 °C of a clean Si(100) wafer under O<sub>2</sub> flux during 40 mn. A 110 nm SiO<sub>2</sub> thickness is obtained, controlled by ellipsometry. In a second step, the PMMA resist is spin coated on the SiO<sub>2</sub>/Si wafer at 3000 rpm using a solution of 15g/l PMMA in MIBK to reach a 50 nm thickness. Then, the resist is annealed at 170 °C during 60s. The e-beam exposure is done using the STEM at a dose of 2000  $\mu\text{C}/\text{cm}^2$  for the multi-scan parts and of 5 nC/cm for the single line scan. The development of the exposed PMMA is done in a solution of MIBK: IPA/1:3 for 15s (Methyl Iso-Buthyl Ketone and IsoPropanol) at 20 °C and then washed in IPA for 30s. Before the metallization, because the pads, the electrodes and the nanowires are buried at the SiO<sub>2</sub> surface, the surface is etched in a very dilute buffer HF solution (5% BHF) in order to create a 10 nm in depth mold for the metallic wire on the surface. The isotropic etching induces an enlargement of the trench under the PMMA resist. The metallisation is performed using 5 nm of titanium for adhesion and 5 nm of gold-palladium for the active metallic part of the nano-electrodes. The process is terminated by a lift-off in hot trichloro-ethylene.

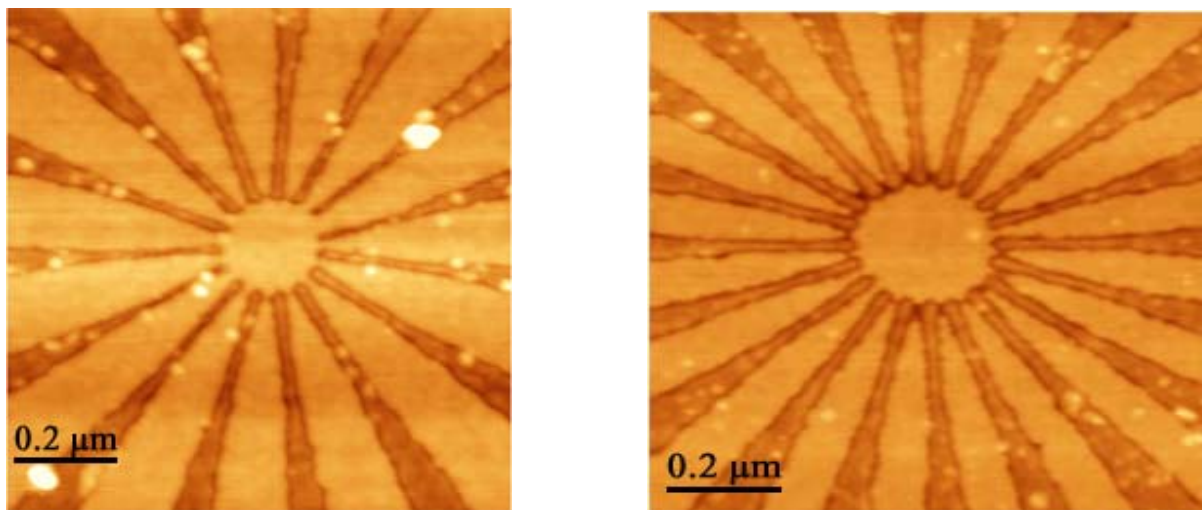


**Figure 50:** The example of a  $N = 15$  and a  $N = 20$  nanojunction with a mesoscopic diameter of 160 nm and 200 nm respectively and an average width of individual nanowire of about 20 nm.

According to the geometrical law  $N = \pi D / (d + \delta)$ , a junction diameter D directly compatible with the dimension of an intramolecular circuit must be of the order of  $D = 10$  nm. This means that for a circuit requiring for example  $N = 10$  interconnections, d and  $\delta$  must be of the order of a nanometer, a very difficult target for e-beam nanolithography. This problem forces BUN to explore a new technology direction in the UHV performing nanolithography without using a resists. This is the nanostencil technique described bellow.

## Vb) I-V characteristics on SWCNT

BUN had taken benefit from its advances in e-beam nanolithography to measure the I-V characteristics of a few macromolecules. Those nano-object are well adapted to the size of the nano-junctions delivered by the e-beam nanolithography technique. This was conducted in parallel with the atomic scale technology of interconnecting a small organic molecule.

The first study was to measure the length dependence of the conductance of a metal-SWCNT-metal mesoscopic junction as a function of the nanotube length. Since the conductance measured on such devices is mostly coming from the nanotube-electrode contact resistance, no notable variation was observed going from inter-electrode distances between 980 nm down to 30 nm. Measures on 30 nm nano-junction are still the smallest nano-junction measurements ever done on a SWCNT. This is due to the specific molecular combing procedure developed in BUN (see section IV). Notice also as presented in fig. 51 that the co-planar nanojunction design mastered in BUN allow to avoid the curvature of the nanotube at the contact to the electrodes, a phenomenon which increased the contact resistance.

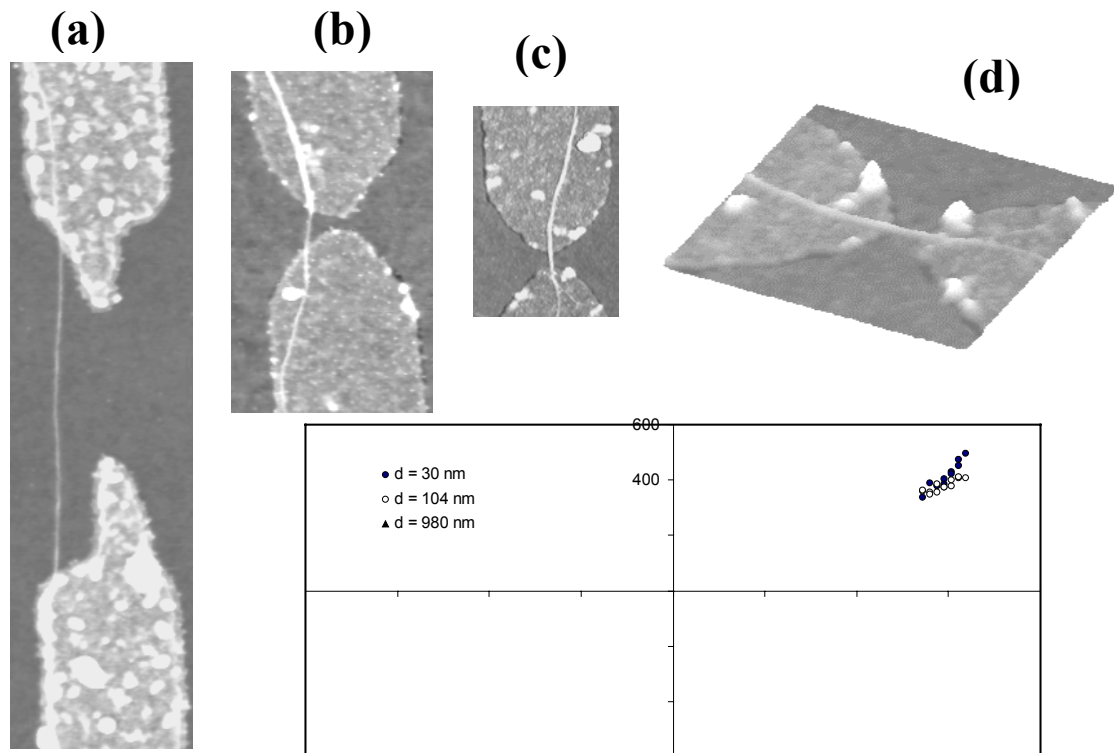


**Figure 51:** Measurement of the dependence of the conductance of the tube as a function of its length. (a) for 980 nm, (b) for 104 nm and (c) for 30 nm. (d) is a 3D version of (c)

In a second step, BUN had also fabricated SWCNT transistor. The originality was here to master a fully planar configuration for the transistor with the source, the drain and the grid electrode fabricated all at the surface of the wafer. The lateral grid effect was first tested on a metallic tube with no clear effect the grid voltage effect applied up to 10 volt as presented in Fig.52. This effect was interpreted as an electromechanical effect on the contact between the electrode and a metallic tube.

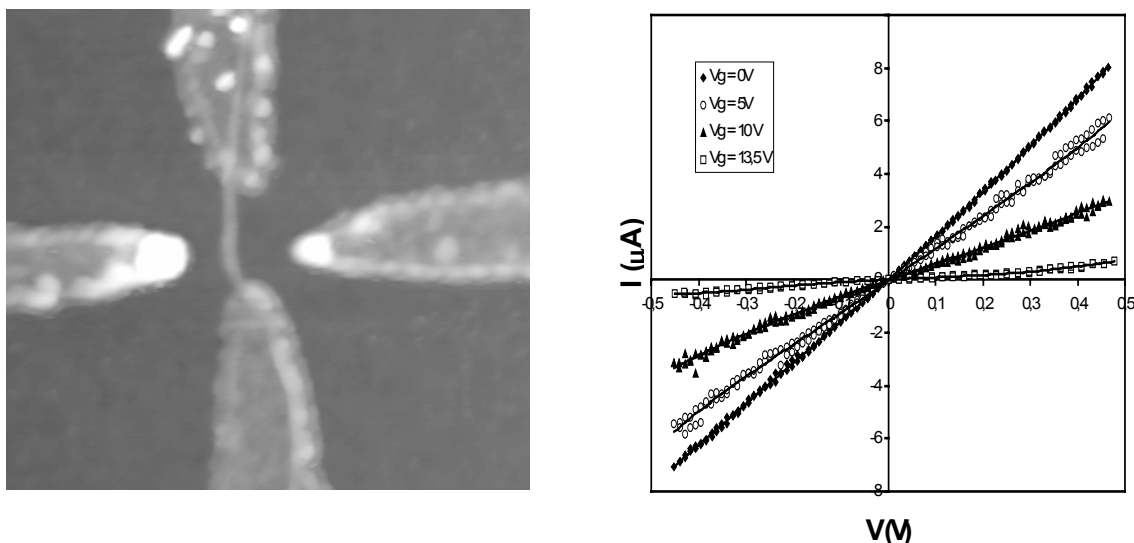


**Figure 52:** The source – drain I-V characteristic of a metallic nanotube under various lateral grid voltage with the corresponding AFM image of the device taken during the I-V measurements. Image size is 400 nm x 400 nm.

For other devices, the lateral grid effect was much larger as evidenced on Fig. 53. This corresponds to semi-conductor tubes. The trans-conductance of these devices is of about 160 nA/V much larger than the values published with a back gate configuration at that time. This strong effect is due to the fact that in our geometry the gate electrode is much closer to the nanotube.

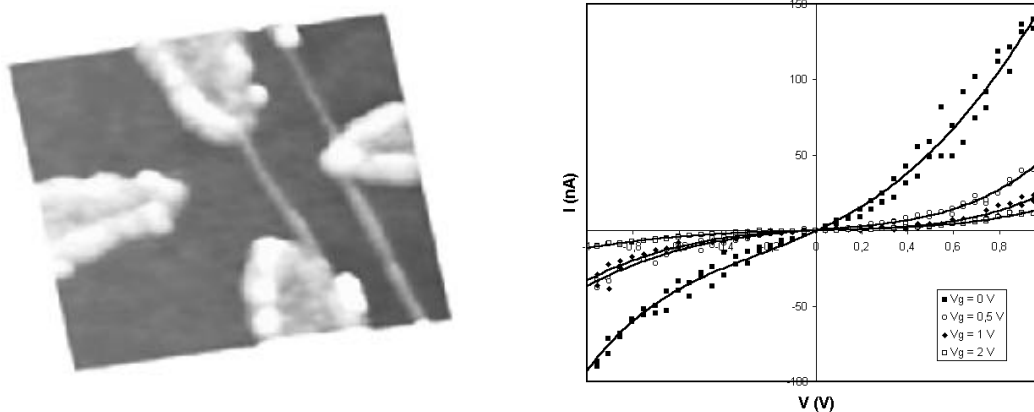


**Figure 53 :** AFM image of a nanotube transistor and its electrical characteristics for different gate voltages. The strong effect is compatible with the behaviour of a semiconductor nanotube.

These results open the way for the fabrication of more complex devices involving several nanotubes that will perform basic logic functions. The combing was tested on the sample whose fabrication and surface treatment was optimised. It appears clearly that the number of nanotubes is larger than on the previous process. In average, we obtain 2 tubes on the active part of the circuit. But as predicted, the combing was less efficient and in particular it appears that the capillary force is not always able to align a SWCNT which is adsorbed between one electrode and the grid. The image of one fabricated circuit is presented in Fig. 54. The 2

SWCNT are not perfectly positioned and electrical measurements confirmed that they are not connected to the electrodes.

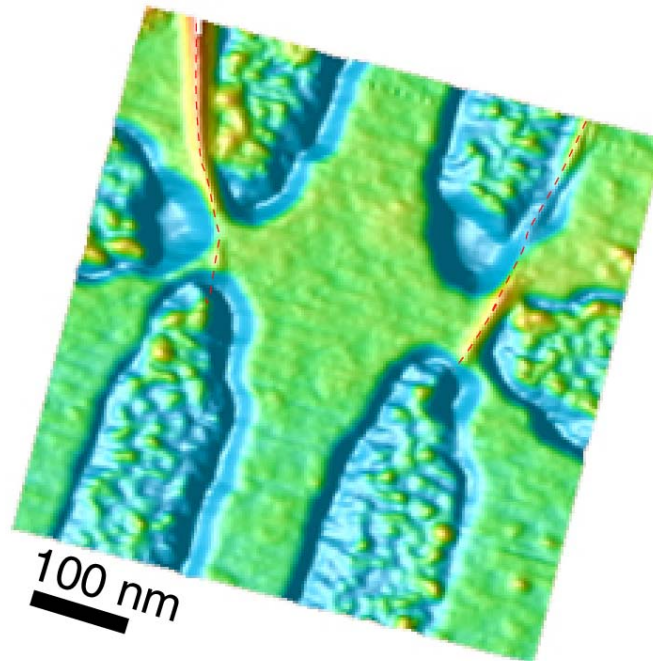


**Figure 54 :** The AFM image of two CNT deposited on an OR circuit.  
The dotted line underline the position of the CNT.

We have also started in BUN to use other semiconductor nano-fibers whose synthesis is better controlled than CNT. The objective was to ensure that any deposited macromolecule is semi-conducting. In collaboration with P. Rozier from CEMES-Toulouse, vanadium pentoxide  $V_2O_5$  nano-fibers were synthesised. These fibres have a ribbon-like shape with dimensions of about  $1.5 \text{ nm} \times 10 \text{ nm}$  for a few microns in length. The great advantage of these objects is that, in principle, their electrical properties can be adjusted during the synthesis (by substitution of  $V^{5+}$  by  $V^{4+}$ ) or by doping. The C. Lieber's group have shown that well-controlled semiconductor meso-fibres can be used to obtain diode and transistor characteristics and all the logic functions that can be built from these basis elements. Again, like for CNT, the objective in BUN with vanadium pentoxide fibers was to decrease the size of these circuits compared to Lieber's mesoscopic ones to find the limit of the hybrid molecular electronic technology.

With this goal in mind, we have tested our combing process on such nano-fibres. The results were even better than for CNT with a yield of about 60% of nanojunctions connected by a nano-fibres. Examples of two such hybrid devices are presented in Fig. 55 with a corresponding semi-conductor like I-V curve. Notice that the electrical characterisations of these nanotube devices were measured systematically using an instrument that we developed in order to perform simultaneous AFM imaging and electrical characterisation of all the devices that can be fabricated in one step on the surface.

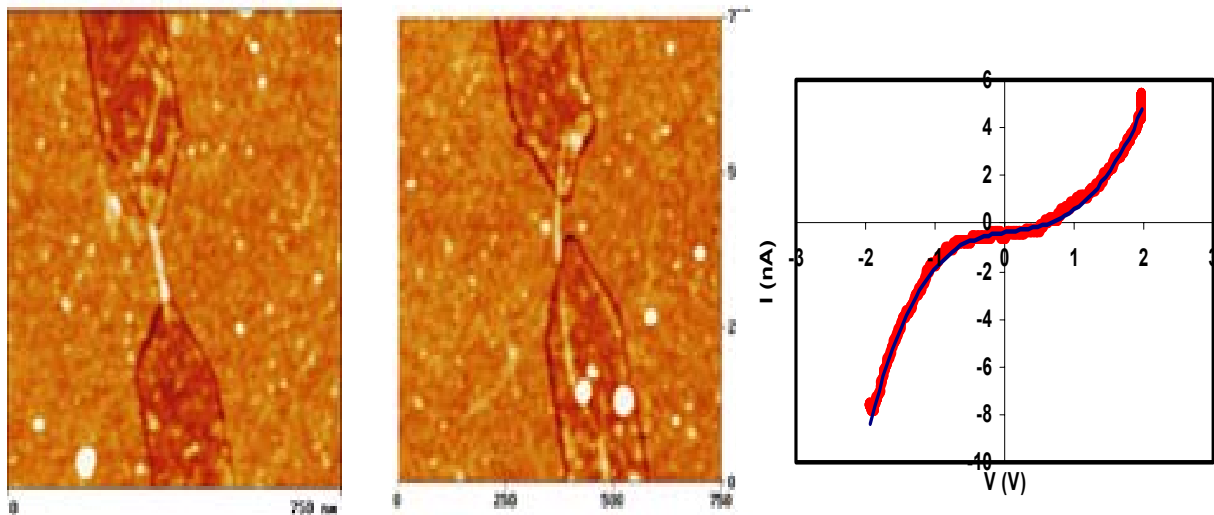


**Figure 55 :** AFM images of  $V_2O_5$  nanofibers deposited by molecular combing on nanojunctions down to 50 nm of inter-electrode distances and the example of an I-V characteristics measured on such a nano-fibre.

### Vc) Is an atomic scale technology possible?

From the experimental knowledge of BUN on SWCNT and also in reference to the vast literature published on SWCNT characterisation, it becomes clear during the BUN project that the interconnection technology provided by e-beam nanolithography is well adapted to macromolecular object but not to small molecules. BUN had therefore put a large experimental effort to move away from this e-beam technology, taking benefit of its expertise in UHV-STM, UHV-AFM and single molecule manipulation. The first step was first to show that, indeed in an almost planar technology, it is possible to keep a small molecule in a good planar configuration to be interconnected to a mono-atomic step on a metal surface. BUN used here its know-how presented in section III and IV to reach this point and push it a step further by contacting the molecule at the end of an atomic wire.

For this first experiment, we have selected a Cu(111) surface because the molecular wire of the single Lander is known to be lower than designed and because the surface states of such a face are very sensible to any atomic scale scatters, an opportunity to probe the interactions of the molecular wire with a mono-atomic step edge. Let us recalled that this mono-atomic step edge is here to mimic the end a contacting metallic pad structure with an atomic precision. To perform this experiment, BUN had contacted the K. H. Rieder group in Berlin which was equipped at the beginning of 2002 with the most stable low temperature UHV-STM in Europe, the only machine able to perform our very precise single molecule STM manipulation at the step edge. F. Moresco agreed to perform the experiment.

The molecule used was the single Lander molecule. Mono-atomic steps were also created by gently crashing the tip in the surface at low temperature. The only difference is that the molecules were sublimated with the substrate kept at low temperature to avoid their spontaneous accumulation at the mono-atomic step edge. The Cu(111) surface states were observed on the clean Cu(111) surface around a single molecule and near the clean mono-atomic step edges. The Lander molecule was manipulated towards the step edge with its molecular wire oriented either parallel or perpendicular to the step edge. Only the perpendicular approach leads to a transformation of the standing electronic wave patterns on

the top terrace (Fig. 56). This is a signature of the interaction of the molecular wire end with the top terrace electronic states.

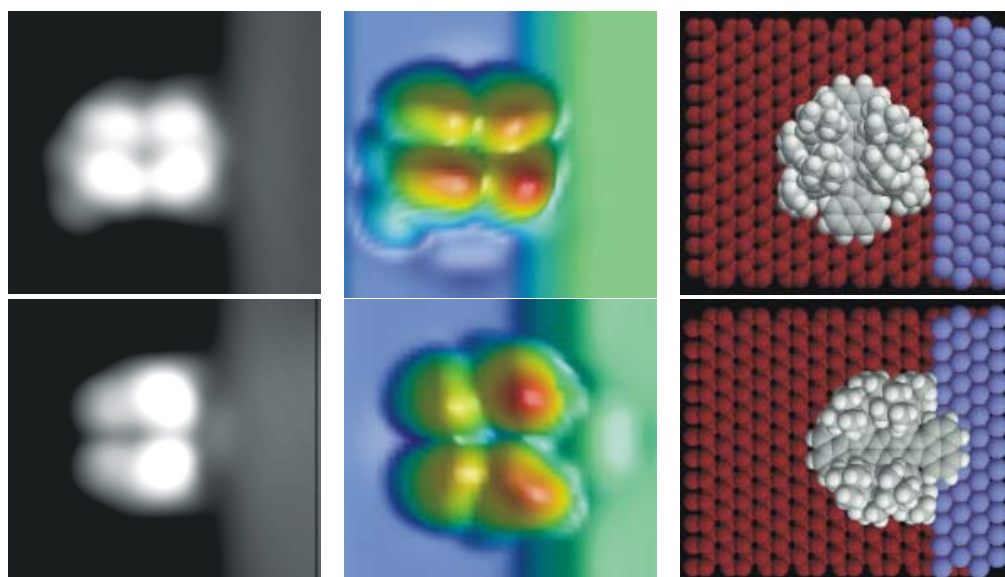


**Figure 56:** image of the Lander molecular wire in its contacted and non contacted conformation together with the extracted conformation obtained using the EHMO-ESQC technique (in collaboration with FU, Berlin).

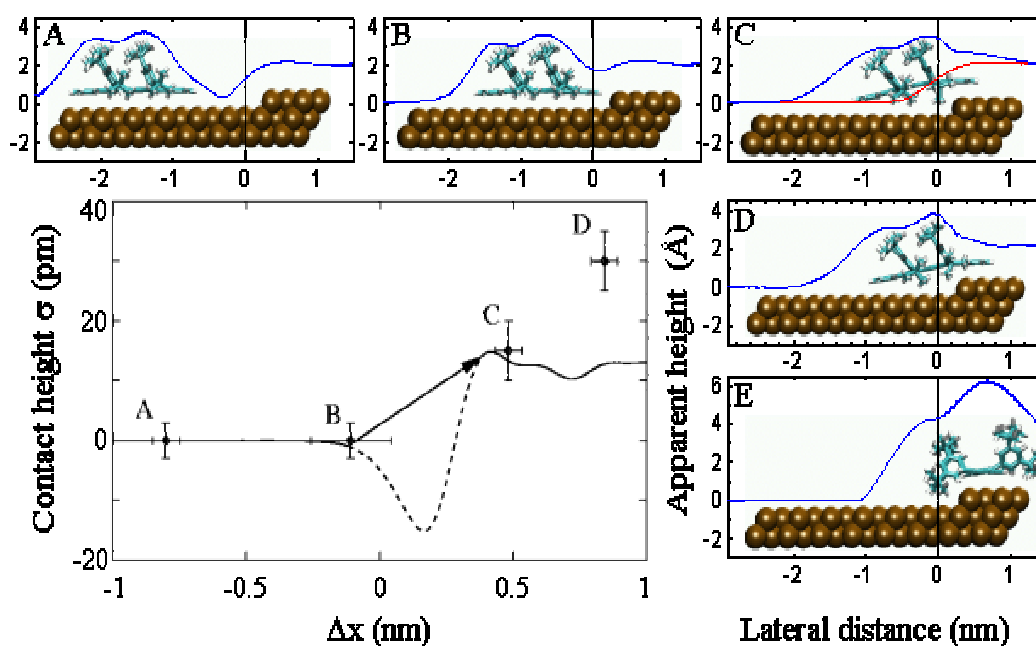


**Figure 57:** The bump height as a function of the distance to the step edge with the corresponding conformations (in collaboration with FU-Berlin).

The BUN know-how on the molecule conformation extraction from an STM image was used here to completely interpret the experiment. For example, the apparent STM bump appearing in the experiment at the contact point is related to the interaction of the molecular wire end to the top Cu(111) terrace. This interpretation was possible by a systematic Lander molecule conformation extraction for each of its position when manipulated towards the step edge for

contact. The contact bump height was calculated for each possible position allowed by molecular mechanics optimisation (Fig. 57). Only a few of these positions are accessible to the measurement because the molecule follows a jump to contact when approach to close to the step edge.

This experiment demonstrate that the electronic interaction between a single molecule and a well atomically ordered and ultra-clean step edge figuring the end of a perfectly faceted end of a nano-electrode is possible. But we went a step further in direction of this future atomic technology. The contact experiment was extended from a step to a single atomic wire because a single Lander molecule is able to self- fabricate a short copper atomic wire at the edge of a Cu(110) mono-atomic step as discussed in section IV. The experience of manipulating a single Lander molecule along the Cu tooth fabricated by the molecule itself was performed again on the FU-Berlin LT UHV-STM.

The transfer of know-how between the Aarhus group and Berlin was the key to reproduce with success the Aarhus Cu tooth experiments on the Berlin Machine. After selecting a single Lander molecule which had fabricated its tooth (Fig. 58c), its conformation was identified (Fig. 58d) by the Toulouse group. At low temperature, we known from the Aarhus know-how that the di-atomic Cu tooth is like a rail for a single Lander. The molecule was STM-manipulated to reach the second equilibrium position of a Lander molecule along this rail. All the different equilibrium position have been determined by molecular mechanics calculation. The one reached at the end of the Cu tooth corresponds to 2 legs out of the rail and the 2 rear legs still on the rail (see Fig. 58d). This conformation was indeed reached experimentally as presented in Fig. 58c. Since the central wire is very near to the underneath atomic wire, this wire is always electronically interacting with it. Positioned at this end of the rail, this contact interaction can be STM imaged only if the rear legs are STM manipulated to leave a free access to the tip for measurement. This phenomenon was observed by the Berlin group and predicted by the Toulouse group (Fig. 59).

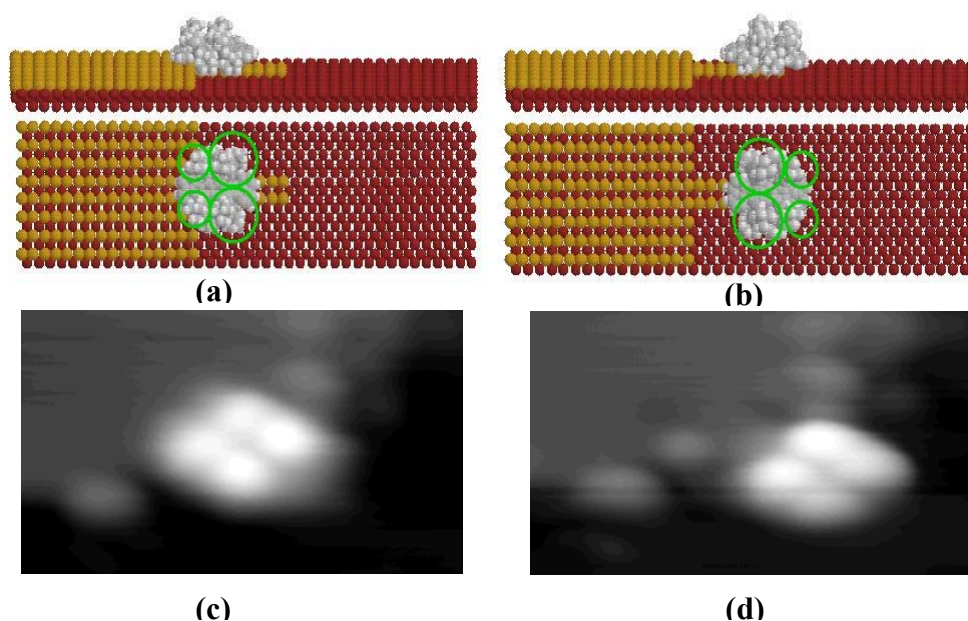


**Figure 58:** (a) the refined conformation of the molecule on the tooth from (c). (b) the refined conformation of the molecule at this second stable position along the tooth from (d). (c) LT UHV-STM image of a single Lander molecule on its wire. (d) LT UHV-STM image of the same spot (molecule and tooth) after the STM manipulation of the molecule along the tooth. The end of the wire is clearly visible. The contact bump becomes visible only after a leg manipulation (in collaboration with FU-Berlin).

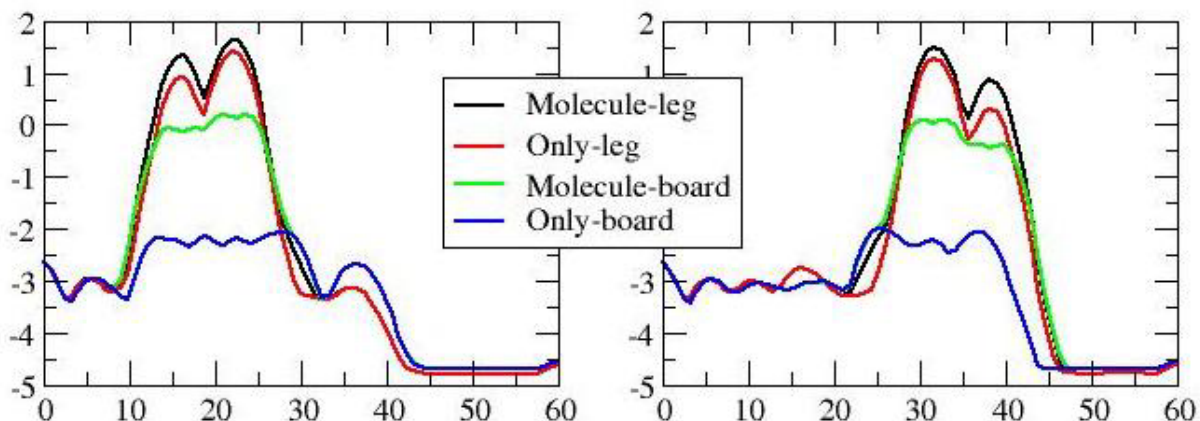


**Figure 59:** EHMO-ESQC calculated STM scans over the centre of the Lander – tooth system when the molecule is (a) near the step edge and (b) at the end of the tooth and the rear legs in the good orientation to observe the contact bump. 4 scans have been calculated to see the influence of each part of the molecule. Notice the contact bump on the (b) scans.

This experiment is the first clear example of an electronic contact between a molecular wire and an atomic metallic wire in ultra-clean and ultimate ordered conditions. Of course, this was done on a metallic surface, the legs of the molecule playing the role of an insulating separator. This is the first convincing step toward the fabrication of an atomic metallic wire on an insulating surface connected to a molecular wire .

In an intermediate step, The Orsay group in BUN had explored how to fabricated atomic wire and circuits on a semiconductor surface. Fig. 60a illustrates the success of this fabrication where 2 parallel Si lines, each 200 Å in length. The background of the image (in grey) shows the rows of hydrogenated Si dimers. Bright spots correspond to individual Si dangling bonds after removal of hydrogen atoms.

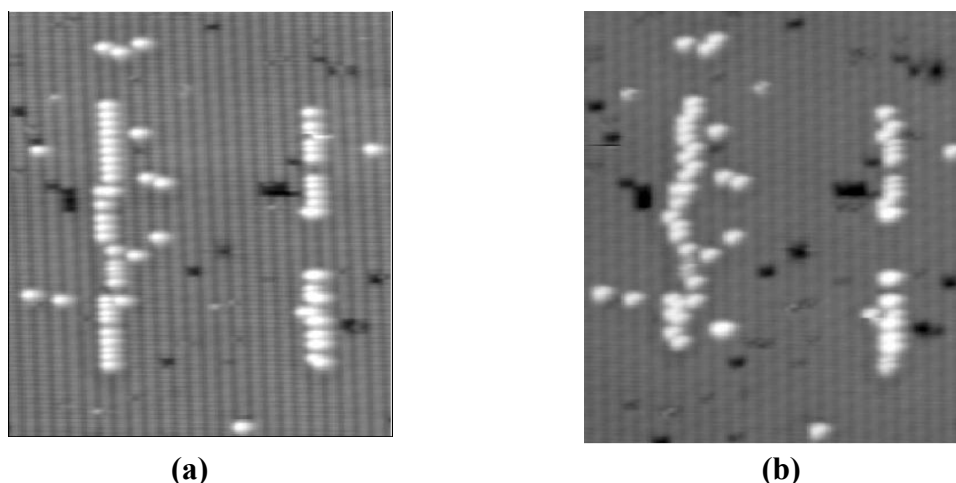


**Figure 60:** (a) 30 nm x 20 nm STM topography of two Si lines STM fabricated on hydrogenated Si(100) ( $V_s = -1.5V$ ,  $I = 1nA$ ). (b) the same surface area than in (a) but after 45 min of scanning.

The lines have been fabricated point by point as follows : the STM tip is positioned successively at 100 points along the line, the separation being  $2\text{\AA}$  between points. At each position, the bias voltage and the tunnel current are set to 2.5 V and 1 nA respectively during 2.6ms, before moving on to the next point.

As seen in Fig. 60, the reproducibility of the method for hydrogen extraction is rather good. However, there are still some defects arising from (i) the fact that the efficiency of the STM tip is not 100%, (ii) the fact that the hydrogen atom can be extracted from either side of the Si dimers, and that both atoms can be desorbed.

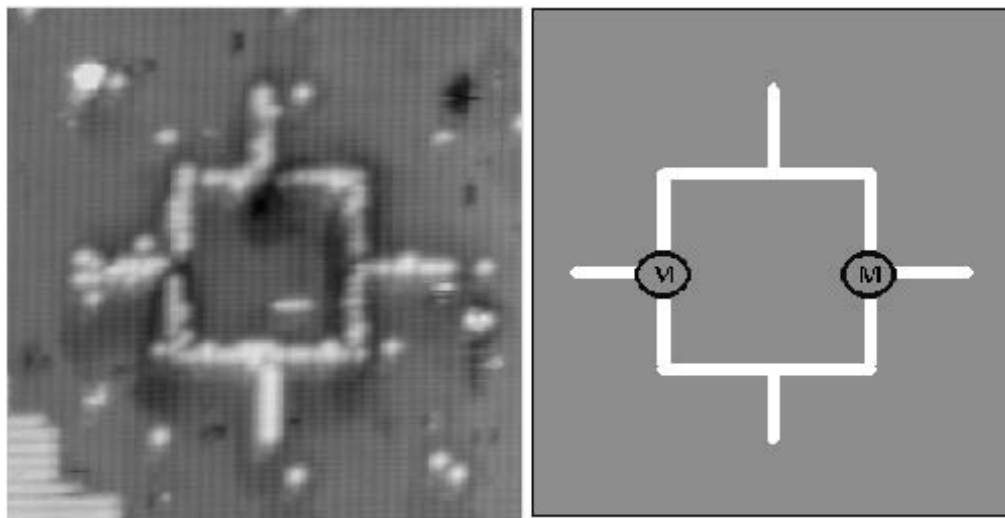


**Figure 61:** (a) 30 nm x 30 nm STM image of the dangling bond pattern of the atomic circuit of an OR logic gate. (b) schematics of the complete OR gate with its 2 molecules for the controlled triode.

In order to demonstrate the feasibility of circuits formed using Si dangling bond lines as surface atomic wires, the atomic circuit of an OR logic gate (similar to the one e-beam fabricated by the Cambridge group (see section IV) was fabricated. Fig. 61a represents an OR logic gate circuit having a total dimension of 20x20 nm and inter-electrode distances of only 2 nm. Molecules can in principle be manipulated inside each atomic scale 3 terminal junction on this surface.

#### **Vd) The Nanostencil: toward an atomic scale technology:**

For interconnecting a single molecule, ideally perfectly clean and crystallographically well defined electrodes at its end is required as demonstrated above. Conventional e-beam lithography produces structures contaminated through the processing steps. But when the electrodes are deposited and defined in UHV, immediately followed by molecular deposition at the required position, no contamination will occur. In this case, the molecule/electrode junction will be atomically ordered and ultra-clean.

The major effort in BUN was to pass from the first in-a-lab demonstration as presented in Fig. 62 to the development of a real machine. The UHV nano-stencil technique combines a tilt evaporation where the material is deposited through a mask and an AFM in non-contact mode. The material passes through the apertures and a pattern is transferred to the substrate surface in the UHV as defined by the shape and the arrangement of the apertures. The mask is defined on a cantilever. The cantilever is programmed to make an arbitrary pattern with respect to the surface. It follows the local surface structure, enabling the device to locate micro and nano-scale features such as mesoscopic-scale interconnects.

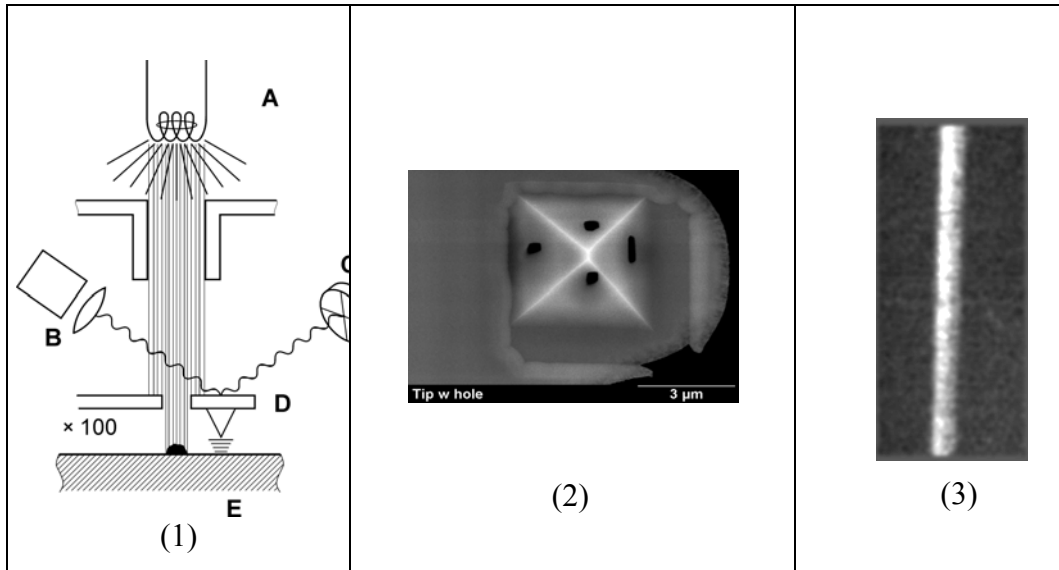


**Figure 62:** Schematic diagram of the nanostencil technique: Material is deposited from a source (A) through a series of collimating apertures. An optical beam from source (B) reflects off an AFM cantilever (D). A position sensitive detector (C) is used to regulate the proximity of the cantilever tip with respect to a substrate surface (E). A series of small apertures in the cantilever (2) define a pattern of deposited material at (E). (3) a first nanostencil result of a 80nm in width metallic nano-wire.

The first nanostencil machine in BUN was built a collaboration between the Zurich and Cambridge group. This machine achieves line width of down to 50 nm using Al deposition and 70 nm using Cu atoms. The shadow mask was generated by using a focused ion beam (FIB) to drill small holes in a commercial AFM cantilever. Fig. 63 shows an example of an AFM Image of 70 nm Cu wires that were directly deposited on CMOS Si. By combining more than one operation junctions are formed as shown in Fig. 63 where two passes of a single aperture formed the junction.

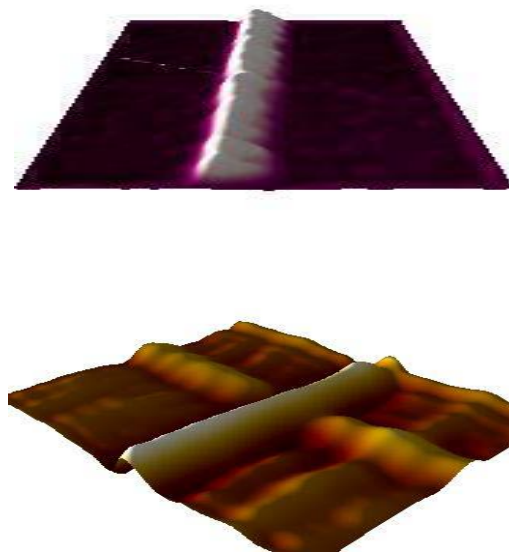


**Figure 63:** 3D AFM image of a 70 nm wide, 30 nm high CU nanowire deposited using an AFM cantilever with a single aperture and of 70 nm high 30 nm wide Cu wire deposited in 2 passes to form a cross junction both on CMOS Si .

In BUN, the Toulouse group had constructed the second generation of a nanostencil machine integrating this time all the micro-tools for multi-pads interconnections in UHV. According to the design the AFM UHV head from Omicron had been totally transformed to leave the access to optics, to the metallic cantilever array for interconnections and to the implantation of a UHV compatible X-Y nano-positioning table. As presented in Fig. 64, the XY table and the XYZ motors for the positioning of the micro-electrodes have been installed on the VT-AFM head.

To achieve nanometer-sized metallic gaps with the nano-stencil method in the UHV requires a two-steps process. A micro scale pattern is first deposited through a static stencil mask. Then, the circuit is completed on the nanoscale, using the dynamic nano-stencil technique. It is essential to limit the region where metallic nanowires have to be deposited by the nano-stencil technique to the smallest possible area in order to delay the unavoidable clogging of the deposition hole in the cantilever.

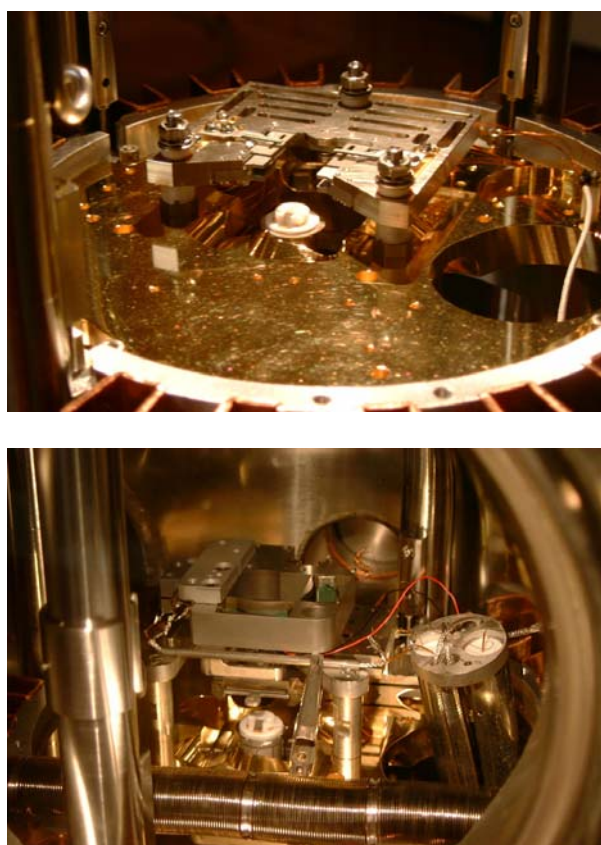


**Figure 64:** The VT-AFM head before and after the installation of the XY table.

Static stencil masks have been fabricated using the expertise gained in ATOM, collaborating with J. Brueger. The two- and four-electrodes patterns which have been elaborated (Fig. 65) are based on a former design of the Toulouse group for two and four-electrodes junctions made by e-beam lithography (see section IV). As it can be seen in the insert on Fig. 65, the area of the central region where the nano-stencil deposition will take place is of the order of  $500 \times 500 \text{ nm}^2$  (Fig. 65). This means that the length of the nano-wire to be deposited will be of the order of  $1 \mu\text{m}$ . Evaporation tests are under progress on these masks.

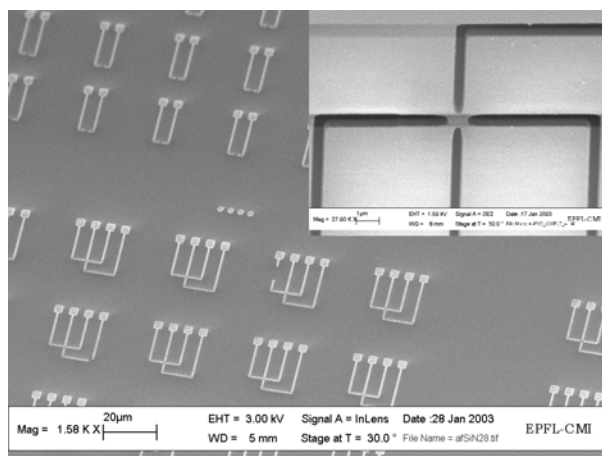


**Figure 65:** Two and four-electrodes stencil masks provided by J. Bruger from the ATOM project.  
Inset : The gap width is of the order of 500 nm in both directions.

The electrical connection of the device to the external world will be achieved by positioning a comb of microelectrodes on the  $3 \times 3 \mu\text{m}^2$  squares that terminate the wires in the mask pattern. The overall size of these patterns is such that it must be possible to keep the device in the shadow of the nano-stencil cantilever during deposition, relaxing the constrain on the focusing of the atomic beam on the cantilever.

In parallel to the transformation of the AFM head for the nanostencil machine, the Toulouse group had tested its ability to NC-AFM image surfaces where the metal patterns will be deposited through the AFM nanostencil and through the larger static mask as presented in Fig. 65. The rutile ( $\text{TiO}_2(110)$ ) surface was used because of its ease of preparation and relatively high reactivity. The possibility to image this surface with STM when the sample is slightly reduced is also useful to control the surface preparation. A lot studied by the Aarhus group in BUN have already been performed. The spatial resolution by NC-AFM is nearly as good as that reached by STM on the same machine (Fig. 66).

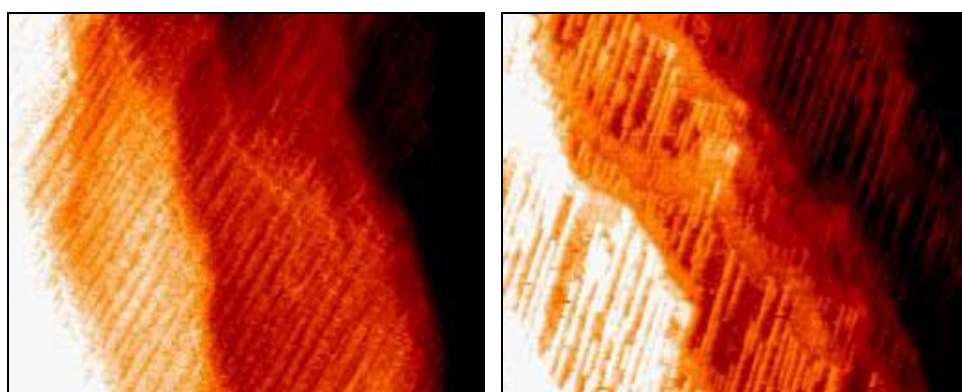


**Figure 66:** (a) NC-AFM and (b) STM image of  $\text{TiO}_2(110)$ . Image size:  $300 \times 150 \text{ nm}^2$

The final goal of the nanostencil machine is to fabricate crystalline nano-electrodes with a well defined epitaxial relation with the underneath crystalline substrate. As now demonstrated in BUN on a metallic surface, this will lead to a much better defined “molecule - metal electrode – surface” system where the imaging and the identification of the adsorbed molecule is facilitated.

## VI) Hybrid molecular electronics circuits

Hybrid molecular electronics circuits are electronic circuits made of molecular devices interconnected by standard metallic wires. Practically, the molecular devices are macromolecular devices made of SWCNT playing the role of the semi-conductor material in a 3 terminal device structure. The interconnecting metallic wires are generally mesoscopic wires around 100 nm in width. Aside from the fabrication of a few devices as reported in section V, BUN focuses its works on the miniaturization limit of the hybrid approach, limitation in the elementary molecular or macromolecular devices and limitation in the circuit design rules. At this point, it must be recalled that the BUN objective was not the fabrication of Hybrid molecular electronic circuits but to open the way to integrate all the functionalities of a calculator (devices, circuits) inside a single and the same molecule.

### VIa) Miniaturisation of the circuit

In BUN, we start with the standard architecture paradigm that each molecular device aside from its molecular or macromolecular character, will look like a standard 3-terminal device as considered from the outside. The wire length of the interconnections is much longer than the electron mean free path. Then, the Kirchoff mesh and nodes circuit laws hold for a mesoscopic circuit. This was very well exemplified by the C. Dekker work using large SWCNT transistors. As recalled in Fig. 67, his team was able to fabricate logic gate, SRAM cell and a ring oscillator where each transistor in the circuit are micron apart.

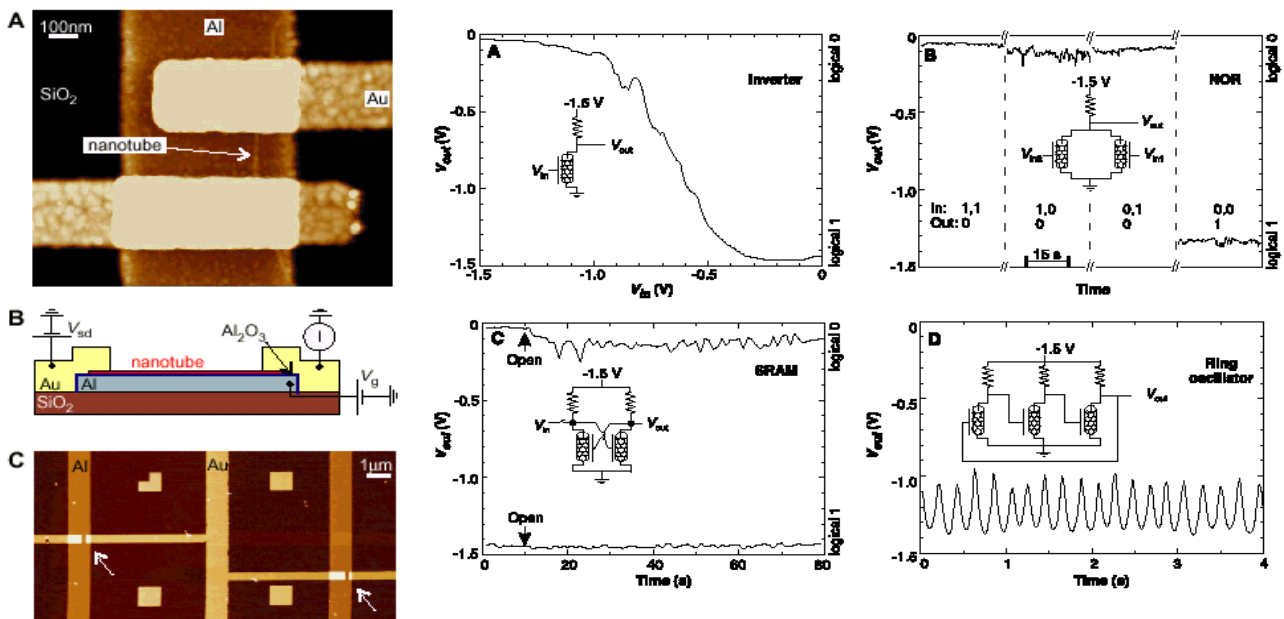
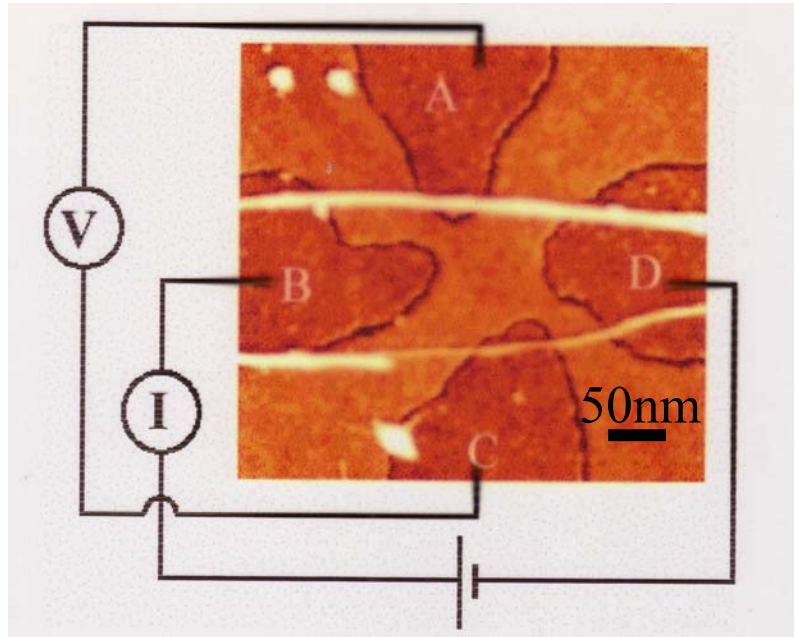


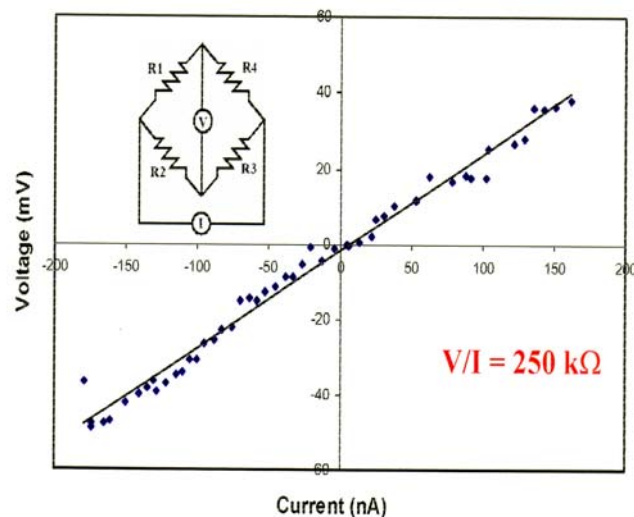
Figure 67: The C. Dekker and co-workers SWCNT transistor micro-circuit.

In BUN, the first practical architecture question we have solved is the limit of application of the standard mesh and node electric circuit laws. For this purpose, the Toulouse group had fabricated simple 4 terminal Wheatstone bridge using 4 mesoscopic electrodes and 2 SWCNT as presented in Fig. 68. The BUN combing technique (see section IV) was used to precisely deposit the 2 tubes in place on this  $N = 4$  mesoscopic junction.



**Figure 68:** AFM image and a schematic of the interconnection used to measure and tune the carbon nanotube Wheatstone bridge.

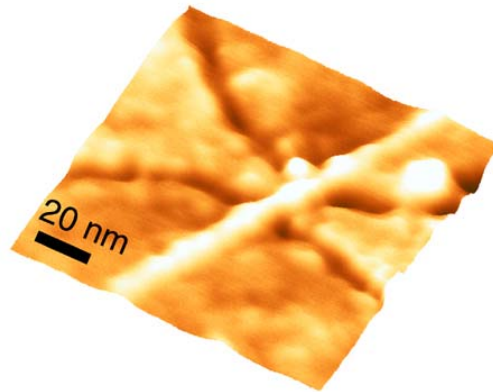
The measurements were performed by interconnecting the 4 electrodes using the Toulouse metallic micro-cantilever technique. The measured bridge resistances are  $R_1 = 570 \text{ k}\Omega$ ,  $R_2 = 20 \text{ M}\Omega$ ,  $R_3 = 16 \text{ M}\Omega$  and  $R_4 = 1,1 \text{ M}\Omega$ . Applying Kirchhoff's laws, the resulting  $V/I$  resistance is  $340 \text{ k}\Omega$ . As presented in Fig 69, the measured resistance is  $250 \text{ k}\Omega$ . The two values are very close, which indicates that down to a few 100 nm in distance, the standard circuit laws of designing electronics circuits are still valid, opening the way to miniaturize further logic circuits in a standard architecture, if necessary or of interest for the technology.



**Figure 69 :** the measured V-I characteristics of the fig. 68 nanotube Wheatstone bridge. After fabrication, this bridge is not tuned. AFM manipulation of the low resistance branches leads to a better equilibration according to Kirchhoff's law. But this required a large torsion of the tube which breaks after the equilibration.

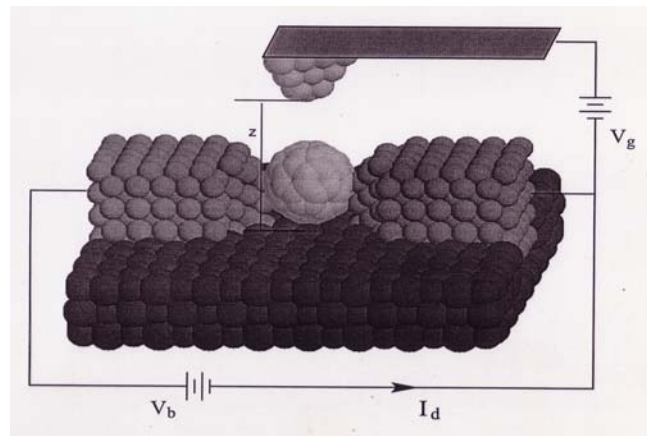
## VIb) miniaturisation of the transistor in an hybrid circuit: the C60 transistor case

After miniaturisation of the circuit in an hybrid version of molecular electronics, BUN look towards the miniaturisation of the transistor device itself. The most accessible experimental device is a SWCNT transistor. In BUN, we have therefore fabricated very small SWCNT transistors with a source-drain distance down to 20 nm as presented in Fig.70 using the BUN combing technique. No gain was measured on those very small transistors.



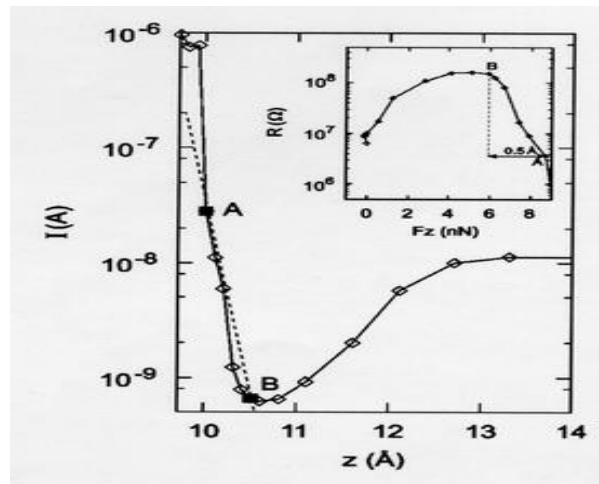
**Figure 70:** An AFM image of the source drain junction of a 20 nm SWCNT 3-terminal device.

To have access to all the problem of circuit architecture while reducing the transistor size down to a few nanometer, we have therefore decided in BUN to return to the single C60 amplifier. Its 3 terminal co-planar version was designed as presented in Fig. 71. To use a standard SPICE electronic circuit simulator, An electronic equivalent circuit was established to emulate all the possible logic function that can be implemented, up to a full processor with more than 400 C60 transistors. The interconnection between the C60 transistors are supposed to be fabricated with standard metallic wire respecting the Ohms law. More important, the equivalent circuit open the way to simulate a dynamic model of the C60 transistor to be able for the first time to test also the response time and clock frequency limits of those hybrid circuit. Notice that such studies were worth to performed because a single molecule transistor, be it electro-mechanic (like the C60) or electrostatic has always a very high impedance and a very low trans-conductance. This imposes specific design rules to reach the targeted logic functions.

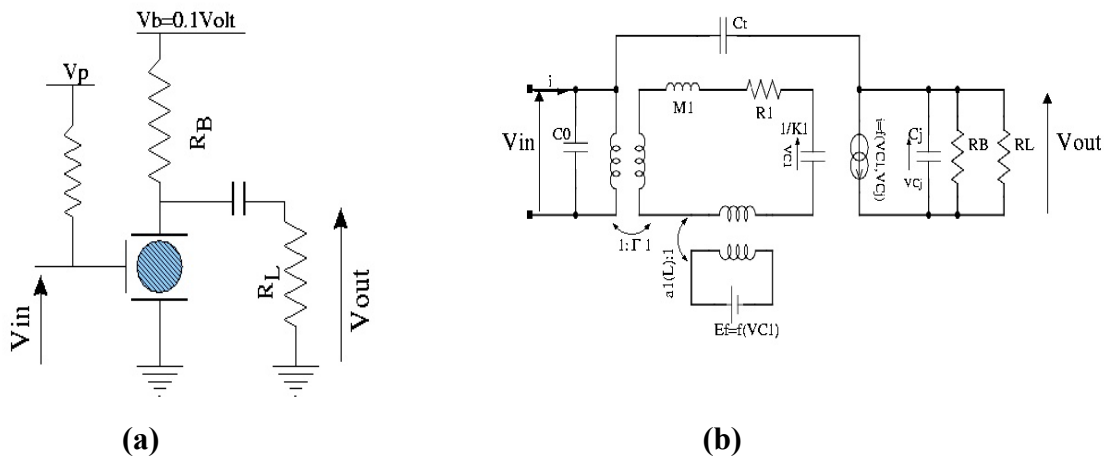


**Figure 71:** the propose implementation of a C60 electromechanical transistor.

A single  $C_{60}$  transistor is made of a single  $C_{60}$  molecule positioned in a nano-junction of gap size 1.25 nm. If the molecule is compressed by the tip on a piezo-electric cantilever, it changes its electronic state and therefore its conductance. The dependence of the current passing through the molecule on the tip position is depicted in Fig.72. If the distance of the cantilever-tip from the electrode where the  $C_{60}$ -molecule is positioned is larger than  $\sim 13 \text{ \AA}$ , then the drain current through the molecule is not affected at all. For positions between 10.5 and 12  $\text{ \AA}$ , the pressure on the  $C_{60}$ -molecule acts as a perturbation creating defect states, thereby diminishing the conductivity of the molecule. In this region the transistor element acts as an inverter. If the molecule is further compressed, its HOMO-LUMO gap becomes filled with defect states and its conductance begins to increase exponentially. In this region the transistor element has only an amplifying effect.



**Figure 72:** Variation of the drain current in the source- $C_{60}$ -drain junction illustrated in Fig.1 as a function of the distance of the cantilever-tip from the surface where the molecule is positioned. The inset shows the ohmic resistance as a function of the force applied to the molecule.



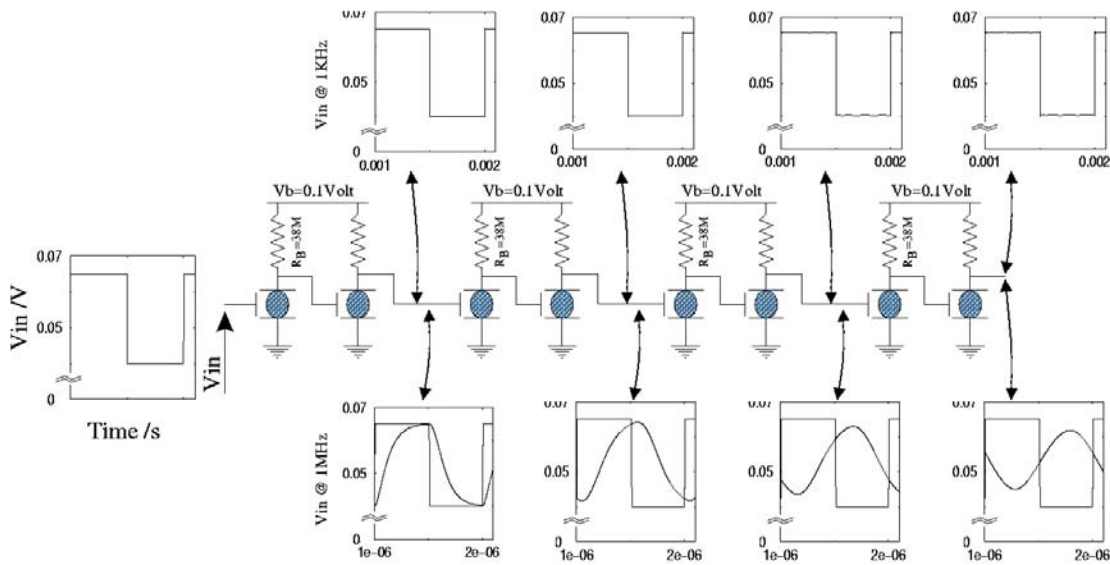
**Figure 73:** (a) Electrical circuit of a  $C_{60}$  transistor, used as a basic element in more complicated circuits in the following chapters. The  $C_{60}$  transistor is depicted as a shaded circle with source, drain and gate electrodes connected to it. (b) Equivalent circuit of the cantilever/ $C_{60}$  system.

Fig. 73 shows circuit diagrams for a single  $C_{60}$ -transistor. All circuit simulations using the commercial electronic engineering software SPICE have been carried out with this basic design, where the piezo-electric cantilever is treated within a equivalent electrical circuit approach, where mechanical forces are transformed into electrical ones.

Apart from its functionality as an electrical resistor in the source-drain-junction, the  $C_{60}$ -molecule enters the circuit as a mechanical resistance to the bending of the cantilever as well, because its mechanical reaction against deformation has to be taken into account as a counter electromotive force  $E_f$  in opposition to the piezoelectric effect in the RLC circuit for the cantilever as is shown in Fig.73 b.

The first logic gate designed in BUN was a NOT-gate. The London group explicitly studied a chain of eight inverters and the result of time-dependant SPICE simulations for two different frequencies are shown in Fig. 74. For a frequency of 1 MHz, the signal decays rapidly, because of RC-time delay. For lower frequencies, the signal proceeds through the gates without distortion..

The top part of Fig. 74 shows a single pulse with a width of  $1.5 \mu s$  travelling through a chain of 20 inverters. From this graph the RC-time delay for a single inverter could be determined to be  $\sim 0.1 \mu s$  numerically by measuring the time between the rising edges of subsequent signals. As illustrated in the lower part of Fig. 74, for a single pulse with a width that equals the time delay, the pulse shape deteriorates rapidly. The RC-time delay is dominated by the resistance of the  $C_{60}$  molecule, which is of the order of  $100 M\Omega$ , and the capacitance of the cantilever, which is of the order of  $10^{-15} F$ . When these two numbers are multiplied, the result for the RC delay ( $\sim 0.1 \mu s$ ) is indeed consistent with the numerical values from the SPICE simulations.



**Figure 74:** Schematic and SPICE results for a circuit of 8  $C_{60}$  transistors in series for signal frequencies of 1 kHz (top) and 1 MHz (bottom). The contact point is at 10.6 Å, the cantilever dimensions are  $l=200$  nm,  $b=50$  nm,  $h=35$  nm and the pull-up resistance  $R_B=38 M\Omega$ .

For real devices the clock period must be at least 10 or ideally 20 times as large as the RC time delay, which therefore limits the bandwidth of the system to less than 1 MHz. Since the capacitance of the cantilever depends on its dimensions and the resistance of the  $C_{60}$  molecule on the chosen contact point, which both might be different for transistors with different functionality's within a complex circuit, the clock frequency might be further reduced by the necessity to synchronise various parts of the architecture.

A very common test piece in electronic engineering is a chain of inverters in series, where the output of the last one feeds the input of the next one in a loop. If a single pulse is sent through this system and if the time delay of the chain is long enough with respect to the pulse-width, then this should result in an output that consists of separated pulses. Such a ring oscillator was tested experimentally with SWCNT transistor at the mesoscopic scale (see above in this section). It was therefore important for BUN to test how a ring oscillator continues to work with real nanoscale molecular transistor.

In Fig. 75 a ring of inverters with  $C_{60}$  transistors is presented. We have tested such a ring up to a chain-length of 51 inverters. Even with 51 inverters and with a cumulative delay of  $\sim 5 \mu\text{s}$ , the residual effects of the RC time constant delay can be seen as a significant rounding-off of the pulses. Hence, this circuit would only be effective at a frequency lower than 200 kHz.

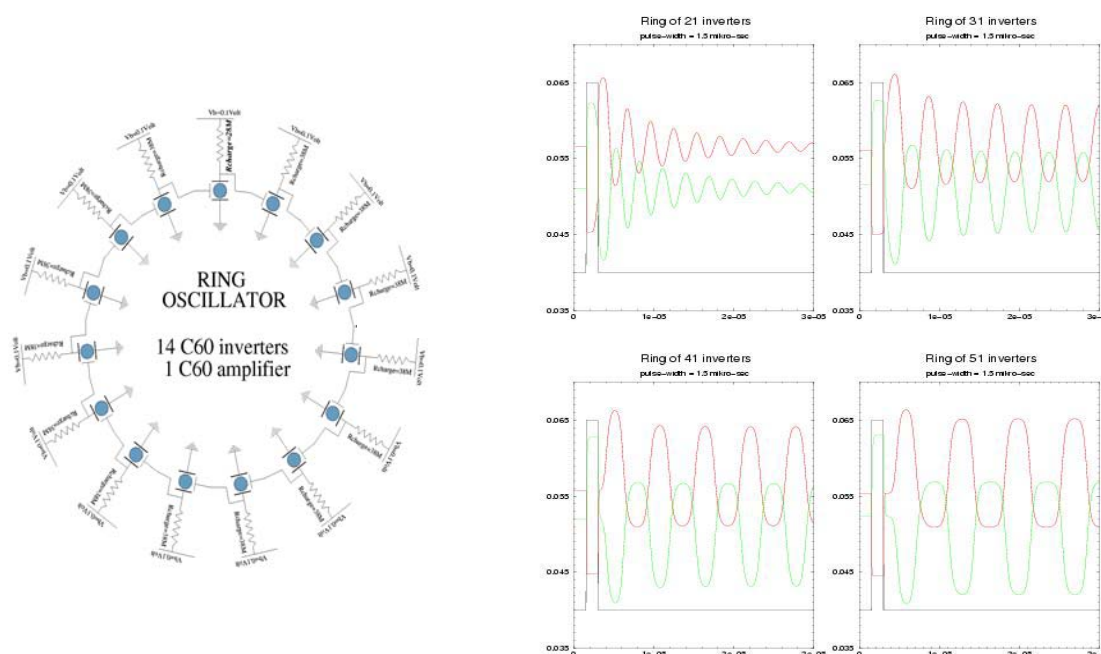


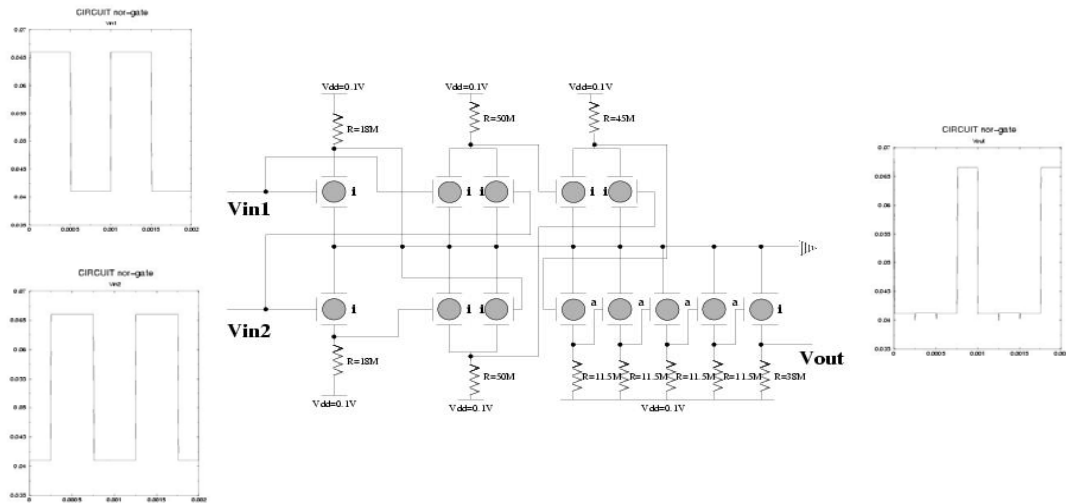
**Figure 75:** SPICE-results for a single pulse moving through rings of 21, 31, 41, and 51 inverters with the same specifications for cantilever dimensions, contact point and pull-up resistance as in Fig. 41. The input pulse is shown as a black line, the output voltage of the 1<sup>st</sup> and 2<sup>nd</sup> inverter as red and green lines, respectively.

Another important property of any logic device is its ability to pass on its output to a large number of subsequent devices in parallel. This number is called fan-out. We have shown in BUN that a fan-out of 30 can be reached with a  $C_{60}$  transistor. Although a fan-out capability of 30 is acceptable for many real circuits, any inverter connected in parallel increases the rise time of the signal by a proportional amount and therefore reduces the bandwidth – for example, a fan-out of 10 reduces the bandwidth from  $\sim 1$  MHz to about 100 kHz.

Larger logic circuits have been designed and tested by the London group in BUN. One of the main dilemmas that had been solved was that output logic levels are in general not compatible with input logic levels of the next logic gate in the circuit due to the high impedance of the molecular transistors used. A way out of this dilemma has been found at UCL by introducing additional degrees of freedom into the circuit. The basic idea was to have three units with two inverters in parallel, where the first unit is fed by the two input signals and the second by signals inverted with respect to the input. Both outputs have three logical levels and are

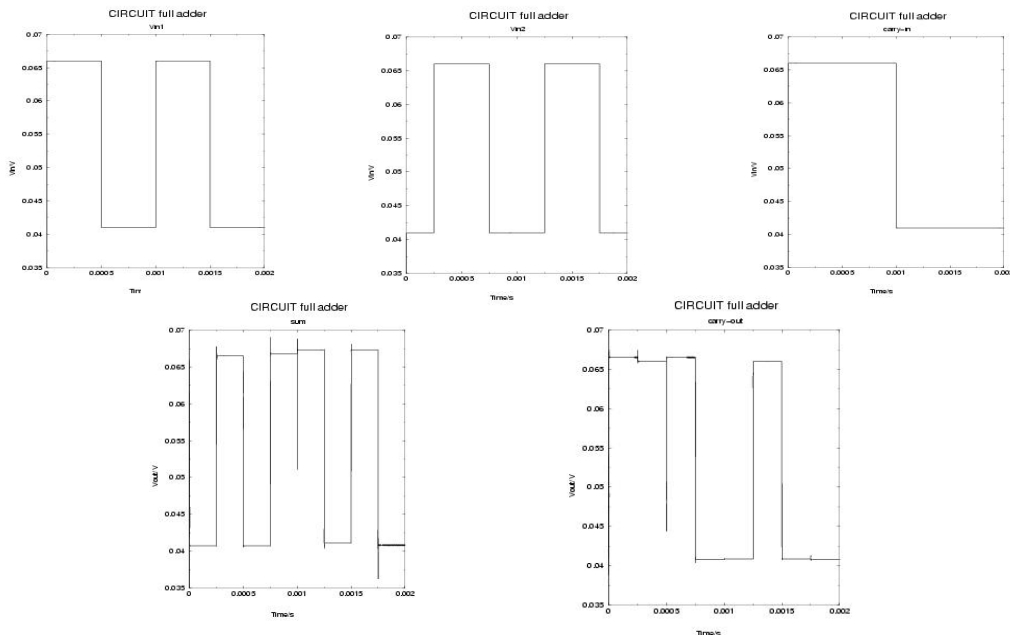
passed through the third two-transistor units, where the lowest and middle level become identical if the values of the resistance for the pull-up resistors are optimised. Since the voltage amplitude of the signal decreases by going through this process, the output must be led through amplifying inverters.

Fig. 76 shows a schematic picture of a circuit for a NOR-gate designed by the London group along these lines with the corresponding SPICE-simulations. The middle logical level has now vanished and the upper and lower level of the output correspond to the same voltages as in the input. XOR and AND gates can be designed following the same principles by adjusting the values of the pull-up resistors. Notice that compared to a solid state transistor technology, there are now 13 C60 transistors instead of 3 to implement the NOR gate.



**Figure 76:** Circuit diagram for a NOR-gate based on C<sub>60</sub> transistors.

Fig. 78 shows how a 1-bit full adder can be implemented with such two-input gates. The SPICE results for this circuit are presented in Fig. 77. The spikes in the output are due to the overlap of rise and fall times of signals that have passed through a different number of gates..



**Figure 77:** SPICE results for the 1-bit adder model in Fig. 78

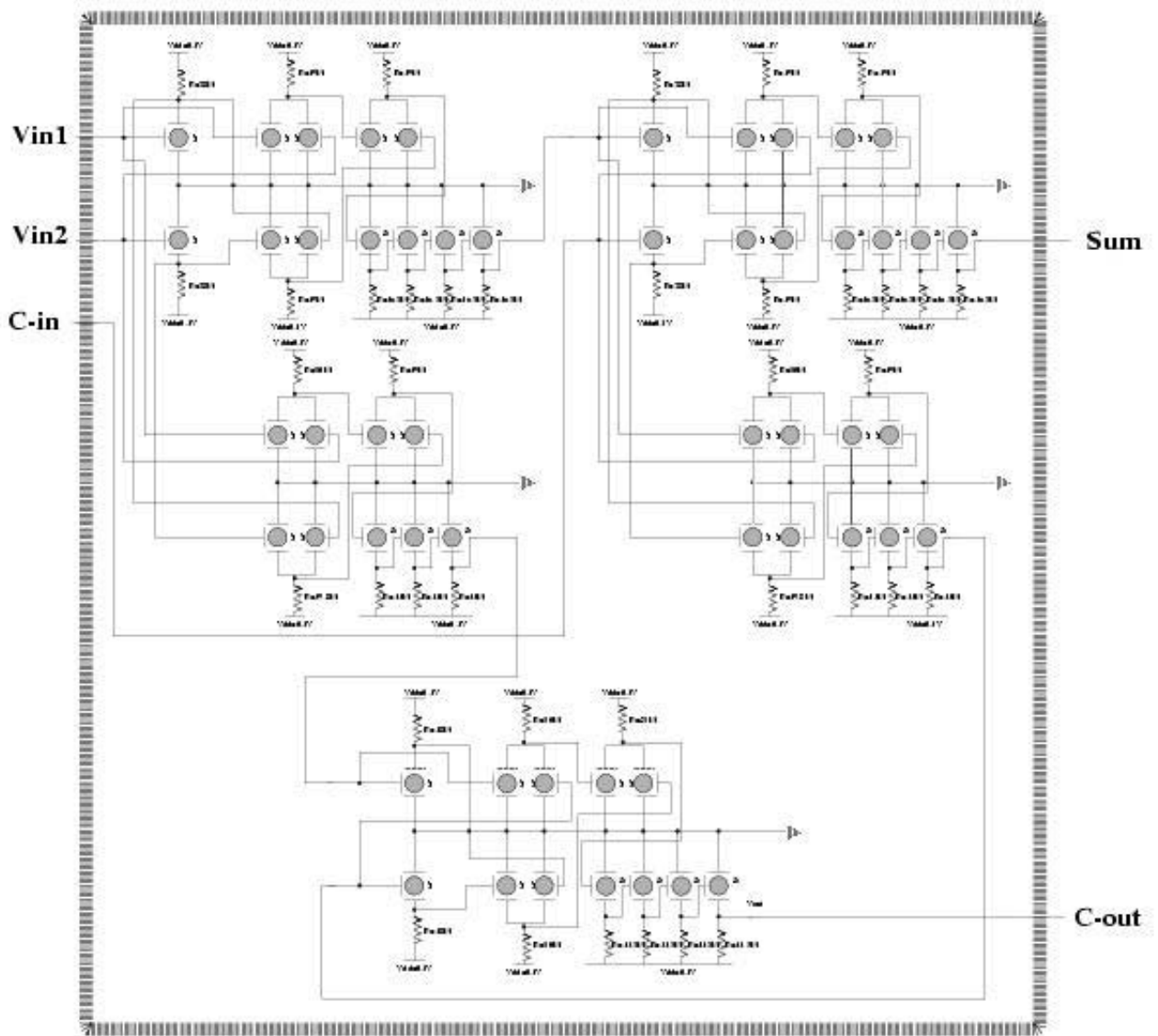
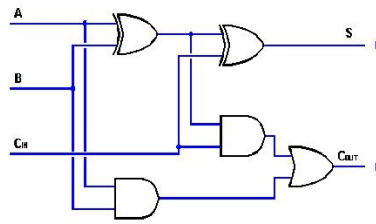


**Figure 78:** Circuit diagram for a 1-bit adder with the detailed outline showing the C<sub>60</sub> transistors, resistors and interconnections involved (on top schematic representation showing the XOR, AND, and OR gates involved)

For the information transfer between memory bits and logic units, registers or latches are needed for temporary storage. A circuit diagram for a clocked D-latch is shown in Fig. 79. It contains 78 transistors. A D-latch incorporates two RS-latches or flip-flops, which consist of two NAND-gates each. The connections to the clock need two AND-gates each as well, which makes a total of eight two-input gates.

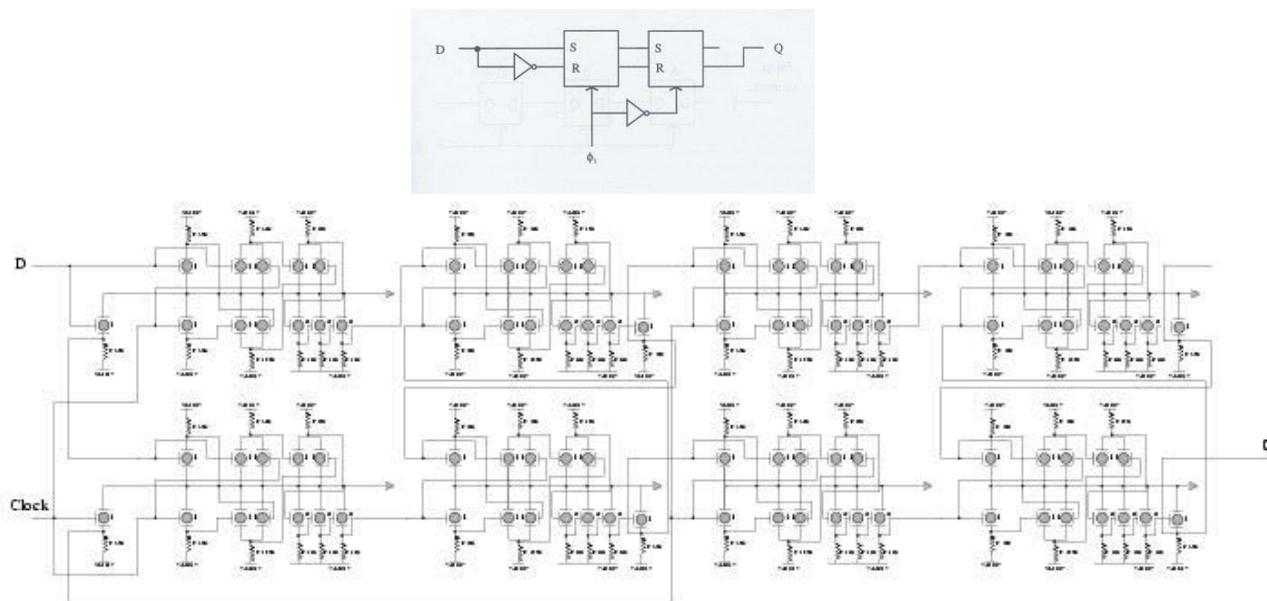


**Figure 79:** Detailed outline of the circuit diagram for a clocked D-latch with C60 transistors (top: schematic representation).

This work has been extended with the simulation of full small processor able to add two 2-bit words. Fig. 80 shows a schematic representation of a memory/adder model. Four bits of information are read from four different memory cells. They are combined to give two 2-bit words by OR gates, which pass the words through registers to a serial adder. The output of the addition moves through another register, from where it can be written on a memory or used in a subsequent computation. Since in a serial adder the carry-out is used as carry-in when the next significant bits are added, the addition involves a clocked RS-latch to store the carry between two steps.

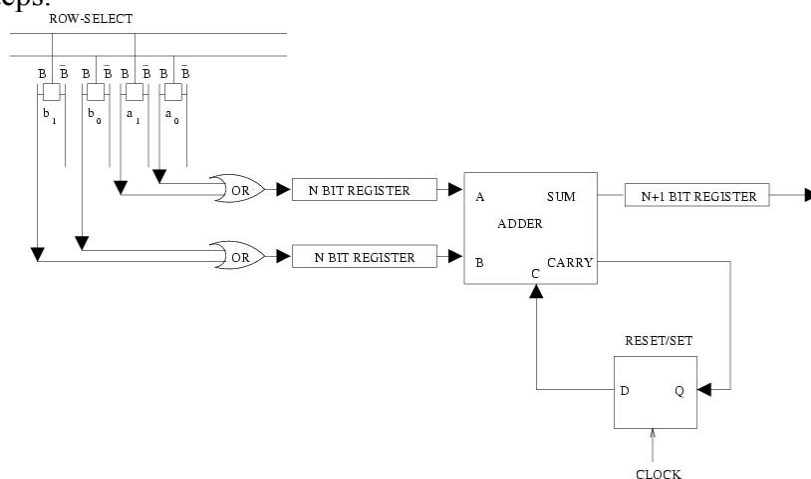


**Figure 80:** Schematic diagram of a memory/adder model. The arrows indicate the directions in which the signals move.

In Fig. 81 a detailed circuit diagram is presented with the 464 C<sub>60</sub> transistors used, also showing the power supply, ground connections and clocking. The RC time delay along the wires was also considered, but was found to be several orders of magnitude smaller than the time delay that arises from the capacitance of the cantilevers compressing the C<sub>60</sub> molecules.

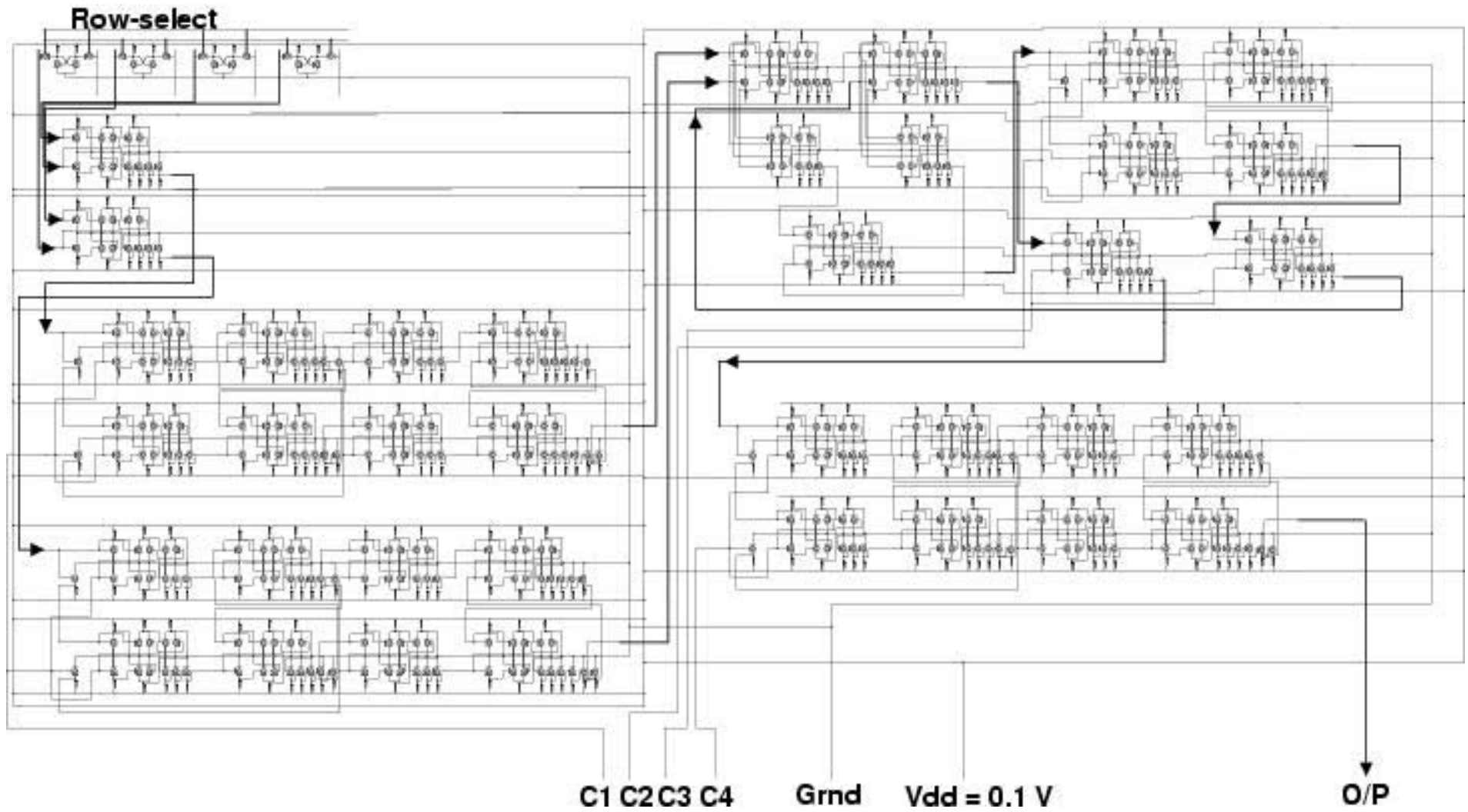


**Figure 81:** Detailed outline of the circuit diagram of a microprocessor with 464 single  $C_{60}$  transistors.

The binary addition  $11 + 11 = 110$  performed with the circuit Fig. 81 has been simulated with the electrical circuit software SPICE, and the results for all stages of the computation are shown in Fig. 82. Although the input read from the memory cells (Fig. 82a) does not have the same logical levels as the logic gates by construction, the signal levels come close to the optimised values after the first OR gate (Fig. 82b) and become equal to them after the signals move through the input register (Fig. 82d).

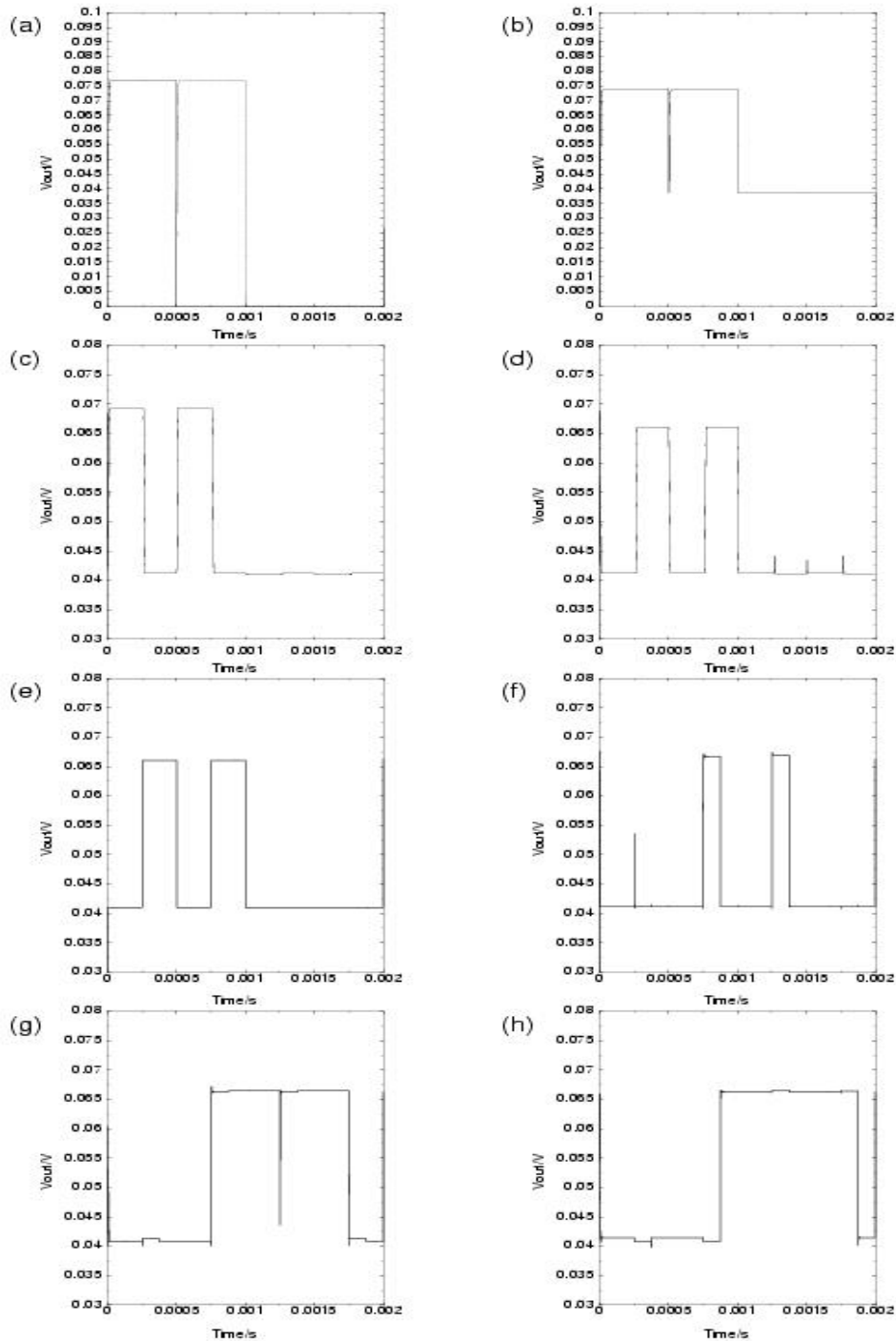


**Figure 82:** SPICE simulation of the addition of two 2-bit words: (a) input of the OR gate in figure 1, (b) output of the OR gate (c),(d) the signal passes through a register from the OR gate to a serial adder, (e),(f) the addition is performed, (g),(h) the output of the addition is passed through another register.

The pulse width of one bit of the signal is reduced by a factor of four during the addition (Fig. 82 e,f) due to the nature of the clocking scheme, but regains its original value again in the output register (Fig. 82g,h) and the output can therefore be directly passed on to be written on memory cells or used in a subsequent computation.

### VIc) Limitations of an Hybrid molecular electronics approach

In BUN, we have studied the principal limitations of an hybrid approach: trans-conductance limitation, power dissipation and breakdown electric field in case of a 3 terminal fully electronic molecular transistor. Table I provides a summary of recent 3-terminal devices whose characteristics are accessible experimentally or have been calculated. At least one dimension of their molecular channel is very small, down to the nanometer scale. The physical effect giving rise to a gain is the increase of the electronic transparency of the metal-molecule-metal source-drain channel induced by a mechanical effect or by an electric field applied to the channel.

	Year	Transcond.	ON resist.	Frequency	Surface size
C <sub>60</sub>	1997	3.9 $\mu\text{A/V}$	500 K $\Omega$	< 100 MHz	10 <sup>4</sup> nm <sup>2</sup>
SWCNT	1998	1.0 $\mu\text{A/V}$	1 K $\Omega$	< 1 KHz	10 <sup>4</sup> nm <sup>2</sup>
HS-C <sub>6</sub> H <sub>4</sub> -SH	2000	0.75 $\mu\text{A/V}$	12.7 K $\Omega$	?	10 nm <sup>2</sup>
NaI	2001	0.07 $\mu\text{A/V}$	150 KW	?	10 nm <sup>2</sup>
HS(C <sub>6</sub> H <sub>4</sub> ) <sub>2</sub> SH	2001	0.2 $\mu\text{A/V}$	600 M $\Omega$	?	?

**Table I:** a summary of the devices characteristics of the main molecular nanomaterial transistors in an hybrid technology. In red are the measured characteristics of some of these devices. (C<sub>60</sub> from C. Joachim, SWCNT from C. Dekker, HS-C<sub>6</sub>H<sub>4</sub>-SH and NaI from N.Lang and HS(C<sub>6</sub>H<sub>4</sub>)<sub>2</sub>SH from E. Schön). Source-Drain voltage were taken at 50 mV, 1 V, 10 mV, 10 mV and 400 mV respectively.

For a macromolecule like a SWCNT, the 3-terminal device works mostly like a FET, playing with carriers population and metal-semiconductor barriers at the SWCNT-electrode interfaces. For small molecules and with no grid applied, the 2-terminal device is usually in a low transparency state because in this case, the electrode Fermi level is located in the Homo-Lumo gap energy range of the molecule. Shifting the molecular orbitals by a grid effect results in an increase of the transparency of the source-drain junction. But such a transparency increase does not guaranty a high gain. For this to happen, the power of the signal used to shift the molecular orbitals must also be much lower than the power of the output signal. This is not always the case because of the high impedance of most of these devices. They suffer from a low transconductance and an ON channel impedance which precludes the expectation for those devices to work at high speed. Furthermore, the overall wafer surface occupied by such devices is usually very large since the physical effects of the grid are not intrinsic to the molecule but results from the action of an external force driven by a macroscopic electrode.

The Fig. 83 presents the decrease of the switching energy of a switch over the years, whatever the technology of this switch. Low power dissipation is clearly a very attractive feature of a single molecular transistor or switch. It had been measured in BUN that the leg porphyrine

switch is very well down a standard solid state transistor in switching energy (see section III). It had also been calculated in BUN that the power dissipation for a NOT-gate based  $C_{60}$  electromechanical transistors is only 0.13 nW at 1 MHz, which is 30 times lower than what can be reached with CMOS at the same frequency and a comparable voltage supply. Still a molecular switch is interacting with at least one thermal bath: the surface supporting the device. Therefore, its switching energy will be bound from below by  $kT \log 2$ . Exploring this limit is very important for hybrid molecular electronics.

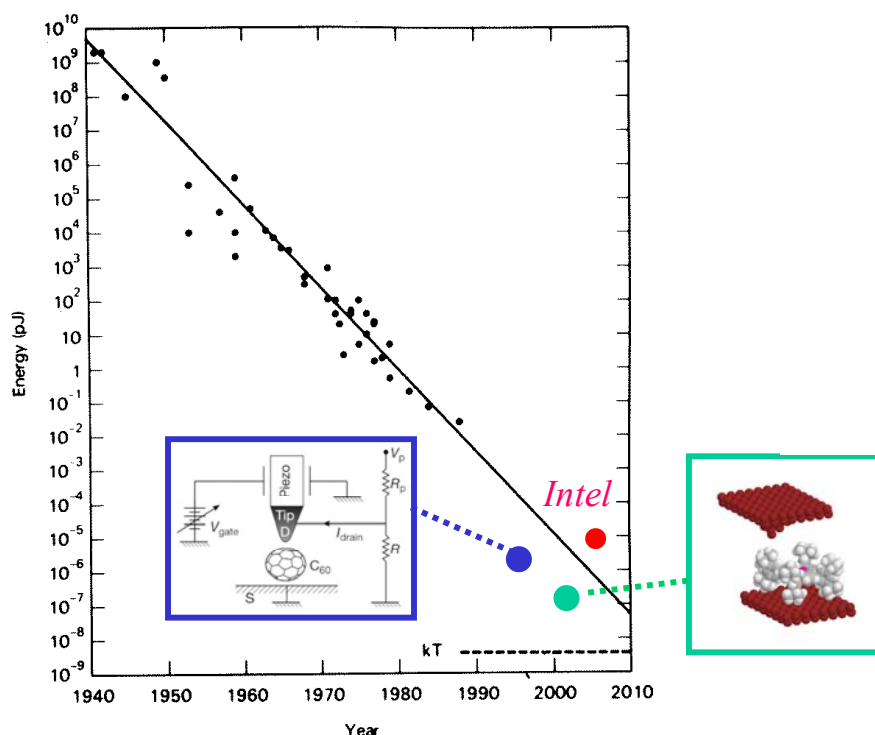


**Figure 83:** the switching energy required by a device all along the years. The  $kT \log 2$  limit is indicated together with the  $C_{60}$  estimated value, the measured Cu-TBP value and the estimated value for the new Intel THz solid state transistor announced at the end of 2001. The data collection on the others devices are from R.W. Keyes (IBM).

However, for a  $C_{60}$  transistor, the power dissipation advantage can only be used if architectures are constructed that operate at 1 MHz or higher frequencies. In BUN, it was also shown that a square wave signal passing through a chain of eight NOT-gates decays rapidly at a frequency of 1 MHz but is undistorted at 1 kHz. The RC-time delay ( $\sim 0.1 \mu s$ ) of a  $C_{60}$  electromechanical transistor is the product of the resistance of the  $C_{60}$  molecule in the compression range defined by the input gate voltages, which is of the order of 100 M $\Omega$ , and the capacitance of the cantilever for this case, which is of the order of  $10^{-15}$  F. Since it is necessary to synchronize various parts of the architecture for real devices, the clock period must be at least 10 or 20 times as large as the RC time delay, which therefore limits the bandwidth of the system to less than 1 MHz. For SWCNTs in an electric field even higher values for the resistance and capacitance ( $R \sim 10$  M $\Omega$ ,  $C \sim 10^{-14}$  F) are to be expected compared with the  $C_{60}$  based device if semiconducting nanotubes are used.

A comparison with current CMOS devices ( $R \sim 0.01$  M $\Omega$ ,  $\sim 2 \cdot 10^{-16}$  F) shows that although the capacitance is higher in hybrid-molecular devices (a factor of 10 for  $C_{60}$  molecules in an electromagnetic grid, two orders of magnitude for SWCNTs in an electric field), it is the high resistance of hybrid-molecular transistors that mainly limits the clock frequency at the device

level. This resistance is not only defined by the conductance of the molecule as a passive device, as in a molecular wire, but also by the requirements of compatible input and output voltages.

In mono-molecular electronics (see section VII) no interplay between the molecule and the grid would be needed inside a circuit. The states of the molecule would still have to be addressed from outside for reading in initial inputs and writing out final outputs. But the speed of a signal passing through the intermediate states of a computation would be limited only by quantum mechanical processes such as tunnelling therefore by the minimum detectable current level. The dimensions of a  $C_{60}$  electromechanical transistor are limited by the length of the cantilever, which has to be larger than  $\sim 100$  nm in order to compress the  $C_{60}$  molecule efficiently. If this is compared with the minimum feature size of CMOS today ( $\sim 150$  nm) and extrapolated to 2012 ( $\sim 50$  nm), the  $C_{60}$  circuit architecture will not be able to compete nor other hybrid molecular transistor.

Quite recently, 4-terminal nano-junctions have been fabricated where two electrodes act as source and drain bridged by a SWCNT and the other two electrodes are used to apply a local electric field. By changing the field the conductance of the molecule can be varied and the whole set-up can be used as a hybrid-molecular transistor. Although device densities of only  $0.1$  Mbit/cm<sup>2</sup> have been experimentally realised, in principle  $100$  Mbit/cm<sup>2</sup> could be achieved. This would still not reach the densities that are expected for CMOS technology in the near future ( $475$  Mbit/cm<sup>2</sup> for SRAM memories in 2006). Wherever electric fields are considered as the 'non-molecular' part of a hybrid-molecular device, the field strength has to be large enough to change the conductance of the molecule inside the nano-junction. Since the field strength depends on the area of the electrodes, there is a natural limit to the minimum feature size of the device for each choice of a particular molecule (see below the experimental part of nano-junction breakdown effects). Therefore, we can conclude that on the device level there are fundamental limits for the miniaturisation of hybrid-molecular electronics, which are governed not by the size of the molecule but rather by the size that an electromechanical or capacitive grid must have in order to influence its energy levels. For an intra-molecular circuit, where the energy levels of a functional group would be addressed inside a molecule, these limits would not occur and the device density would be determined by the size of the molecule.

This breakdown field effect was deeply studied in BUN. According to Table I, a way to increase the trans-conductance of an hybrid molecular device is to used high electric field for the grid effect. This seems to be compulsory for small molecule where the electric field is supposed to change the Homo-Lumo gap of the molecule. This requires extremely large electric field.

In order to test this limit, we have performed in Toulouse a systematic study of the electric field breakdown of planar nano-junctions as a function of their size. For electrodes separations in the millimetre range and larger, the voltage threshold is well described by the end of the 19 century Paschen's law. D. Germer and more recently P. Torres investigated smaller dimensions (down to 500nm). They have found large deviations from the Pashen's law. We extended this study down to 5 nm electrodes separations. The nano-junctions were contacted using our micro-contactor set-up while imaged permanently by AFM during the experiment. This allows us to follow in real time the modifications of the electrodes as a function of the applied voltage. The results of a typical experiment on a 11nm nano-junction are reported in Fig. 84.

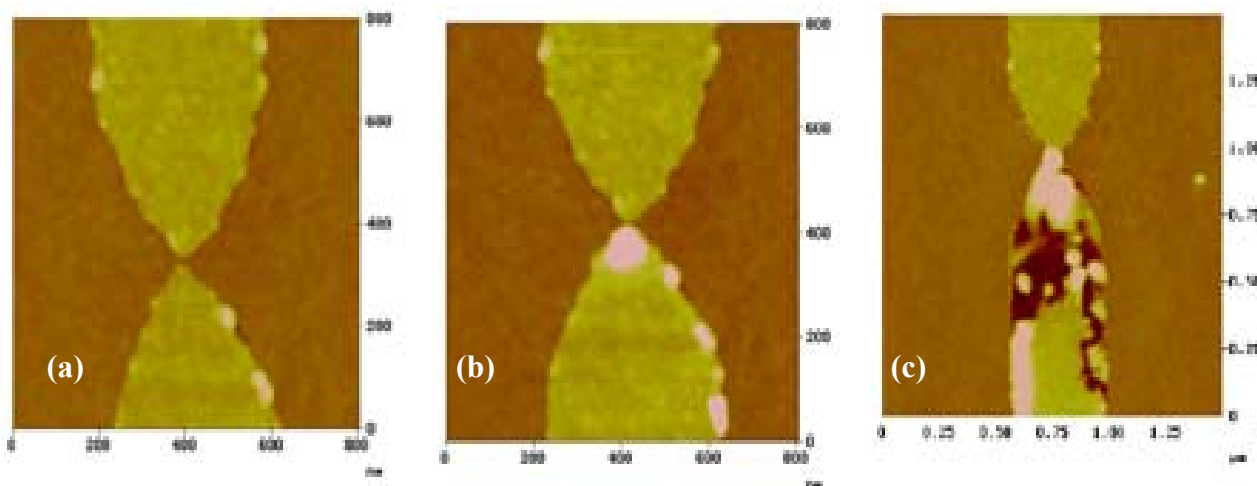


**Figure 84 :** AFM images of a 11 nm nano-junction (a) before any bias voltage have been applied, (b) after the accumulation process at low bias voltage (c) after breakdown at a larger voltage.

Two different regimes are identified in air: (i) when the applied voltage is slowly increased, a small bump suddenly appears at the end of one electrode, probably due to an accumulation of matter resulting from the large electric field. (ii) When the voltage is increased further, a dramatic breakdown occurs leading to the destruction of one electrode and of the silica in the gap. The electrode being destroyed depending of the bias polarity.

The measured accumulation and breakdown voltages are reported in Fig.85 below. They show how the threshold voltage increases linearly with distances. The good agreement between the resulting electric field and the electric field strength of silica suggests that the breakage occurs in the silica between the electrodes. This gives the order of magnitude of the maximum voltage that can be applied to a nano-junction without breaking it. For example, a 2 nm nanojunction can not support bias voltages larger than 3V.

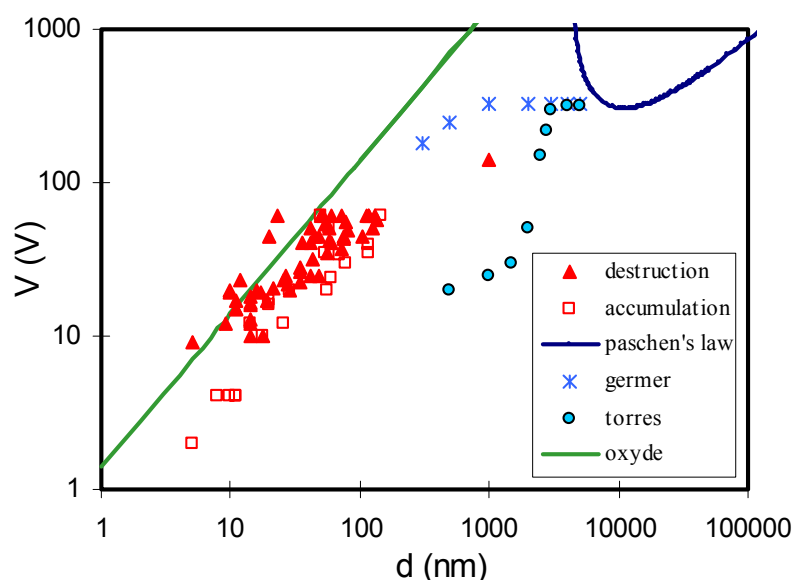


**Figure 85:** Voltage threshold measured on nanojunctions compared with Paschen's law, oxyde breakdown and previous measurements of Germer and Torres.

A molecular nano-FET with high gain based on an electric field effect to change the position of the molecular electronic level of the canal would be at the stability limit of the junction for junction below 5 nm. There is here a limit of reliability which will be very hard to overcome for an hybrid molecular electronic technology.

## VII) Mono-molecular electronics circuits

Mono-molecular electronics circuits are electronic circuits integrated inside a single molecule. In principle and in this fully miniaturised approach, a single molecule is an electronic circuit by itself. This mono-molecular approach was explored by BUN with the prospect to improve reliability and to solve the assembling cost at the molecular scale. Like for the invention of the monolithic approach in the 60's for solid state electronics, it will be very costly to assemble many molecules at the good place on a pre-defined circuit of the Hybrid molecular electronic approach and self assembly will reduce a lot the reliability of the full circuit. To explore this new mono-molecular approach foreseen by F.L. Carter in the 80's, the BUN strategy was three folds: to explore more the tunnel transport regime, to develop a true intramolecular circuit simulator and to start the experimental approach by experimenting on intramolecular switches at the atomic scale.

### VIa) The tunnel transport regime

When a molecule is closing an electrical circuit, the metal-molecule-metal junction is like a leaky capacitance. The leakage conductance  $G$  varies following a  $G = G_0 \exp - \Gamma L$  decay law with  $L$  the distance between the 2 electrode in the junction. For time independent current measurements, the physics of the electron transfer through the molecule and of the tunnel junction is all summarized in  $G(E_f)$  and on its variations over the bias voltage.  $G_0$  is the so-called contact conductance and  $\Gamma$  the inverse decay length.  $\Gamma$  is usually very large of the order of  $0.2 \text{ \AA}^{-1}$  for a conjugated molecule. For a molecule longer than 10 nm, it will be very difficult with such decay to pass a measurable current through a long molecular wire. So, where this fast decay comes from and how to control it? The theoretical work in BUN over those 3 years on this decay problem was first to secure a mono-electronic approach for  $G$  and then to identified the controlling parameters of both  $\Gamma$  and  $G_0$ .

For the mono-electronics  $G(E)$  calculation problem, all calculation techniques are now based on a scattering matrix approach either via a spatial propagator or via the Green function techniques where the Green function is essentially the kernel of the spatial propagator. On usually calculated the Transmission coefficient  $T(E)$  through the full junction and gets  $G(E)$  via the Landauer formula. In BUN we have improved the ESQC technique introduced by the Toulouse group 10 years ago by exploring self-consistent quantum chemistry approaches instead of semi-empirical techniques like EHMO. This started by the experimental fact that the I-V conductance spectrum calculated by the EHMO-ESQC spectrum is very close to the experimental spectrum compared for example to a multi-excitation MNDO-ESQC spectrum. Therefore, the Toulouse group had developed the concept that among all the possible excitations a tunnel electron can create in the molecule electron cloud, only a small number can contribute to  $G(E)$ . This is a sort of super-selection rule due to the fact that after an electron transfer event, the state of a tunnel electron will decoher on the reservoirs defined by the electrodes. One consequence is that any precise tunnelling current intensity calculation beyond the mono-electronic precision will require a determination of this selection rule. Another consequence is that the experimental peaks observed in a  $dI/dV$  tunnel spectrum are not exactly corresponding to mono-electronic states of the molecule. They correspond to states dressed by the  $n$ -electrons excitation of the electronic states and filtered by the decoherence process occurring inside the electrodes.

To demonstrate this hypothesis, the Toulouse group used a very simple model of a tunnelling process through a model system made of a full (2 electrons) ground state and an empty excited

state. Such a 2-level system interconnected to a source of electrons delivering one electron at a time has 12 possible excitation states as presented in Fig. 86. This means that the full  $T(E)$  spectrum of the system looks like the one presented in Fig. 86 with 12 resonant or anti-resonant peaks and a difficulty to recover a mono-electronic like Homo-Lumo gap.

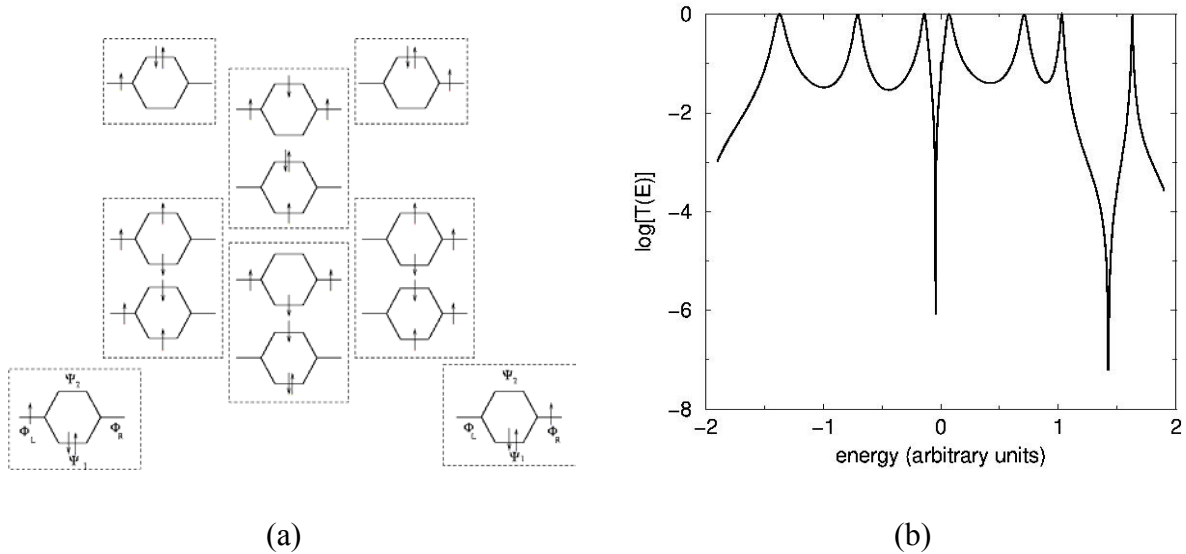


**Figure 86:** (a) representation of the 12 possible electronic excitation of our model 2-level system under the excitation of a single electron transfer event defined by the electrodes. (b) the full  $T(E)$  spectrum calculated from the (a) configuration using the same weight for each configuration. This results from a multi-excitation ESQC calculation.

In the mono-electronic approximation that everyone uses at present, the  $T(E)$  spectrum will simply present 2 peaks corresponding to the Homo and the Lumo of this system (Fig.87). Performing a simple effective Hamiltonian transformation of this full multi-excitation spectrum on a target state space corresponding only to the 2 n-electronic states with a highest weight on the descendant of the Homo and Lumo mono-electronic states, we get a new spectrum with 2 peaks but with a different conductance (Fig. 87). This shows that a specific transformation of the full n-excitation spectrum is able to approach the intuitive experimental result. Certainly, we have not yet found the full transformation adapted to the tunnel decoherence effect on the reservoir. But this shows the robustness of the mono-electronic approach.

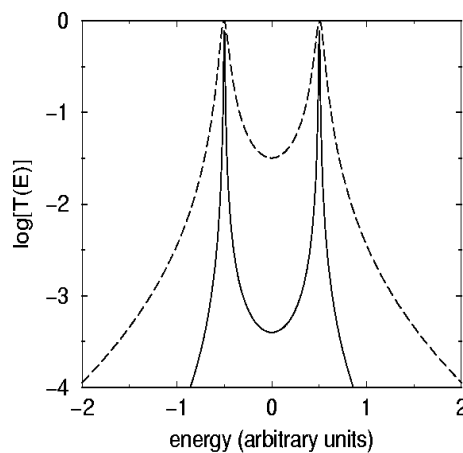


**Figure 87:** the dashed curve is the mono-electronic  $T(E)$  spectrum of our simple model 2-level system and the continuous one the  $T(E)$  spectrum after the effective transformation of the full  $T(E)$  spectrum given in the Fig. 34b below.

Returning to the mono-electronic approximation, the Toulouse group had demonstrated that the inverse decay length  $\Gamma$  can be written analytically:

$$\Gamma = [(8\pi^2 m^*(E)/h^2) (E_l - E) (E - E_h) / \chi ]^{1/2}$$

Aside from the standard dependence of  $\Gamma$  on the homo-lumo gap of the molecular wire, the interesting part of this formula is the  $m^*(E)$  effective mass of the tunnelling electrons. Near the Fermi level, the Toulouse group had demonstrated that  $m^*(E)$  is the curvature of the complex valued band structure of the molecular wire. This complex valued band structure is calculated using the analytic expansion of the molecular wire Hamiltonian, a mathematical technique introduced in the 50's by W. Kohn for low gap semi-conductor. We have calculated a lot of effective mass, showing that tunnelling electrons through the conjugated organic molecules considered up to now as good molecular wires have very heavy tunnelling electron. Consequently, their respective  $\Gamma$  is very large.

Interacting with 2 electrodes, the number of molecular orbital contributing to  $G_0$  and  $\Gamma$  is very small. We have extracted this number as a function of the length of the molecular wire. This was performed by identify the molecular orbitals per categories and by recalculating the  $G = f(L)$  curve for each selected molecular orbital. This work is tedious because of the destructive and constructive interference effects. It is facilitate by the ESQC technique which permit at the molecular wire Hamiltonian diagonalisation step to suppress molecular orbitals at wish. The Fig. 88 presents the series of molecular wires chosen for this study. It is essentially the central molecular wire on the Lander series extended to very long members of the series.

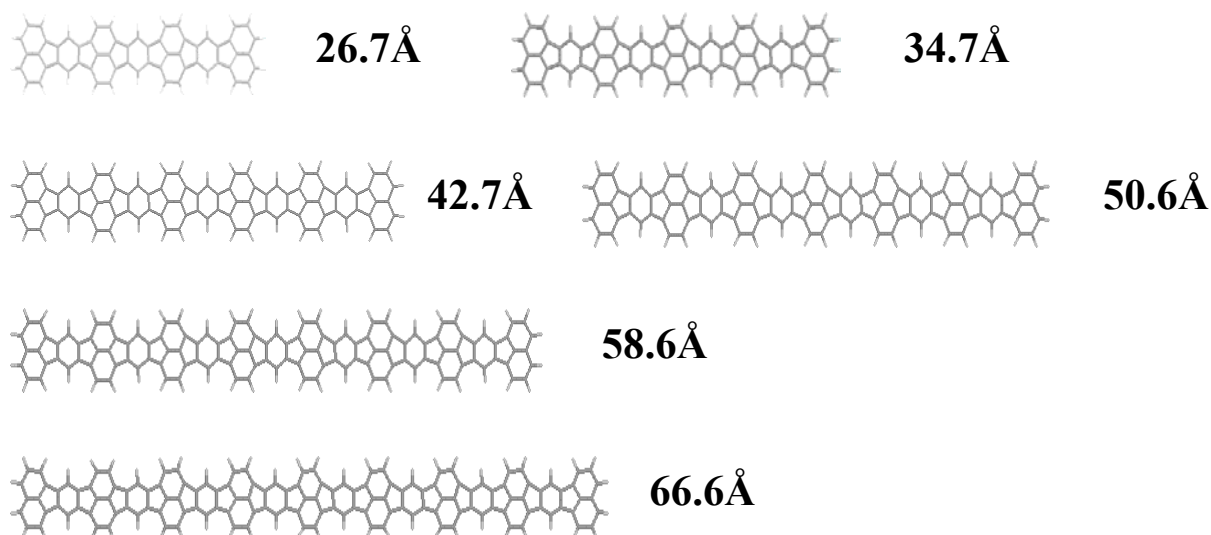


**Figure 88:** the molecular structure of the wire series used in the decomposition of molecular orbitals contribution to  $G$ .

For each of the Fig. 88 molecular wires, we have determined the number of  $\pi$  molecular orbital contributing to  $G$  for 2 different adsorption distances: in physisorption and in chemisorption as presented in the Table II below. It remains to separate the molecular orbital contributing to  $G_0$  or to  $\Gamma$ .

N (and L)	Total MO	Total $\pi$ MO	$\pi$ MO (G at 4 A)	+ $\sigma$ MO at 2 A
3 (2.67 nm)	258	58	33	53
4 (3.47 nm)	328	74	42	68
5 (4.27 nm)	398	90	51	83
6 (5.06 nm)	468	106	60	171
7 (5.86 nm)	538	122	69	195
8 (6.66 nm)	608	138	78	220

**Table II:** number of molecular orbital active in the through molecule tunnel process as a function of the molecular wire length L for 2 adsorption altitude 0.4 nm and 0.2 nm. The molecules are given in Fig. 88.

In the 80's, the Toulouse group had largely contributed in the understanding of the electronic super-exchange phenomenon through a single molecule. At that time, it was demonstrated that the effective electronic coupling  $V$  through a molecular wire between 2 metal atoms varies like  $V = V_0 \exp - \gamma L$ . For long molecular wires,  $V$  is very small (below 10 meV) and according to J. Bardeen,  $G$  is proportional to  $V^2$ . Therefore, the way to optimise  $\Gamma$  via  $m^*$  depends directly on the way to optimise  $\gamma$ . Notice that this inverse decay length is independent of any transport phenomenon. By building a family of formal molecular wire, we have now succeeded in BUN to demonstrate that  $\gamma$  is depending on the precise distribution of the molecular level away from the homo-lumo gap. This distribution can be summarized under the so-called spectral repulsion parameter, a statistical parameter well know by the nuclear physicists community.

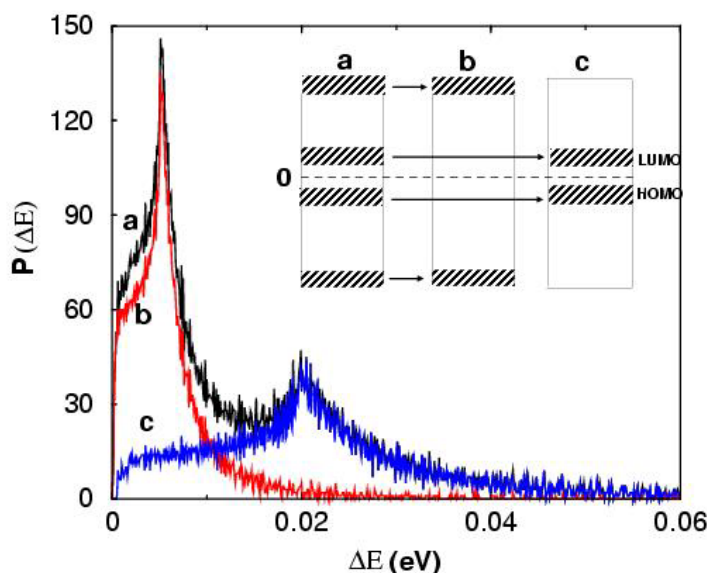


**Figure 89.** Example of the statistical analysis  $P$  of the 1-spacing distribution of the levels of a given molecular wire. The tail of this distribution for the large spacing  $\Delta E$  values can be fitted to get the repulsion parameter which controls  $\Gamma$ .

When a regular molecular wire is elongated by one unit cell, the spectral repulsion parameter describes how its molecular levels are pushed by the new molecular levels brought by this new unit. This parameter can be quantified by performing a statistical analysis of the spacing distribution of the molecular wire levels as presented in Fig. 89. At constant homo-lumo gap,

the repulsion parameter  $\rho$  is extracted by fitting the tail of this 1-spacing level distribution. The expression for  $\Gamma$  can be written:

$$\Gamma/2 = [(a)^{1/2} - b]/\rho$$

with  $a = 0.0123$  eV and  $b = 0.039$  eV for the formal selected molecular wires. Putting the equality  $\Gamma = 2\gamma$  as proposed by J. Bardeen for simple tunnel junctions and for standard homo-lumo gap  $\chi$  larger than 1 eV,  $m^*$  is directly proportional to  $1/\rho$ . This opens a new way to design super-tunneling molecular wires by adjusting the 1-spacing level distribution using for example side groups along the molecular wire.

A large part of the theoretical BUN work was also devoted to the contact conductance  $G_0$ . The starting example was of course the end contact of the single Lander molecule to the copper atomic wire on Cu(110) (see section V). The calculated images are presented in Fig. 90. There is a tiny increase in the contrast between the 2 rear legs. This provides a trace of the interaction of the board end with the copper wire end. To confirm the origin of this small contrast increase, we have recalculated the same STM image but now without the 4 legs (Fig. 90).

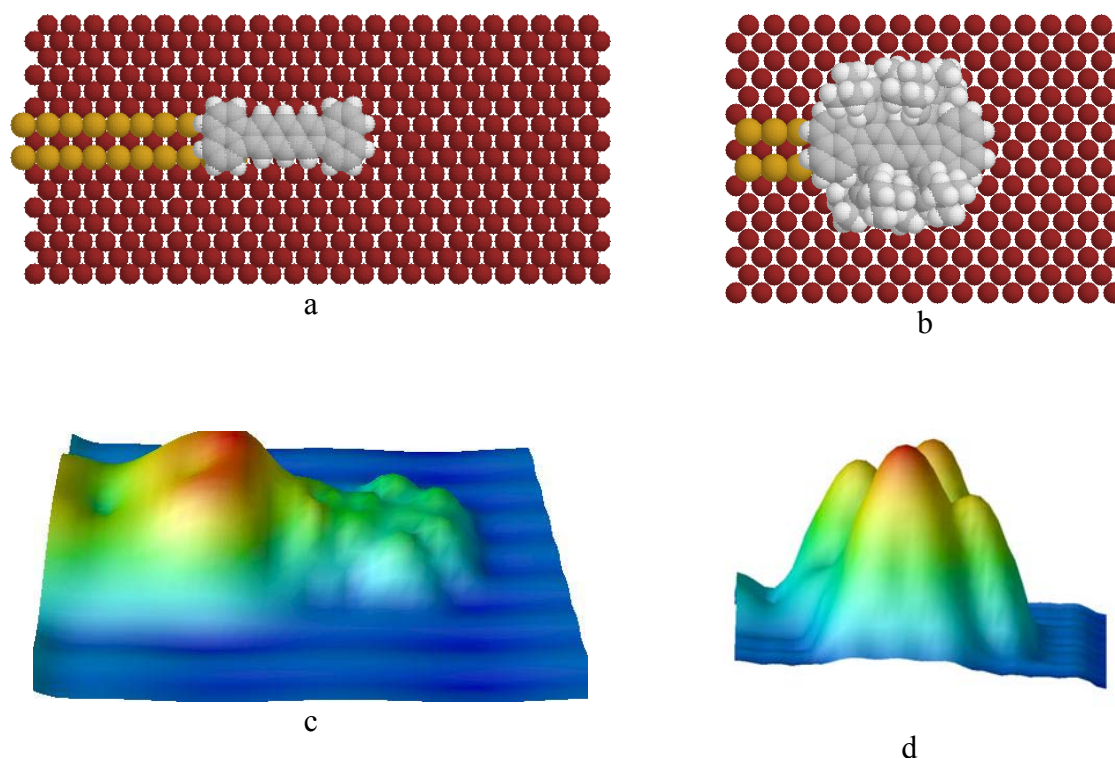


**Figure 90:** Calculated images and molecular model of the Lander molecule adsorbed at the end of the copper sub-nanowire. (a) and (c) without the legs and (b) and (d) with the 4 legs on the Lander. The big red bump in (c) is corresponding to the small blue bump between the 2 rear legs in (d).

Clearly the interaction between the end of the board and the 2 copper atoms at the end of the surface wire creates this contrast of about 50 pm. This is overshadowed by the usual 0.4 nm contrast given by the legs. We have also systematically study how this contact bump is related to the molecular orbitals represented at the end of the molecular wire by calculating for example the conductance of a given molecular wire with 2 different end groups: a standard naphthalene group and a naphthalene group equipped with 2 thiols. As presented in Fig. 91, the

two  $T(E)$  spectrum are not exactly the same. But at the centre of the gap, the two tunnel conductance's have the same order of magnitude.

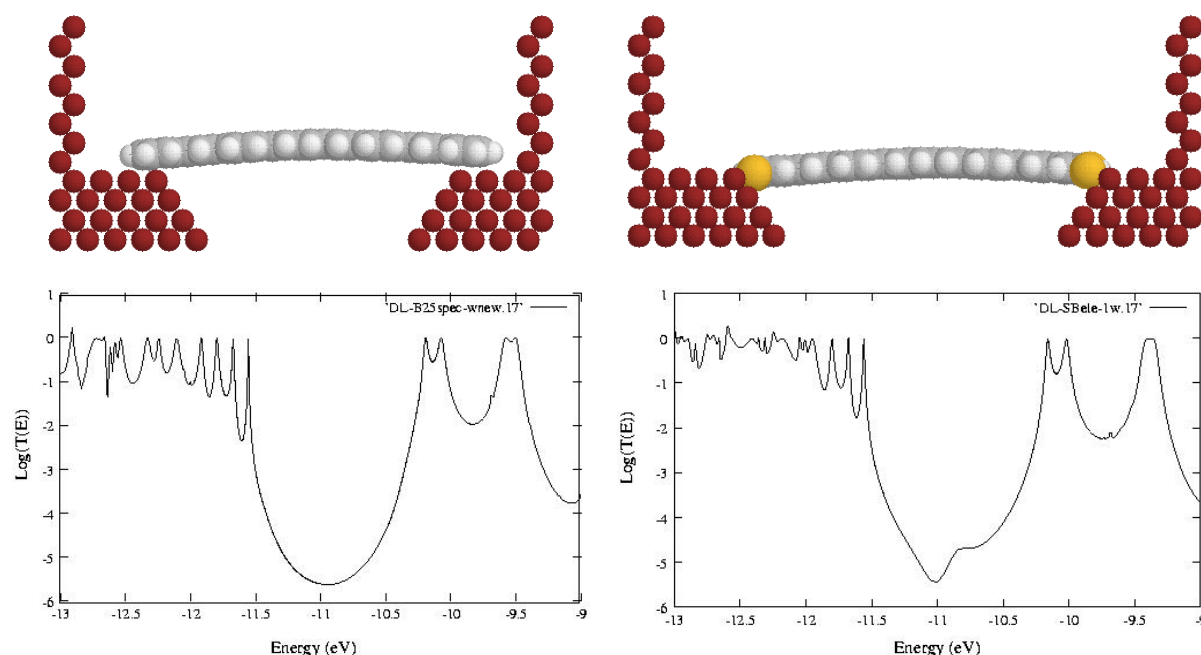


**Figure 91:** Calculated  $T(E)$  spectrum and the conformation of a molecular wire electronically connected to 2 massive electrodes. The molecular wire has the same chemical structure than the board of the molecular wires. The thiol are indicated by the yellow sulfur atoms.

For a non-thiol molecular wire we have plotted  $G_0$  as a function of the distance  $X$  of the end group towards the electrodes. As presented in Fig. 92, there is an optimum distance around  $X = 0.2$  nm which provides the better conductance. This  $G_0$  can be correlated to the contact bump height measured by the STM. This open a nice way to measure the contact conductance by recording the STM corrugation image at the molecule-wire contact location.

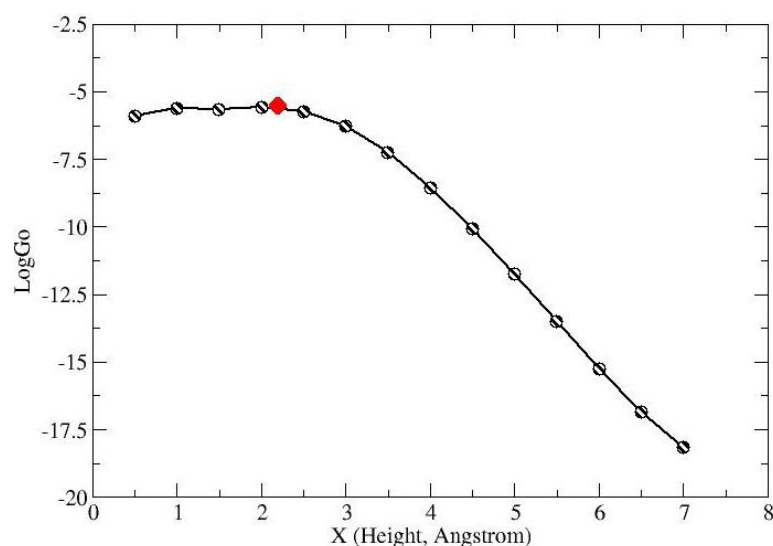


**Figure 92:** Variation of the contact conductance as a function of the distance  $X$  between the wire end and the contact electrode for the molecule series presented in Fig. 88. The red point is for thiol end groups.

## Vib) The intramolecular circuit laws and circuit simulator

To establish the intramolecular circuit law and build the first intramolecular circuit simulator, the Toulouse group had developed for BUN the N-ESQC extension of the standard ESQC technique. This N-ESQC calculation technique was shown stable enough to handle very large molecule up to the size of the largest logic circuit proposed for example by the MITRE corporation in the US. The integration of the EHMO semi-empirical quantum chemistry technique have been completed. It's not possible yet to go over this approximation due the thousand of molecular orbitals required in such a calculation pushing the computation time for a large molecule up to a month. To compare with, the  $N = 2$  standard ESQC technique can now compute at the DFT level of approximation the conductance of a few atomic junction with a computation duration of a few days.

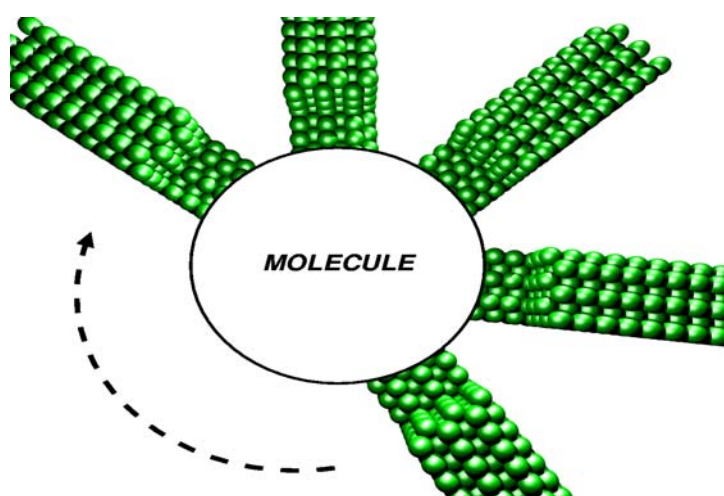


**Figure 93:** representation of the type of scattering experiment the EHMO-NESQC calculation technique can handle:  $N$  interconnect electrodes a single large molecule interacting with each of the electrode. The electronic band structure and surface states available are well described by the EHMO semi-empirical approximation together with the molecular orbital structure of the central molecule-circuit.

One difficulty was the correct matching of the electrodes Bloch waves with the central defect in the  $N$  electrodes junction presented in Fig. 93, when the section of the electrodes is becoming large enough to represent realistic nano-wires. A special effective Hamiltonian like technique was developed with a specific choice of the propagative channel state vectors to be kept. We are now able to compute the I-V characteristics from any 2 set of electrodes of for example the large intramolecular circuit presented in Fig. 94.

In parallel, the Toulouse group had extended its understanding of the intramolecular circuit rules to define simple design rules. This will avoid the very lengthy calculation of the N-ESQC technique in the first design step of an intramolecular circuit. These laws are summarized in Fig. 95. All these association rules results from 2 simple properties of the well studied electron super-exchange mechanism. If  $V_a$  and  $V_b$  are 2 super-exchange electronic interactions through 2 different molecular wires  $M_a$  and  $M_b$ , the overall coupling is proportional to  $V_a \cdot V_b$  if the new molecule results from the chemical bonding of  $M_a$  and  $M_b$  in series and  $V_a + V_b$  if they are bond in parallel. Since The conductance of a molecular junction is proportional (in first approximation) to the square of the electronic coupling

between the 2 electrodes introduced by the molecule-circuit, these 2 laws explain the circuit rules presented in Fig. 95.

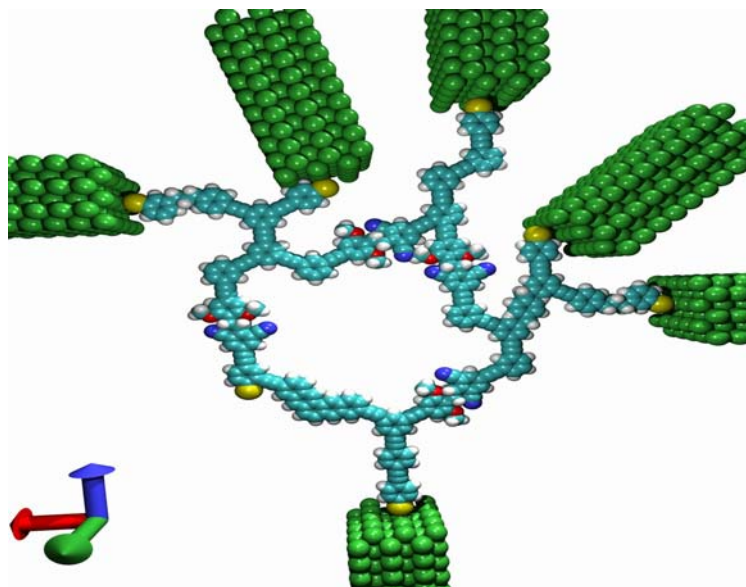


**Figure 94:** A 6 electrodes intramolecular logic circuit inspired from the MITRE corporation design whose I-V logic functionalities had been fully calculated using the NESQC technique.

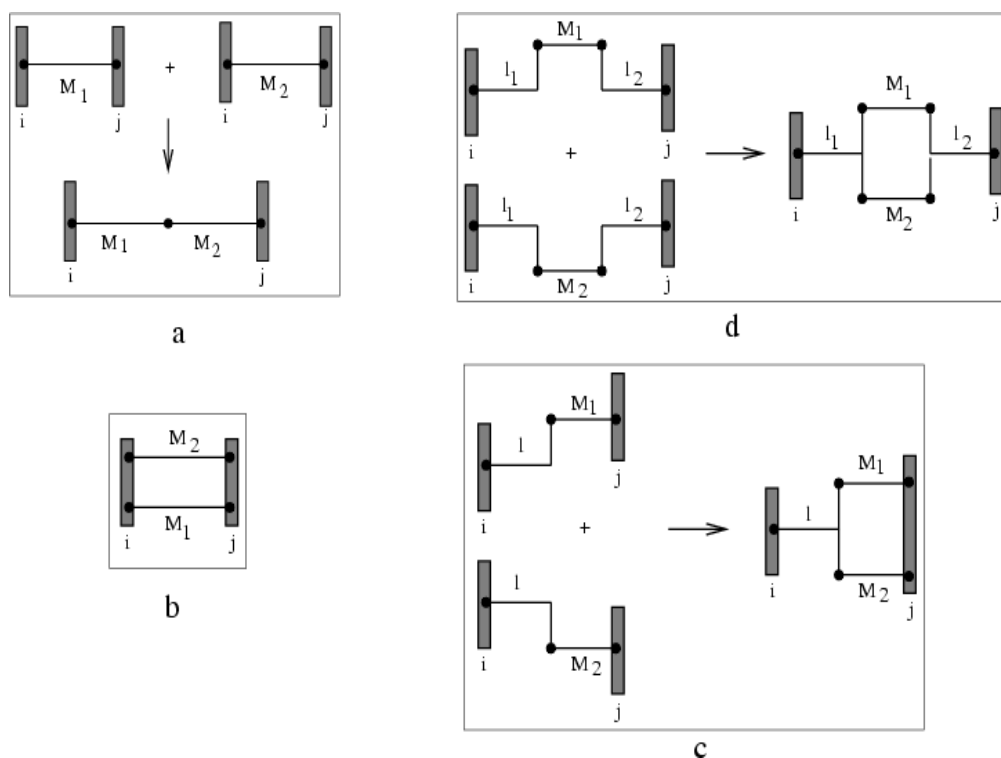


**Figure 95:** An example of 4 circuit rules of association that can be deduced from the super-exchange interaction superposition properties with (a) 2 molecular wires in series, (b) 2 molecular wires connected in parallel on a single junction, (c) a single node integrated inside the molecule and (d) 2 nodes integrated inside the molecule creating an intramolecular mesh.

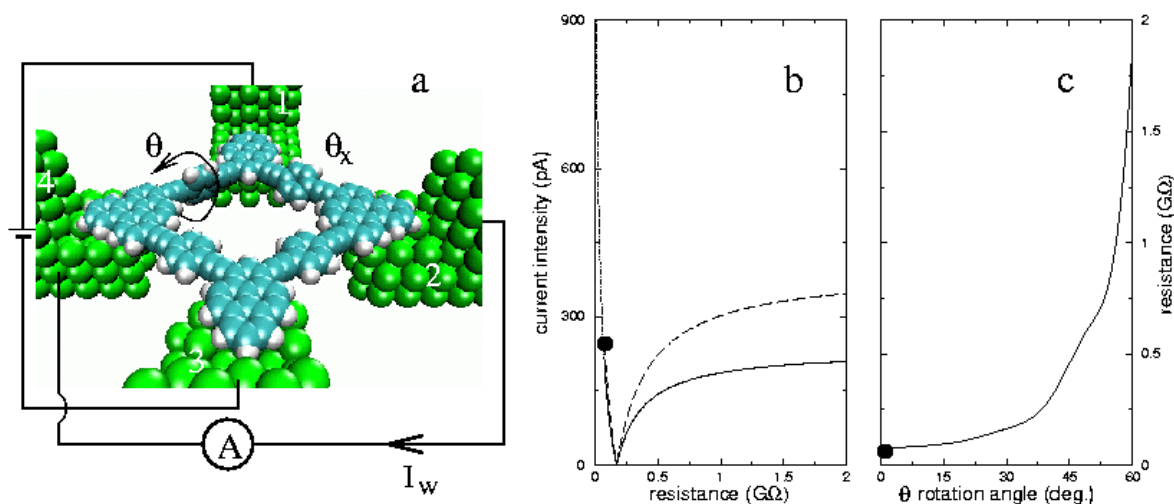


**Figure 96:** The balancing of the intramolecular wheatstone bridge presented in (a) using the N-ESQC calculation and intramolecular circuit rules. The bridge is tuned by changing  $\theta$  as a function of the unknown value of  $\theta_x$ . (b) is the balancing curve as a function of the variable resistance of the 1-4  $\theta$  branch. Full line for the standard Wheatstone rules and dashed for the NESQC quantum rules. (c) gives the relation between the resistance of a branch as a function of the phenyl rotation angle.

The first real molecular scale application of the circuit rule Fig. 95 was the balancing of the monomolecular Wheatstone bridge presented in Fig. DDD. The Toulouse group had studied this bridge because it is the first complex circuit where simple rules can be compared with a total N-ESQC calculations. The corresponding molecule can be synthesised and such macrocycle are already known in the literature. For this 4 electrodes connected molecule, the resistance of each molecular branch is calculated taking the corresponding molecular wire alone connected between 2 electrodes. When the phenyl in the molecular branch 1-2 is rotating by an unknown angle  $\theta_x$ , the bridge is balanced for example by rotating the 1-4 phenyl of the same angle or its complementary. As presented in Fig. 96, the approach to equilibrium is not the same applying the standard mesh and node Wheatstone rules or our new intramolecular circuit rules.

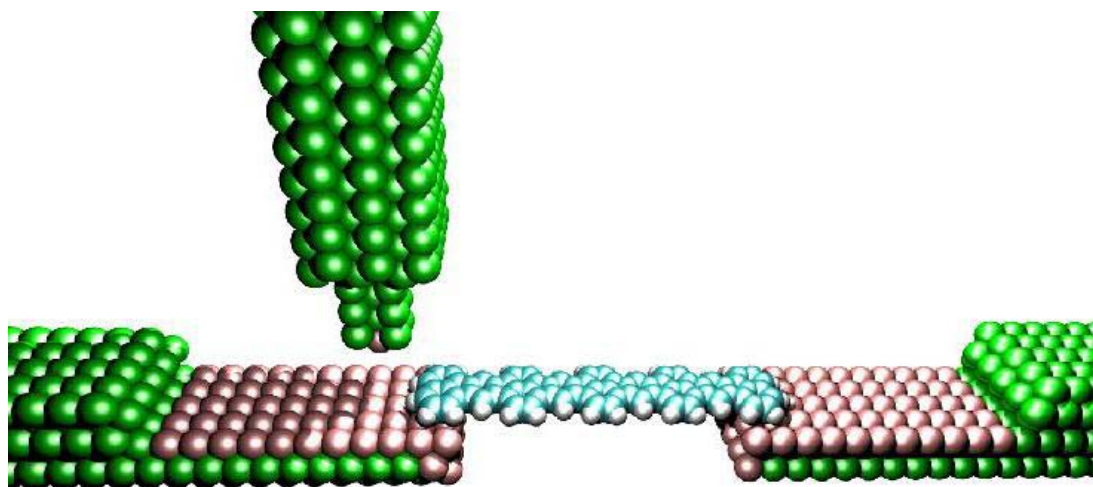


**Figure 97:** the atomic model of a N=3 tunnel junction made of 2 pads to electronically connect the central molecular wire and an STM tip. The central scattering defect is made of 2 surface pads (in pink and green), a molecule (in blue) and the tip apex. The 3 electrodes are the same on this model but can be chosen different.

Another application of the EHMO-NESQC technique is the calculation of the STM image of a molecule interconnected at least to one electrode. In this case, one electrode in the formal Fig. 93 circuit becomes the tip of the STM and the other electrodes continued to be use as the surface and the interconnections (see Fig. 97 for an example). This calculation technique can for example serve to identify the molecular orbital contribution in a molecular switch interconnected between 2 electrodes or to follow the tunnelling current path along a more complex intramolecular circuit.

### VIc) The design and function of a full tight binding half adder

For complex logic systems like a digital 1-bit half adder integrated inside a single molecule, the circuit diagram to be integrated in given in Fig. 98. The tight-binding version of N-ESQC was used by the London group to design this half adder inside the molecule first in the ballistic electron transport regime and after in a tunnel regime.

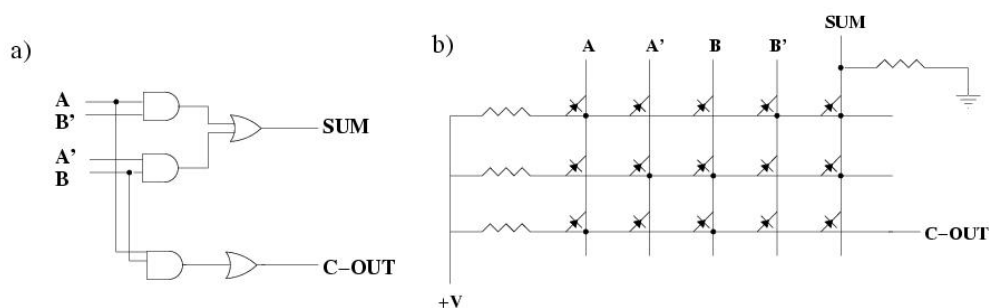


**Figure 98:** (a) Schematic logic gate structure and (b) detailed circuit diagram based on programmable gate logic arrays (PGLAs) for a 1-bit half-adder.

Fig. 99 a and b present the circuit diagram of the diode logic AND gate part of the Fig. 98 circuit and its schematic tight binding representation. This mono-molecular circuit is defined by atomic orbitals with on site-energies  $\epsilon, \epsilon_1$  which are coupled to each other by parameters  $h, \alpha$  and is connected to four electrodes A, ..., D.

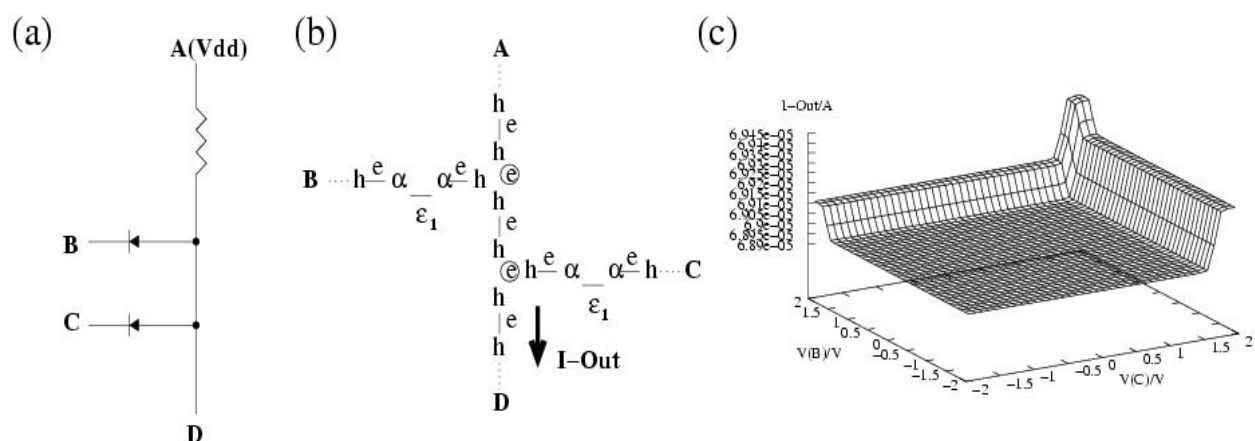


**Figure 99:** a) Diode logic circuit diagram and b) schematic representation of the tight binding (TB) Hamiltonian of an AND-gate. c) Output current on electrode D as a function of the input voltages on electrodes B and C. The coupling parameters are  $h=1, \alpha=0.05$ , the onsite energies are  $\epsilon=0, \epsilon_1=-1.7$  eV and the voltage supply  $V(A)=2$  V.

Depending on the voltages on input electrodes B,C the output current at electrode B should be a logic ‘1’ and ‘0’ representing a logic AND. However, as illustrated in Fig 98 c, instead of the desired two, there are 4 logical levels for the output current intensity. In order to understand this result, the contributions of the different branches of the circuit to the current have been analysed in BUN.

The electron transport between the voltage supply A and the output electrode D was found to be the dominant contributor to the total current. The differences between output currents for different inputs have their origin in the small contributions from electrons tunnelling through the defect orbitals between the two input electrodes and the output electrode, when their incident kinetic energy matches the onsite energies of the defects.

There are some properties of the tight binding diode AND-gate driven in the ballistic regime that are different from its classical counterpart in the Boltzmann regime. The contribution of a path through a tunnelling diode depends on the number of orbitals that have to be passed. For circuit design this means that two inputs will contribute different amounts to the output current, depending on their respective distances from the output electrodes. This is a consequence of the transformation of the Kirchhoff laws (see above). Although this could be compensated for by adjusting coupling parameters, it becomes very cumbersome for large circuits to analyse full branch by full branch the circuit. Finally, the form of the transmission coefficient of a path depends on the positions of connections to the corresponding wires, which makes it impossible to decompose molecular circuits into their individual parts in the ballistic regime.

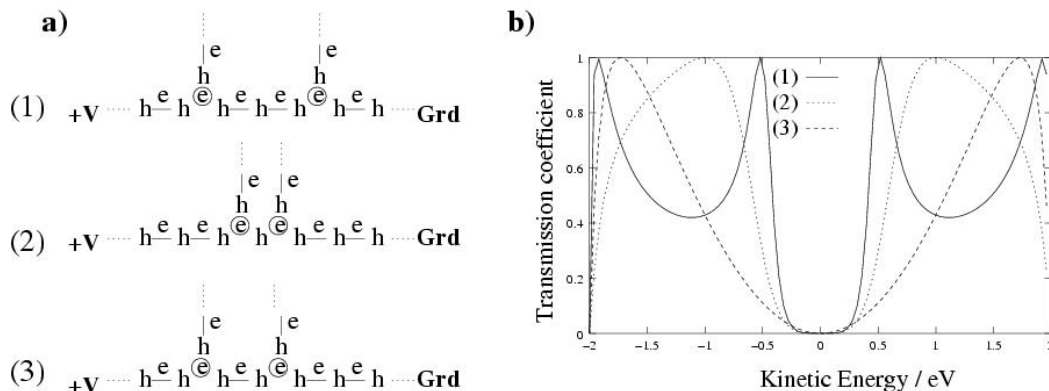


**Figure 100:** a) Schematic representations of the TB-Hamiltonians and c) transmission coefficients for the wires in the AND-plane of the PGLA half adder (Fig. 98), which all have connections to different pairs of wires in the OR-plane.

This behaviour has been expected for intra-molecular electronics in the ballistic regime, because ballistic circuits show the same effects whether they are implemented in microwave computing, photonics or mesoscopic ballistic electron devices. Fig. 100 presents this effect for PGLA given Fig. 98 and a tight-binding representation of the three wires in an AND-plane is used. These wires have been connected to single atomic orbitals in our calculation, since our analysis for the AND-gate (Fig. 99) had shown that the current flowing through such a wire depends primarily on the positions of the connections, rather than on electrons tunnelling through them by passing diodes. The results for the transmission coefficients for these three cases are shown in Fig. 100b. The variation of the current due to different positions of

connections to the wire is about an order of magnitude larger than that due to different inputs to the AND-gate

In order to illustrate further this architecture problem, the output current for the sum of a half-bit adder had also been calculated. Fig. 101 shows a ‘dedicated’ architecture for this logic function, the corresponding total current output. The details of connecting wires indeed make a difference for the output that is about ten times larger than the input variations. Furthermore, whereas the output of the XOR-gate of the dedicated architecture (Fig. 101 c) has only three logic levels due to the high symmetry of the circuit, this number rises up to five levels for the PGLA case. This signal mismatch illustrates the serious problems that would have to be solved if intra-molecular circuits of different types would have to be combined. In conclusion, a ballistic version of the circuit presented in Fig.98 cannot be directly integrated inside a single molecule without a severe adaptation of its local electronic structure.

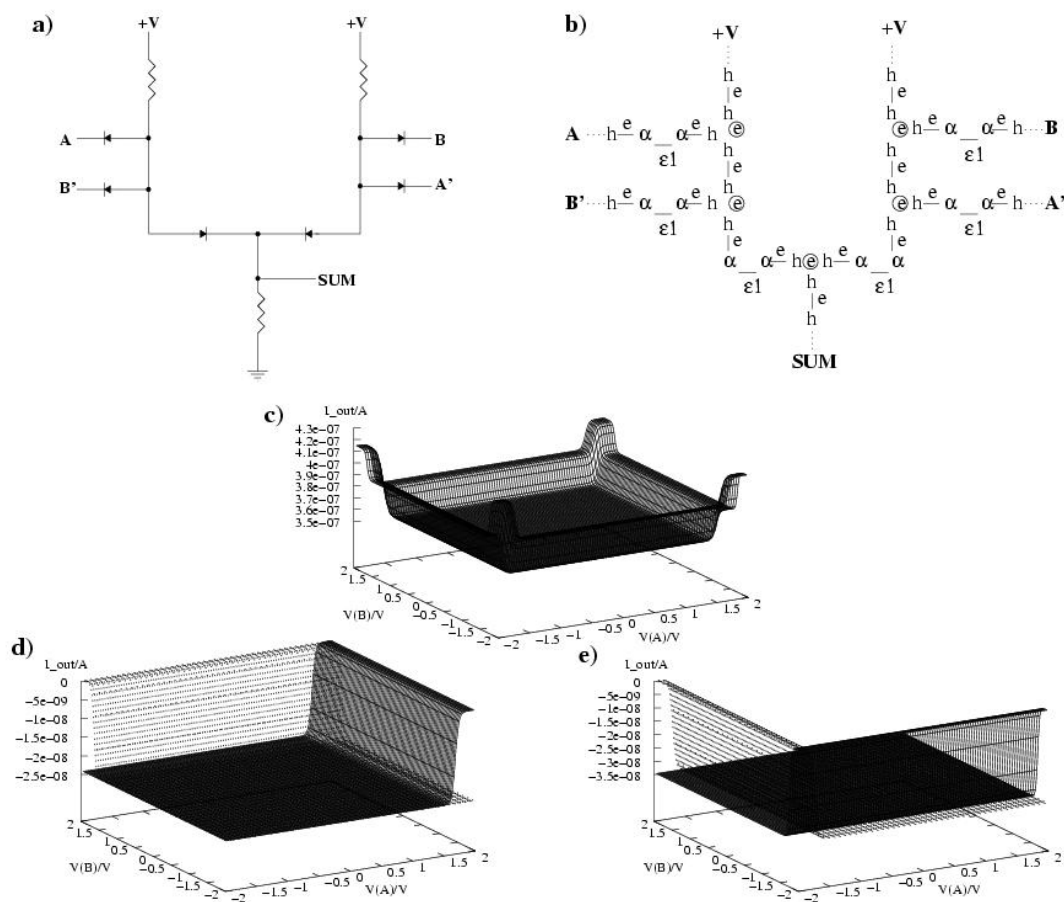


**Figure 101:** (a) Diode logic circuit diagram and (b) schematic representation of the TB-Hamiltonian of a XOR-gate, which is the logic function defining the sum of a half adder. (c) Total output current. (d) Contributions to the current/voltage dependence coming from electrodes A,B., (e) contributions from electrodes A',B'.

After the ballistic regime, the London group had studied the FPGA design of an half adder given in Fig. 98 but in the tunnel transport regime where for example, the interferences effect due to mesh of different lengths in a ballistic circuit have a smaller effect. In the tunnelling regime, the output current of the PGLA half adder presented in Fig. 102 depends strongly on

the symmetry of the molecular circuit due to the occurrence resonance states which dominate electron transport through the molecule.

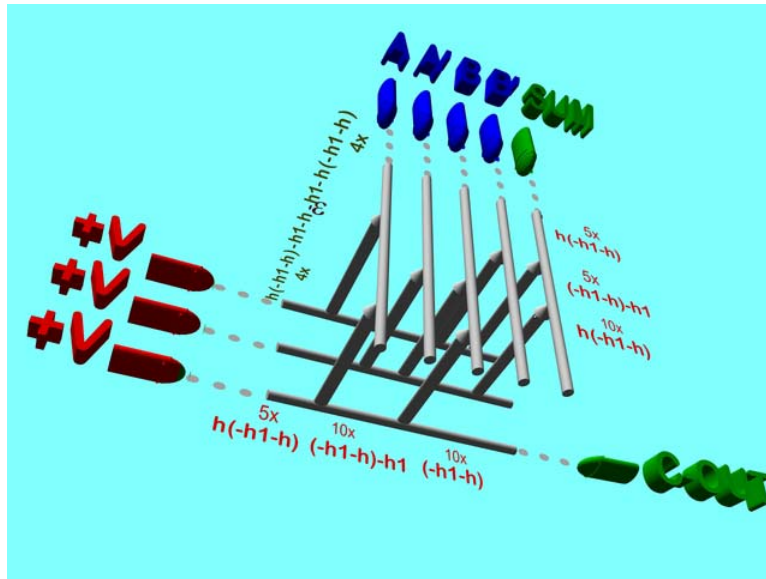


**Figure 102:** a 3D perspective of a schematic representation of the TB levels for a PGLA half adder in the tunnelling regime  $h=1$ ,  $h1=1.2$ ,  $e=0$  eV,  $\varepsilon=6$  eV, all lines represent levels with onsite energy  $e$ , where only diodes  $\varepsilon$  are an exception; for the sake of clarity only one wire of each plane and one connecting wire with diode has been explicitly labeled in the figure. All connecting wires have identical TB levels and the wires in the OR- and AND-planes are constructed from wire segments with 5, 10 or 15  $(h-h1-)$  segments depending on the respective length between connections in the architecture. There are 510 atomic orbitals in the model.

Fig. 103 shows the total output current intensities for the SUM and C-OUT electrodes for the PGLA half adder Fig. 102 in the tunnelling regime and its individual voltage dependent contributions coming from the four input electrodes. The differences between the individual contributions are much larger than the level splitting due to the voltage variation, an effect which also occurred to a lesser degree for the ballistic circuit. Furthermore, the total variation of the output current for the SUM is entirely determined by the variation of the voltage at input electrode A'. For the C-OUT, it is determined by the current flow due to varying the voltage at electrode B. For C-OUT, this is consistent with the fact that the wire length is the decisive aspect in the tunnelling regime, because electrode B has the shortest TB PGLA path to the C-OUT electrode. For the SUM logic output, the path from the dominating input electrode A' to the SUM electrode is distinctly longer than those from electrodes B or B'.

The transmission coefficient of the SUM-A' and C-OUT-B paths have the highest peak in the relevant energy region (also in the ballistic case) the SUM-A' path gives the strongest contribution to the output at SUM and C-OUT-B at electrode C-OUT, although it is less pronounced. The reason why this contribution still completely determines the output pattern at the SUM electrode can only be found in the complex symmetry properties of the circuit and cannot be predicted by a simple comparison between the path lengths. The symmetry properties will change entirely with any new piece bonded to the circuit, which means that it will not be possible simply to join such circuits together to form a larger TB PGLA architecture.

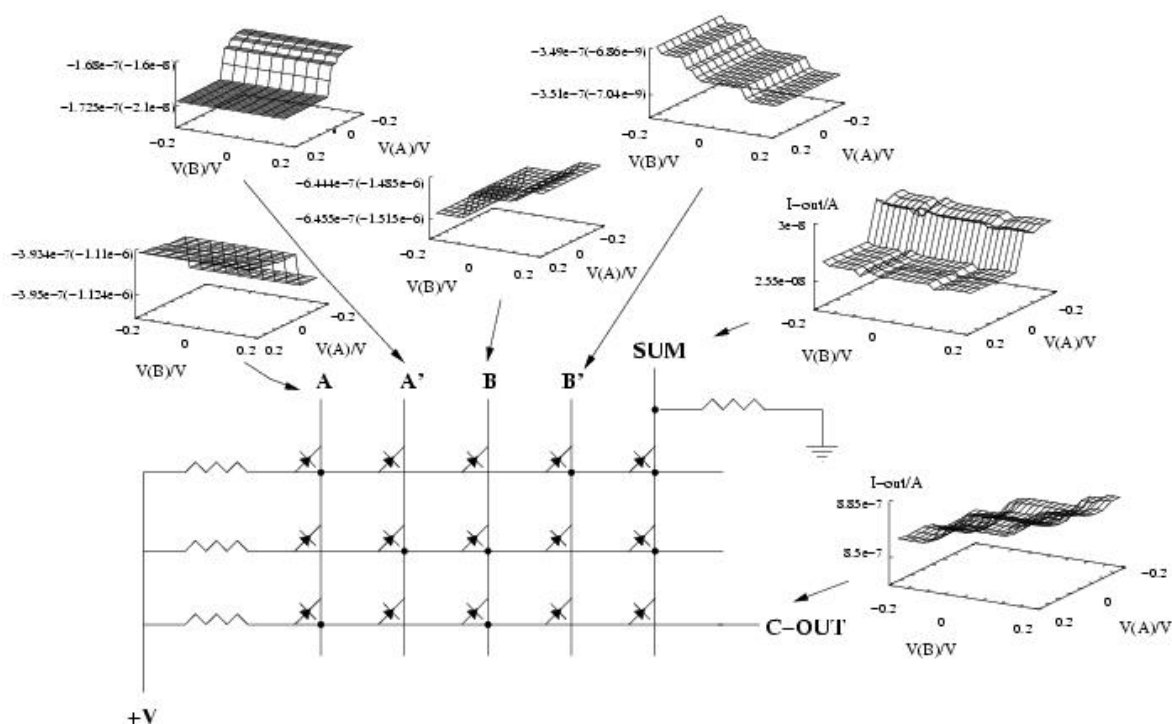


**Figure 103:** Output currents for sum and carry-out for a PGLA half adder in the tunnelling electron transport regime. The individual contributions coming from different input electrodes are also shown, where the first value is the contribution to the SUM and the value in parenthesis is the contribution to C-OUT.

In completing the comparison for PGLA adders in the two intra-molecular transport regimes, we note that whereas for the ballistic case the output current has a similar maximum as in the dedicated architectures for the AND- and XOR-gate, for the tunnelling circuit it is an order of magnitude smaller, which is due to the exponential decrease of electron transmission with the wire length in the tunnelling regime.

### VI d) The design and function of a molecule-OR and a molecule AND

To complete this analysis of the problem of designing digital logic circuit integrated inside a single molecule, we have in BUN used the full EHMO-N-ESQC to design a molecule with a OR and a AND logic function. Compared to the TB version, the expectation was that a complete set of molecular orbital, especially in the definition of the rectification effect will compensate part of the architecture difficulties discussed above.

As demonstrated by the London group, an OR-molecule gate does not introduced great challenge for the design at the tight binding level. Only one intramolecular node is required in diode logic for an OR gate. This results in the Fig. 104 molecular design of our proposed OR-gate with 2 intramolecular Aviram-Ratner diodes and one central node connect to a third electrode.

Using the Buttiker-Landauer formula and starting from the Fig. 104 spectra, The 3 electrodes I-V characteristics of the Fig. 104 junction was calculated using electrodes B and C as voltage input and electrode A as a current input. Input logic level are 0 V for “0” and > 0.2 V for “1”.

For a working Or logic function, the threshold output current must be 2 fA for output logic level “1”. The full logic surface of the propose Molecule-OR is presented in Fig. 105. Notice that input B and C are naturally decoupled as a consequence of the series superposition law presented Fig. 95a.

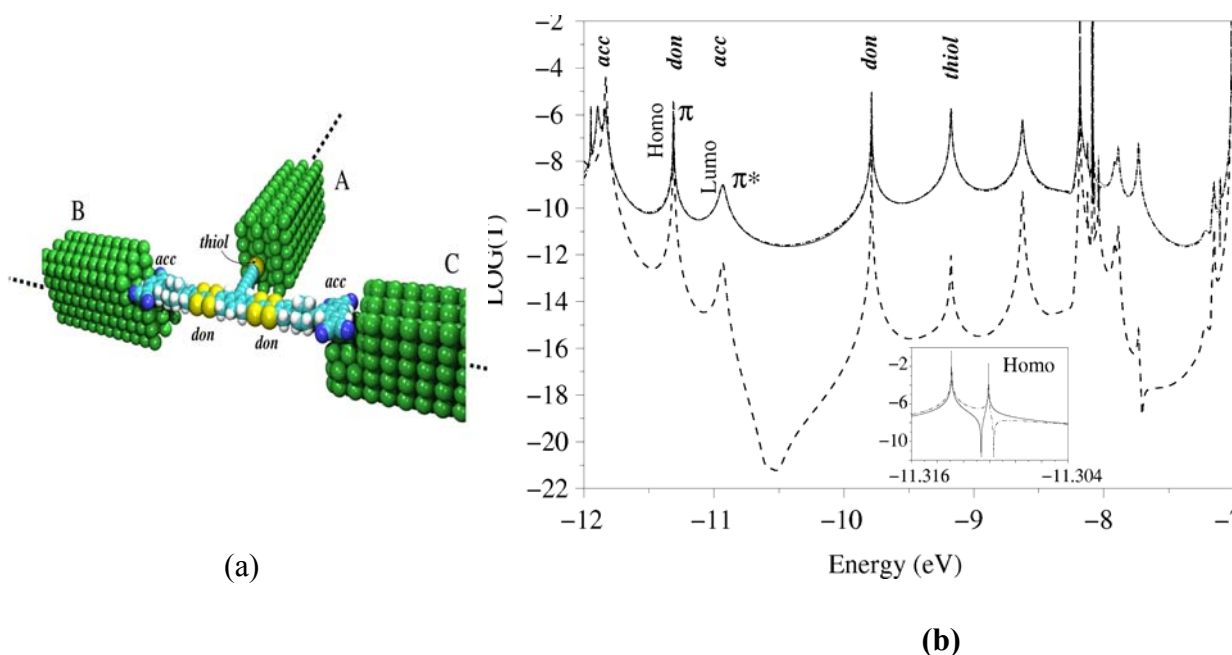


**Figure 104:** (a) Chemical structure, molecular conformation and interconnection set up for our Molecule-OR. EHMO-NESQC  $T(E)$  spectra calculated for the (a) scattering system. The HOMO-LUMO gap is indicated together with a chemical identification of the electronic resonance near the gap.

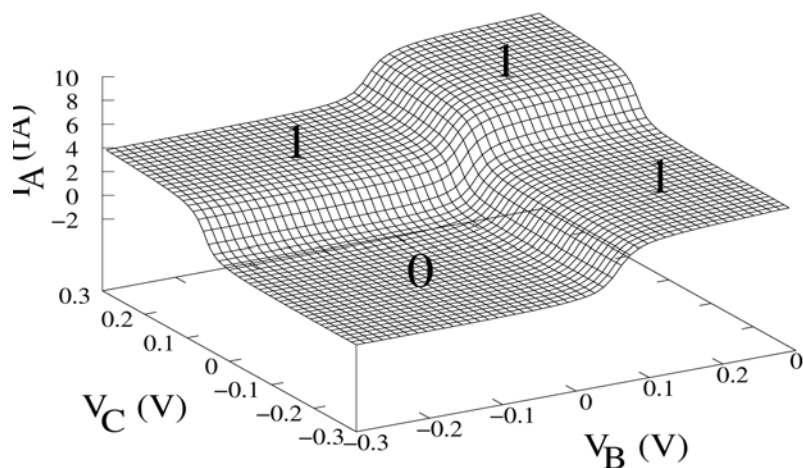


**Figure 105:** The calculated logic surface of the molecule-OR described in Fig.104. Notice the 2 values for the output logic “1” as already identified in a simple TB approach by the London group.

The Toulouse group had also designed and calculated the logic surface of a challenging AND gate. Contrary to the TB model, it was possible to choose the chemical composition to almost design a molecule-AND. The reason is that a lot molecular level are available to describe such a molecule at the semi-empirical EHMO level and the T.B. level appears to poor in molecular orbital. Furthermore, we have not selected an FPGA design to be able to adjust each wire length independently to compensate for example for the intramolecular interference effect. This results in the Fig. 106 design. The kernel of the molecule is identical to the OR gate. As it is well known is diode logic design, a change in the external driving electrical circuit

permits to pass from a OR to an AND with one electrode more. Electrodes B and C are still the voltage input, electrode D is connected to the ground and the voltage output is taken on electrode A. The logic surface is almost the one of an AND gate.

Notice that the main drawback of those logic function integrated inside a single molecule is the extremely running tunnelling current intensity in the fA regime. Shorter molecular rectifier may bring the design up to a few nA. But this will be still too low to pill up a lot of logic layer inside a single molecule.

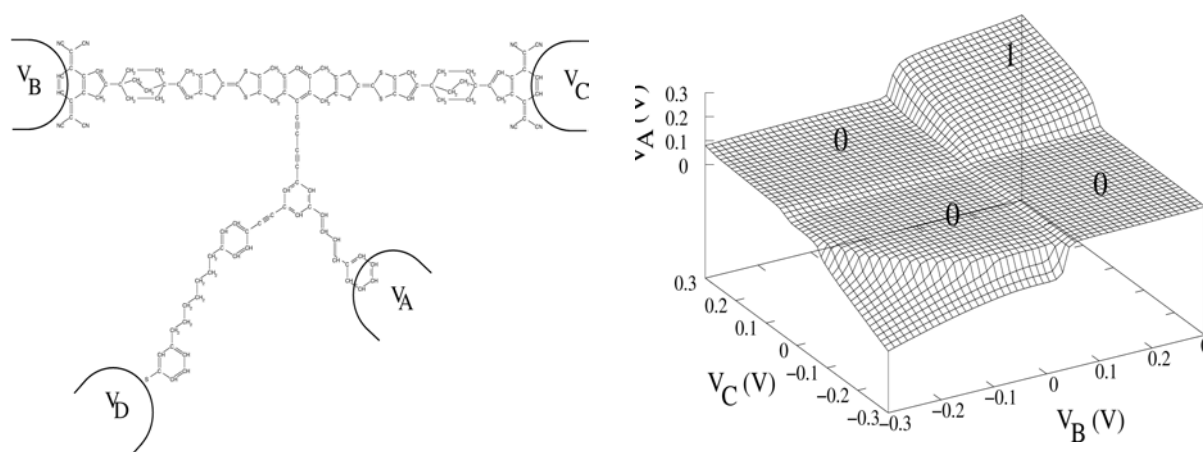


**Figure 106:** The proposed molecular structure and calculated logic surface of an AND gate integrated in a single molecule. There is only a logic level “1” and a bit of leakage current in the reverse bias.

This problem was known in the 50’s with semiconductor diode logic and compensated by inserting amplifier stage between logic stage. This approach is very difficult to be implemented inside a single molecule since no intramolecular amplifier exists today. It is even not certain that it will be possible to design one due to the quantum nature of the electron transfer process through a molecule.

### **VIe) Staring of the mono-molecular experimental approach**

The first molecule studied in BUN to open the mono-molecular era was an extended in 2 directions  $\pi$  molecule to have access with the STM tip to the quantum superposition and interference effects within this corral like molecule. The molecule is presented in Fig. 107. It is a molecule known as super-benzene or hexa-peri-hexabenzocoronene(HBC).

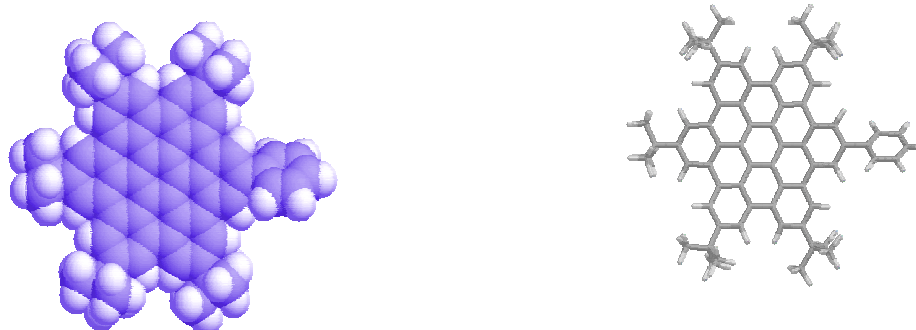


**Figure 107:** Space filling (left) and stick models of the corral molecule

The molecules were synthesised in Toulouse and have been substituted with six peripheral groups. 5 t-butyl substituents were added plus a phenyl ring substituted on place of the 6<sup>th</sup> one. This molecule is designed to couple electronically to a metallic mono-atomic step. This molecule provides very nice UHV-STM images as obtained by the Zurich group. The molecules self-assembled with an amazing degree of perfection and extend the order over large areas in which they exist as one rotational domain. Different orientation domains are observed in islands separated by steps. In the step regions molecular disorder is evident. The phenyl tail appears to play an important role in which they align in rows with each other as shown in Fig 108.

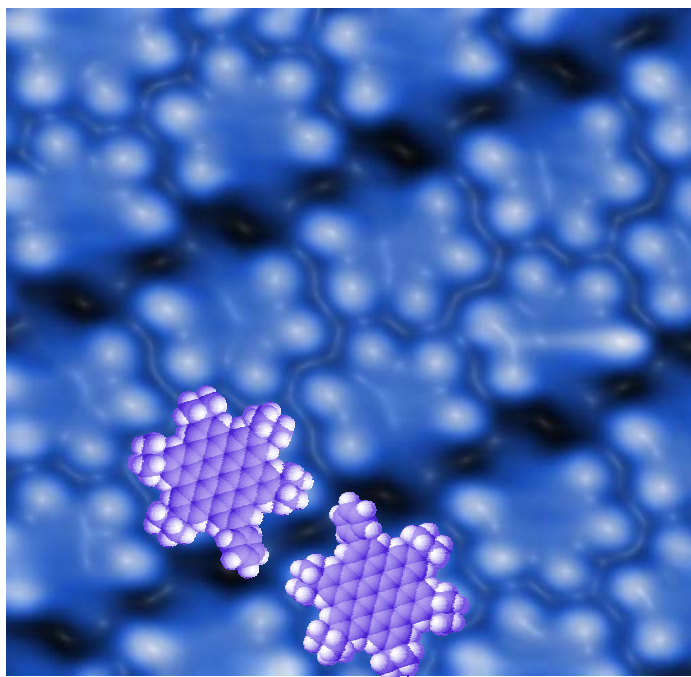


**Figure 108:** STM image of the corral molecules. The overlays of molecular models areas a guide to the eye. The phenyl groups are clearly resolved and the orientations of the phenyl groups in the model don't reflect their orientation in the image.

The phenyls are imaged with a lower apparent height than the t-butyl groups probably because they are electronically decoupled to a greater extent from the surface. But the polyaromatic ring system is also imaged and it is possible to resolve structure within the planar ring system. This is an indication that the central part of the molecule is electronically coupled to the surface via the 5 legs. The tunnel current decays exponentially from the centre of the polyaromatic ring towards the phenyl group.

In BUN, we went a step further by starting imaging conformational intramolecular switches which may be able to be integrated inside a molecule of the corral type for example at the place of a leg to control intramolecular interference effects. The Aarhus group had first as Monophenyl rotating -Lander (MphL). The board of this Lander is divided to two pieces connected via a single phenyl group  $\sigma$  bonded to the different parts, which is off axis (see section IIc). This phenyl group is expected to rotate under the action of the STM tip, either by direct manipulation or as a result of an excited state induced by inelastic tunnelling. As presented in Fig. 109, the molecules were deposited and STM imaged with success on the Cu(110) surface. It is apparent from the pictures that, whereas some molecules have the legs oriented along the close-packed direction of the substrate (right most molecule), some others

present a different axis (left most molecule). This is due to different molecular conformations related to different rotations with respect to the phenyl group.

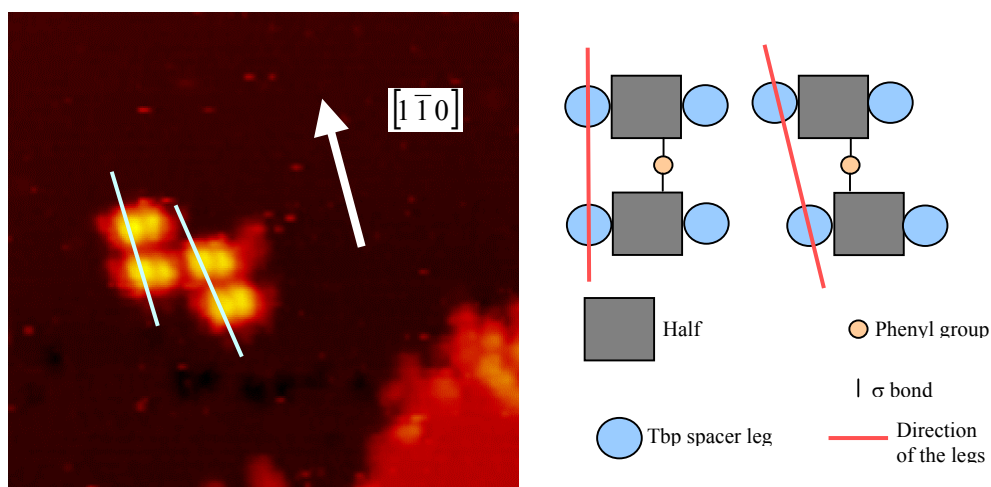


**Figure 109:**  $18 \times 18 \text{ nm}^2$  STM image of two MphL on Cu(110) showing two different conformations. The right panel shows a schematic representation of the proposed conformations, and how this leads to different directions of the axis that links the two legs in the same side of the molecule

When deposited at RT, most molecules appear attached at the step edges (see Fig. 110), although a number of them can be found also on the terraces. The molecules anchored at the step edge also lead to the reconstruction already reported for the SL and the VL. As shown in Fig. 110, a number of the MphLs attached at the step edge present still a new molecular conformation that reminds somehow of the conformation with the displaced half-boards reported above.

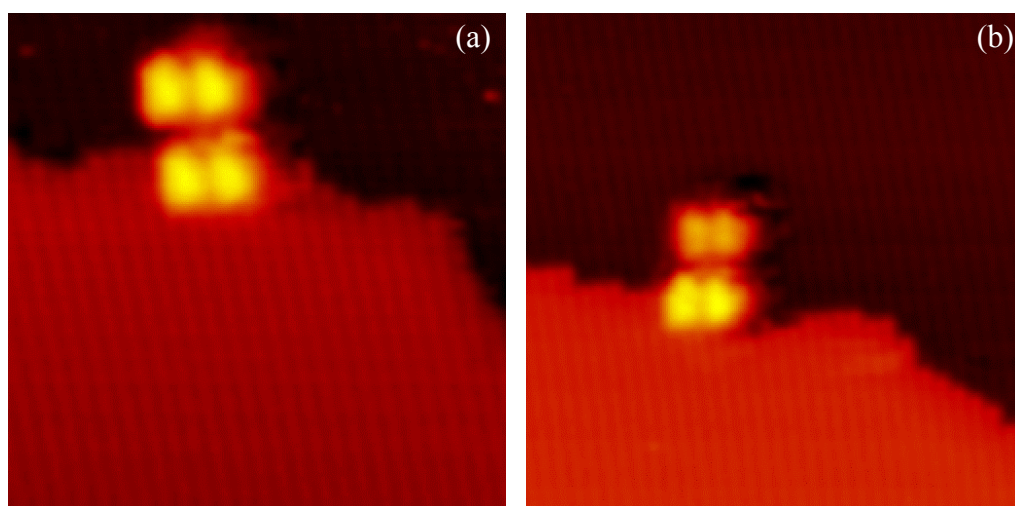


**Figure 110:**  $9 \times 9 \text{ nm}^2$  (a) and  $1.2 \times 1.2 \text{ nm}^2$  (b) STM images of MphL attached at the step edge. The conformation in (b) is of rotated type (see Fig. 109) and the two legs closer to the step edge appear brighter

The Aarhus had also investigated another 'rotating' lander ( $\text{C}_{126}\text{H}_{114}$ ) where the rotating part is an anthracene unit instead of a phenyl ring (see section IIc). The interest of this design is that upon rotation, the central anthracene will interact strongly one side or the other with the underneath copper surface. This will create a bistable intramolecular switch whose double well is created by the molecule-surface interaction. An example of the STM images obtained

is given in Fig.111. The lobes are going by four lobes (2 x 2 attached ones) in a somewhat rectangular geometry, corresponding to tunneling through the four spacer legs.

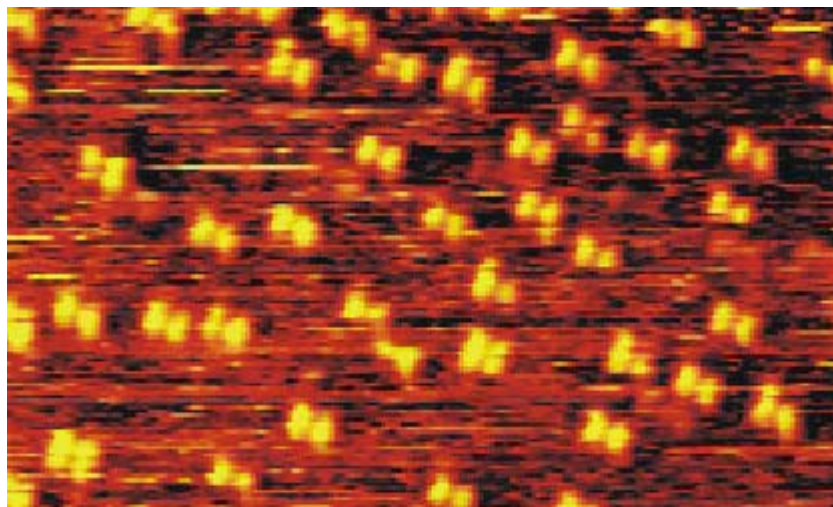


**Figure 111:** Constant current images of the 'rotating' lander after attempted deposition on Cu(110) ( $V=1250$  mV,  $I=0.3$  nA,  $200 \times 100 \text{ \AA}^2$ ).

A last example on an intramolecular switch is given by the TRIMA molecule (Fig. 112). Instead of lateral legs, this molecule was equipped with 2 grafting end groups to be adapted to a Si(100) surface.

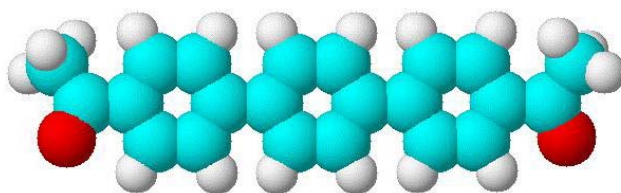


**Figure 112 :** The Trima molecule is the 1,4 para triphenyl dimethyl ketone with a length of 1.56 nm.

Through STM imaging (Fig. 113), the Orsay group has shown that the TRIMA molecules adsorb along the silicon dimer rows of the reconstructed Si(100) surface. NEXAFS spectroscopy using the synchrotron radiation has shown that the molecule is chemisorbed through the two end oxygen atoms to the silicon surface. Furthermore, NEXAFS spectroscopy has shown that the phenyl rings interact only weakly with the surface. This makes the TRIMA molecule a very good candidate for testing the change of molecular configuration through electronic excitation.

The Orsay group had succeeded in changing the TRIMA molecular conformation through an electronic excitation on the Si(100) surface. This is shown in Fig. 113 which displays three STM images ( $5 \times 5$  nm,  $V_S = -1.5$  V,  $I = 1$  nA) of the same area of the Si(100) surface. The left image shows 2 Trima molecules adsorbed on the surface. The middle image indicates the position of the STM tip during the electronic excitation ( $V_S = +4$  V,  $I = 10$  nA, time of excitation = 160 ms). The right image shows the result of the electronic excitation. It seems that the geometry of the central phenyl ring of the Trima molecule has been modified although a more definitive assignment of the change will require a comparison between the experimental and calculated STM images. It has been found by varying the surface voltage

during the electronic excitation that the efficiency of the STM tip induced process has a voltage threshold at 4-5 V. This indicates that the involved electronic excitation has an energy of 4-5 eV. This energy coincides with the energy of the  $\pi \rightarrow \pi^*$  electronic transition of the Trima molecule as determined from UPS and NEXAFS spectroscopy using the Synchrotron Radiation. Although it seems possible to achieve the change of molecular configuration through electronic excitation, the detailed understanding of the processes is still under debate. Indeed, it has been found that three different kind of molecular changes can be produced, namely rotation of the whole molecule, change the geometry of the central part (as presented in Fig. 113) and fragmentation of the molecule, depending on the exact value of the voltage applied to the surface.

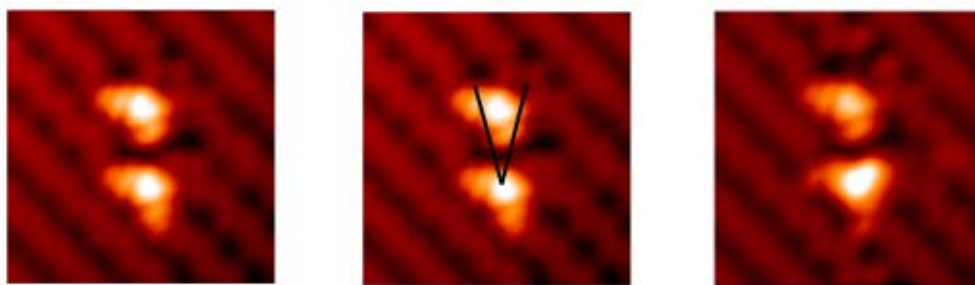


**Figure 113** : Change of configuration of a Trima molecule through electronic excitation with the STM tip. After the imaging, the tip apex is positioned on one TRIMA and a voltage pulse applies. The STM image recorded after the pulse shows a notable modification of the conformation of the molecule

#### **Vif) conclusion**

There is no physical limitation for the integration of an electronic circuit inside a single molecule. BUN was first in exploring in detail this new avenue of molecular electronics from a theoretical and from an experimental point of view. There are a lot of practical difficulties in reaching this ultimate stage in miniaturisation. Chemistry is first because the molecule must be larger and larger to open a reasonable growth margin in term of circuit complexity. The decay of the tunnel current intensity with an increase of the spatial extension of the molecule is also a very challenging problem. In a way, integrating an electronic circuit inside a molecule with identified meshes, nodes and functional groups is like forcing a molecule to behave classically. The very original architecture research performed in BUN opens a new avenue between this semi-classical view and a purely quantum computer architecture point of view. Why not benefiting from the intramolecular quantum behaviour of a molecule without separating the molecule in qubits? This is the new architecture paradigm for mono-molecular electronics in a quantum sense with the necessary companion atomic scale technology as presented in section II, IV and V.

## VIII) Conclusion

To reach the dream of an ultimate miniaturisation at the atomic scale, Molecular Electronics must imperatively re-enforce the knowledge in 2 major fields: atomic scale technology and architecture. To ensure a powerful roadmap, Molecular Electronics will have to abandon the hybrid approach which belong to the Moore roadmap. The mono-molecular approach requires a new architecture direction because a molecule is not a classical physics object. Forcing a molecule to resemble an electronic circuit poses the problem of the spatial extension of the molecule to reach a large computation functionality in the same molecule.

We will have to think quantum inside the molecule together with the use of our capacity to have access to this single molecule. This grand marriage between the quantum realm and a new picotechnology approach is challenging for science and for technology. BUN enters in picotechnology. We have pushed the UHV-STM and UHV-STM tool outside surface science to start the creation of a new technology at the atomic scale. The chemists have designed very specific molecule adapted now to the atomic scale of the nano-machines to be built. The physicists have started to explore another way of exchanging information, orders, results in and out of a single molecule. The problem here is no more to master the interconnection (the electronic interaction) between a molecule and an ultra-clean and ordered metallic electrode. The problem is to pass the required information through this link for the nano-machine to work.

The BUN consortium activity has generated 64 publications in journals of international reputation. May be more important, BUN has generated fundamental links between very good research groups all around Europe. This had formed the kernel of many new projects for the 6<sup>th</sup> framework in the spirit of what was explored by BUN. The CHIC project for quantum architecture, NAPA for atomic scale technology, Nanoplasmon for optical nano-communication and Nanoman to push forwards the atom and molecule manipulation techniques. We thanks the European Commission for the support of the BUN project during these 3 <sup>1/2</sup> years.



## BUN Publications list

Electronics using Hybrid-Molecular and Mono-molecular Devices

C. Joachim, J.K. Gimzewski and A. Aviram

Nature, **408**, 541 (2000)

Molecular and intramolecular electronics

C. Joachim

Superlattice & . Microstructure, **28**, 305 (2000)

Co-planar carbon nanotube hybrid molecular transistor fabricated in parallel

T. Ondarcuhu, C. Joachim and S. Gerdes

Europhys. Lett., **52**, 178 (2000)

Towards 4-electrodes co-planar metal-insulator-metal nanojunctions down to 10 nm

S. Cholet, C. Joachim, J.P. Martinez and B. Rousset,

Nanotechnology, **12**, 1 (2001)

Conformation change of a single molecule induced by STM manipulation: a route to molecular switching

F. Moresco, G. Meyer, K.H. Rieder, H. Tang, A. Gourdon and C. Joachim,

Phys. Rev. Lett., **86**, 672 (2001)

Logic gates and memory cells based on single C<sub>60</sub> electromechanical transistors

S. Ami and C. Joachim,

Nanotechnology. **12**, 44 (2001)

Relative performance of three nanoscale devices – CMOS, RTDs and QCAs – against a standard computing task

K. Nikolić, D. Berzon and M. Forshaw

Nanotechnology, **12**, 38 (2001)

A fast-scanning, low- and variable-temperature scanning tunneling microscope

L. Petersen, M. Schunack, B. Schaefer, T. R. Linderoth, P. B. Rasmussen, P. T. Sprunger, E.

Lægsgaard, I. Stensgaard, and F. Besenbacher

Rev. Sci. Instr. **72**, 1438 (2001).

Anchoring of Organic Molecules to a Metal Surface: HtBDC on Cu(110)

M. Schunack, L. Petersen, A. Kühnle, E. Lægsgaard, I. Stensgaard, I. Johannsen,

and F. Besenbacher

Phys. Rev. Lett. **86**, 456 (2001).

A Chiral Metal Surface

M. Schunack, Erik Lægsgaard, Ivan Steensgaard, Ib Johannsen, and Flemming Besenbacher,

Ang. Chem., International Edition, **40**, 2623 (2001).

Conformational changes of single molecules induced by STM manipulation for molecular switching

F. Moresco, G. Meyer, K.H. Rieder, H. Tang, A. Gourdon and C. Joachim

Phys. Rev. Lett., **86**, 674 (2001)

Inelastic transport of tunnel and field emitted electrons through a single atom

G. Dujardin, F. Rose, J. Tribollet and A. Mayne

Phys. Rev. B, **63**, R81305 (2001)

Toggling the local surface work function by pinning individual promoter atoms

G. Dujardin, F. Rose and A. Mayne

Phys. Rev. B, **63**, 235414 (2001)

Inelastic interactions of tunnel electrons with surfaces

A.J. Mayne, F. Rose and G. Dujardin

Faraday Discussion **117**, 241 (2001)

Atomic-scale imaging of insulating diamond through resonant electron injection

K. Bobrov, A.J. Mayne and G. Dujardin

Nature, **413**, 616 (2001)

A memory/adder model based on single C<sub>60</sub> molecular transistors

R. Stadler, S. Ami, M. Forshaw and C. Joachim,

Nanotechnology **12**, 350(2001)

Conformation of a long molecular wire with legs on a Cu(100) surface

T. Zambelli, H. Tang, J. Lagoute, S. Gauthier, A. Gourdon and C. Joachim

Chem. Phys. Lett., **348**, 1 (2001)

Forces with submolecular resolution between the probing tip and Cu-TBPP molecules on Cu(100) observed with a combined AFM/STM

Ch. Loppacher, M. Bammerlin, M. Guggisberg, E. Meyer, H.-J. Güntherodt, R. Lüthi, R. Schlittler, J.K. Gimzewski:

App. Phys A **72**, S105-S108 (2001).

Contrast inversion in NC-AFM on Si(111) 7x7 due to short-range electrostatic interactions

M. Guggisberg, O. Pfeiffer, S. Schär, V. Barwich, M. Bammerlin, C. Loppacher, R.

Bennewitz, A. Baratoff, E. Meyer

Appl Phys A **72**, S19-S22 (2001).

Atomic-resolution images of radiation damage in KBr

R. Bennewitz, S. Schär, V. Barwich, O. Pfeiffer, E. Meyer, F. Krok, B. Such, J. Kolodziej, and M. Szymonski.

Surf. Sci. Lett. **474**, L197 (2001).

The performance of hybrid-molecular architectures with current CMOS technology as a reference

R. Stadler and M. Forshaw,

Physica E, in press (2002)

Single Crystals of Single-Wall Carbon Nanotubes Formed by Self-Assembly,

R.R. Schlittler, J.W. Seo, J.K. Gimzewski, C. Durkan, M.S.M. Saifullah, and

M.E. Welland,

Science, **292**, 1136 (2001).

Synthesis of Polyaromatic Hydrocarbons with central rotor  
Christine Viala, Andrea Secchi and André Gourdon  
EurJOC, 4185-4189 (2002).

Long Jumps in the Surface Diffusion of Large Molecules  
M. Schunack, T. R. Linderoth, F. Rosei, E. Lægsgaard, I. Stensgaard and F. Besenbacher  
Physical Review Letters **88**, 156102 (2002).

Bonding and Ordering of Decacyclene Molecules on Cu(110) Studied by Scanning Tunneling  
Microscopy  
M. Schunack, E. Lægsgaard, I. Stensgaard and F. Besenbacher  
Journal of Chemical Physics **117**, 8493-8498 (2002).

Temperature control of electronic channels through a single atom  
G. Dujardin, A.J. Mayne and F. Rose  
Phys. Rev. Lett. **89**, 36802 (2002).

An STM study of the growth behavior of the oxidation of the Ge(111) surface  
A.J. Mayne, F. Rose and G. Dujardin  
Surf. Sci. **523**, 157 (2002).

Different role of filled and empty surface states in a polyfunctional molecule adsorption :  
Geranyl Acetone on Si(111)7x7  
M. Carbone, G. Comtet, G. Dujardin, L. Hellner and A.J. Mayne  
J. Chem. Phys. **117**, 5012 (2002).

Resonant electron injection as an atomic-scale tool for surface studies  
K. Bobrov, L. Soukiassian, A.J. Mayne, G. Dujardin and A. Hoffman  
Phys. Rev. B, **66**, 195403 (2002).

Toluene adsorption on Si(111)7x7 studied by synchrotron radiation photoemission and  
photodesorption  
M. Carbone, M.N. Piancastelli, M.P. Casaletto, R. Zanoni, G. Comtet, G. Dujardin, L. Hellner  
Surf. Sci., **498**, 186 (2002).

AFM tip nanoprinting of gold nanoclusters  
M. Ben Ali, T. Ondarcuhu, M. Brust and C. Joachim  
Langmuir, **18**, 872 (2002).

Large molecules on copper surfaces: A low temperature scanning tunneling microscope investigation  
F. Moresco, G. Meyer, K.H. Rieder, J. Ping, H. Tang and C. Joachim  
Surface Science, **499**, 94 (2002).

Tunneling heating of a single Xe adsorbate  
M. Hliwa and C. Joachim  
Physical Review B, **65**, 085406 (2002).

Electron effective mass when tunnelling through a molecular wire  
C. Joachim and M. Magoga  
Chemical Physics, **281**, 347 (2002).

Intramolecular circuits connected to N electrodes

S. Ami and C. Joachim

Physical Review B, **65**, 155419 (2002).

Conformation of a molecular wire at step edges on a metal surface

J. Kuntze, R. Berndt, J. Ping, A. Gourdon and C. Joachim

Physical Review B, **65**, 233405 (2002).

A tight binding study of logic gate circuits for adding numbers inside a molecule

R. Stadler, S. Ami, M. Forshaw and C. Joachim

Nanotechnology, **13**, 424 (2002).

The Lander molecule as a template on Cu(110)

F. Rosei, M. Schunack, P. Jiang, A. Gourdon, C. Joachim and F. Besenbacher

Science, **296**, 328 (2002).

Adsorption Behaviour of Lander Molecules on Cu(110) Studied by Scanning Tunneling Microscopy

M. Schunack, Y. Naitoh, F. Rosei, P. Jiang, A. Gourdon, E. Laesgaard, I. Stensgaard,

C. Joachim and F. Besenbacher,

J. Chem. Phys., **117**, 6259 (2002).

Bonding more atoms together for a single molecule to compute

C. Joachim

Nanotechnology, **13**, R1 (2002).

The deformation of a 3.7 nm long molecular wire at a metallic step edge

T. Zambelli, P. Jiang, J. Lagoutte, S. Gauthier, A. Gourdon and C. Joachim

Physical Review B, **66**, 075410 (2002).

A reliable scheme for fabricating sub-5 nm co-planar junction for molecular electronics

MSM Saifullah, T. Ondarcuhu, D.F. Koltsov, C. Joachim and M. Welland

Nanotechnology, **13**, 659 (2002).

Chiral Recognition in Dimerization of Adsorbed Cysteine Observed by Scanning Tunneling Microscopy

A. Kühnle, T. R. Linderoth, B. Hammer and F. Besenbacher

Nature **415**, 891-893 (2002).

Mechanics of Nanosprings: Stiffness and Young's Modulus of Molybdenum Nanocrystals,

C. Durkan, A. Ilie, M. S. M. Saifullah & M. E. Welland,

Applied Physics Letters, **80**, 4244 (2002).

Adsorption of Dodecanethiol on Cu(110): Structural Ordering upon Thiolate Formation

A. Kühnle, S. Vollmer, T. R. Linderoth, G. Witte, Ch. Wöll and F. Besenbacher

Langmuir **18**, 5558-5565 (2002).

Theory of near-field optical imaging with a single molecule as light source

G. Colas des Francs, C. Girard and A. Dereux

J. Chem. Phys., **117**, 4659 (2002).

Spatially resolved photonic transfer through single mesoscopic heterowire  
R. Quidant, J.C. Weeber, A. Dereux, D. Peyrade, C. Girard and Y. Chen  
Phys. Rev. E, **65**, 036616 (2002).

Oxygen Mediated Diffusion of Oxygen Vacancies on the TiO<sub>2</sub>(110) Surface  
R. Schaub, E. Wahlström, A. Rønnau, E. Lægsgaard, I. Stensgaard and F. Besenbacher  
Science **299**, 377-379 (2003).

Low temperature electron transport on semiconductor surfaces  
M. Lastapis, D. Riedel, A.J. Mayne, K. Bobrov and G. Dujardin  
J. of Low Temp. Phys., **29**, 196 (2003).

Direct determination of the energy required to operate a single molecular switch  
Ch. Loppacher, M. Barmmerlin, M. Guggisberg, O. Pfeiffer, E. Meyer, R. Luthi, R. Schlitler,  
J. K. Gimzewski, H. Tang and C. Joachim  
Physical Review Letters, **90**, 066107 (2003).

Molecular “OR” and “AND” logic gates integrated in a single molecule  
S. Ami, M. Hliwa and C. Joachim  
Chemical Physics Letters, **367**, 662 (2003).

Modulation of electron transmission for molecular data storage  
R. Stadler, M. Forshaw and C. Joachim  
Nanotechnology, **14**, 138 (2003).

Balancing a single molecule nanoscale Wheatstone bridge  
S. Ami, M. Hliwa and C. Joachim  
Nanotechnology, **14**, 283 (2003).

Atomic wire fabrication by STM induced hydrogen desorption  
L. Soukiassian, A. J. Mayne, M. Carbone, and G. Dujardin  
Surf. Sci., **528**, 121 (2003).

Atomic-scale desorption of hydrogen from hydrogenated diamond surfaces using the STM  
K. Bobrov, A.J. Mayne, A. Hoffman and G. Dujardin  
Surf. Sci., **528**, 138 (2003).

A tight binding study of a 1-bit half adder based on diode logic integrated inside a molecule  
R. Stadler, S. Ami, M. Forshaw and C. Joachim  
Nanotechnology, **14**, 722 (2003).

Lander on Cu(211): selective adsorption and surface reconstruction by a molecular wire  
L. Gross, F. Moresco, M. Alemani, H. Tang, A. Gourdon, C. Joachim and K.H. Rieder  
Chemical Physics Letters, **371**, 750 (2003).

Properties of large organic molecules on metal surface  
F. Rosei, M. Schunack, Y. Naith, P. Jiang, A. Gourdon, E. Laesgaard, I. Stensgaard,  
C. Joachim and F. Besenbacher,  
Progress in Surface Science, **71**, 95 (2003).

Probing the Probing the different stages in contacting a single molecular wire  
F. Morecsco, L. Gross, M. Alemani, K.H. Rieder, H. Tang, A. Gourdon and C. Joachim  
Physical Review Letters, 91, 036601 (2003).

Fabrication of N electrodes nano-junction for mono-molecular interconnects  
O. Cacciolati, C. Joachim, J.P. Martinez and F. Carsenac  
Nanotechnology, submitted (2003).

Syntheses of Hexabenzocoronene Derivatives  
Subir K. Sadhukhan, Christine Viala, André Gourdon  
Synthesis, submitted (2003).

Atomic-scale visualization and surface electronic structure of the hydrogenated diamond  
C(100)-(2x1) :H surface  
K. Bobrov, A.J. Mayne, G. Comtet, G. Dujardin, L. Hellner and A. Hoffman  
Phys. Rev. B, submitted (2003).

Self-assembled molecular chains formed by selective adsorption of lead-phthalocyanine on  
InSb(100)-(4x2)-c(8x2)  
N. Papageorgiou, H. Oughaddou, A. J. Mayne, G. Dujardin, Y. Ferro, L. Giovanelli, J. M.  
Layet, and G. Le Lay  
Appl. Phys. Lett. , submitted (2003).

Atomic-scale desorption of H atoms from the Si(100)-(2x1) :H surface : Are so many  
electrons really necessary ?  
L. Soukiassian, A.J. Mayne and G. Dujardin  
Phys. Rev. B, submitted (2003).

A chemisorbed bistable molecule: Biphenyl on Si(100)-2x1  
A.J. Mayne, G. Baffou, L. Soukiassian, L. Hellner, G. Comtet and G. Dujardin  
Phys. Rev. B, submitted (2003).

Numerical simulations of a phase locked loop based NC-AFM  
L.Nony, D.Schär, A.Baratoff, R.Bennewitz, A.Wetzel, E.Meyer  
Applied Surface Science, submitted (2003).

Investigation of organic molecules on insulating surfaces by NC-AFM  
L.Nony, O.Pfeiffer, E.Gnecco, R.Bennewitz, E.Meyer  
Applied Surface Science, submitted (2003).

Decay of the molecular wire conductance with length: the role of spectral rigidity  
A. Lahmidi and C. Joachim  
Chem. Phys. Lett., submitted (2003).

Experimental investigation of resonance curves in dynamic force microscopy  
J. Polesel-Marais, A. Piednoir, T. Zambelli, X. Bouju and S. Gauthier  
Nanotechnology, submitted (2003).